Doctor Dissertation

Regulation of steroidal glycoalkaloid biosynthesis by jasmonate-responsive Ethylene Response Factors in tomato

Chonprakun Thagun

Laboratory of Plant Cell functions,
Graduate school of Biological Science,
Nara Institute of Science and Technology

2016

バイオサイエンス研究科　博士論文要旨

所属 （主指導教員）	Laboratory of Plant cell function (Prof. Takashi Hashimoto)		
氏名	Chonprakun Thagun	提出	平成　　年　　月　　日
題目	Regulation of steroidal glycoalkaloid biosynthesis by jasmonate-responsive Ethylene Response Factors in tomato		

Yield of tomato, an economically important crop in the Solanaceae family, can be adversely affected by pathogens and insect herbivores. Tomato genes involved in the regulation and biosynthesis of defense compounds, which often cause food poisoning, may be exploited to breed new tomato cultivars that benefit human health. Among tomato defense compounds, steroidal glycoalkaloids (SGAs) are the major cholesterol-derived pseudo-alkaloids. Although many enzyme genes in the biosynthetic pathway of SGAs have been recently cloned, it is not well known how these enzyme genes are up-regulated after the herbivore attack. By combining approaches using molecular biology, transcriptomics, and metabolite analysis, I found that a group of jasmonate-responsive ETHYLENE RESPONSE FACTOR (JRE) transcription factors, which are close homologs of alkaloid regulators in *Catharanthus roseus* and tobacco, regulate SGA biosynthesis genes in tomato. Alteration of JRE functions in transgenic plant or hairy root lines by overexpression or dominant suppression caused drastic changes in SGA accumulation and in expression patterns of enzyme genes involved in the whole multistep pathway, starting from the mevalonate substrates and leading to the final SGA products. Transactivation and DNA-protein binding assays demonstrated that JRE4 activates the transcription of SGA biosynthetic genes by binding to the GCC-box-like elements in their promoters. I also found that jasmonates act upstream of the induction of JRE4-mediated SGA biosynthesis. The JRE4-binding elements occur at significantly higher frequencies in the proximal promoter regions of the genes regulated by JRE4, supporting the JRE4-mediated transcriptional coordination of a series of metabolic genes involved in the SGA biosynthesis. My research results provide the novel insights of regulatory mechanism of tomato toxic compound biosynthesis mediated by a conserved jasmonate-inducible ERF transcription factors in tomato, and will be useful for elucidating regulatory mechanisms of defense compounds found in related *Solanaceae* crops, such as potato and eggplant.

Contents

Introduction

Tomato (*Solanum lycoopersicum*) is a *Solanaceae* vegetable rich in vitamins, antioxidants and other nutrients (Kimura and Sinha 2008). In US alone, fresh tomatoes of 27.3 million pounds, worth $1.14 billion, were harvested in 2014 (USDA NASS 2015). Although originated in warm climate area, tomato is widely cultivated across all continents in part because of its high adaptability to various environments (UGA Extension 2014). Tomato, as a model species of plant biology, has been intensively studied to understand the genetic and evolutionary bases of fruit development (Ososio et al. 2011, Seymour et al. 2013), flowering (Samach and Lotan 2007), and biotic and abiotic responses (AbuQamar et al. 2009). Genetic modification though transformation is readily available for the species, and has been used to develop cultivars with novel genetic traits (Shikata and Ezura 2016). Whole genome sequence of a domesticated cultivar of tomato (cv. Heinz 1706) was determined (The tomato genome consortium 2012)

Plants, as sessile organisms, have evolved multitudes of defense and adaptation mechanisms to endure in fluctuating environments. To ward off biotic threats imposed by pathogens and pests, plants produce and accumulate toxic substances, including a diverse array of alkaloids, terpenoids, and other metabolites with bioactive properties (Bednarek and Osbourn 2009). For instance, saponin from *Avena sativa* disrupt cell membrane of pathogens (Osbourn et al. 1996), morphine from opium poppy (*Papaver somniforium*) blocks specific receptors in central nervous systems (Moriyama et al. 2001), and DIMBOA-glucoside from *Zea mays* inhibits nutrient absorption in insect gut (Frey et al. 2009). Plant-derived chemicals, being widely exploited by human as valuable compounds, are often considered unwanted ingredients in food crops because of their adverse impacts on human health (Betz 1999), and elimination or reduction of such phytochemicals has been considered critical in plant breeding. Complex metabolic pathways, encompassing precursor-supplying primary pathways and downstream specialized pathways, are engaged in the production of defense chemicals, and the regulation of the pathways, often represented with transcriptional coordination of structural genes, is required to ensure the restrained implementations of costly chemical defense, which usually impose burdens on growth and development in plants (Baldwin 1998).

Solanaceae plants synthesize steroidal glycoalkaloids (SGAs) (Itkin et al, 2011,

Itkin et al. 2013, Iijima et al 2013, Chowański et al. 2016); over a one hundred of SGAs, including α-tomatine, dehydrotomatine, and esculeosides in tomato (Itkin et al. 2011, Cárdenas et al. 2015), α-solanine and α-chaconine in potato (Itkin et al. 2013, Cárdenas et al. 2015), and α-solasonine and α-solamargine in eggplant (Mennela et al. 2012), has been found in *Solanaceae* (Chowański et al. SGAs are mainly produced and accumulated in green parts of plants, such as leaves and immature fruits in tomato, and sprouting shoots in potato. When consumed, most SGAs have lethal or sub-lethal effects on herbivorous insects (Itkin et al. 2013, Chowański et al. SGAs have cholesterol-derived steroidal backbone attached with a chain of three or four sugar residues (Cárdenas et al. 2015). All of the steps involved in SGA biosynthesis starting from acetyl-CoA are schematically shown in **Fig. 1**. Steroidal backbones of SGAs, such as tomatidine and solanidine, are synthesized from cholesterol by a series of enzymes encoded by *GLYCOALKALOID METABOLISM* (*GAME*) genes in potato and tomato (Itkin et al. 2011, Itkin et al. 2013, Cárdenas et al. 2015) (**Fig. 1**). Like other metabolic genes forming the clusters in plants (Boycheva et al. 2014, Osbourn 2010a and 2010b), *GAME* genes were found to be clustered together in tomato and potato genomes (Itkin et al. In the final part of the biosynthesis, three and four sugar moieties are attached to the steroidal aglycones by multi-step glycosylation steps catalyzed by GAMEs with UDP-glycosyltransferase activities (**Fig. 2**). During ripening of tomato fruits, α-tomatine is converted to lycoescoleosides, e.g. esculeoside A, less toxic and health benefit-compounds (Iijima et al. 2008, Yamanaka et al. 2009) (**Fig. 2**).

Jasmonates (JAs) play central signaling roles in a wide range of plant resistance and developmental responses (Wasternack and Hause 2013), including the elicitations of defense chemical pathways. Among different forms of JAs synthesized in plants, isoleucine-conjugated jasmonate (jasmonoyl-L-isoleucine; JA-Ile) is the most effective form of naturally occurring JAs (Fonseca et al. 2009) (**Fig. 3**). Methyl jasmonate (MeJA) has been widely used as effective elicitors to induce the production of secondary metabolites in plant cultures (Yukimune et al. 1996). Perception of JA signals and following steps, mediated by CORONATINE INSENSITIVE 1 (COI1), JASMONATE ZIM-DOMAIN proteins (JAZs) and JAZ-interacting transcription factors, have been elucidated through molecular and genetic studies and found conserved among the plant species (Wasternack and Hause 2013) (**Fig. 3**). JA-Ile promotes the COI1/JAZ complex formation and degradation of JAZ repressor proteins by 26S proteasome complex

(Pauwels and Goossens 2011). The degradation of JAZs releases basic helix-loop-helix (bHLH)-family MYC2 and other transcription factors bound by JAZ repressors in the absent of JA-Ile, leading to the activation or repression of genes responsible for JA-mediated transcriptional control (Zhang et al. 2015) (**Fig. 3**). The molecular mechanisms linking the conserved JA signaling with downstream defense metabolisms have been intensively studied (De Geyter et al. 2012). Plant secondary metabolisms can also be controlled by JA-mediated COI1/JAZ signaling cascade via bHLH-family MYC2 transcription activation. A group of JA-inducible ETHYLENE RESPONSE FACTOR (ERF) transcription factors, categorized in clade 2 of group IXa (Nakano et al. 2006, Shoji et al. 2010, Shoji et al. 2013), including OCTADECANOID-DERIVATIVE RESPONSIVE CATHARANTHUS 3 (ORCA3) from *Catharanthus roseus* and ERF189 from tobacco, have been found to play similar regulatory roles in JA-induced alkaloid biosynthesis in distinct species; ORCA3 controls the JA-dependent production of monoterpenoid indole alkaloids, including clinically important compounds, in the medicinal species (van der Fits and Memelink 2000), whereas JA-induced formation of ornithine-derived nicotine is regulated by ERF189 in tobacco (Shoji et al. 2010) (**Fig. 4**). JA-inducible *ORCA3* and *ERF189* mediate the coordinated transcription of a series of metabolic and transport (Shoji et al. 2009) genes involved in the alkaloid pathways by recognizing specific GCC box-like elements found in promoters of the targeted genes (van der Fits and Memelink 2001, Shoji et al. 2010, Shoji and Hashimoto 2011a). JA-inducible expression of *ORCA3* and *ERF189* is regulated by bHLH-family MYC2 transcription factor (Zhang et al. 2011, Shoji and Hashimoto 2011b), one of the JAZ-interacting factors, involved in the regulation of a wide range of JA downstream responses (**Fig. 4**).

Tomato has six *JA-Responsive ERF* (*JRE*) genes, phylogenetically related to alkaloid-regulating *ORCA3* and *ERF189*, and five of the *JRE*s are clustered together on chromosome 1 (**Fig. 5**). In this study, I performed the transcript profiling and metabolite analyses of transgenic tomato lines with altered *JRE* function, and demonstrated that *JRE*s play central roles in the transcriptional regulation of a long multi-step pathways leading to SGAs, from isoprenoid-supplying mevalonate pathway to GAME-mediated steps after cholesterol. Transactivation and DNA-protein binding studies indicated that JRE4 positively controls the biosynthesis genes by recognizing GCC box-like elements in their

promoters. Amino acid substitution in the DNA-binding domain of JRE4 causes loss-of-JRE4 function to recognize with JRE-binding site in promoter region of SGA gene. Significantly frequent occurrences of putative JRE-binding elements in proximal 5'-flanking regions of *JRE*-regulated genes, including genes involved in SGA biosynthesis, implicated the *JRE*-mediated transcriptional coordination of the genes.

Experimental procedures

Plant growth, transformation and treatment

Sterilized seeds of tomato, *Solanum lycopersicum* cv. Micro-Tom, were germinated and grown to the seedlings on half-strength Gamborg B5 medium solidified with 0.6% (w/v) agar and supplemented with 2% (w/v) sucrose. Two-week-old seedlings were transferred onto the soil in pots and grown to maturity in greenhouse.

A coding region of *JRE4* was cloned into the *Bam*HI and *Sac*I sites on pBI121 to generate a binary vector *p35S::JRE4* for overexpression. The *p35S::JRE4* vector was introduced into *Agrobacterium tumefaciens* strain GV2260 by electroporation. *Agrobacterium*-mediated transformation to generate transgenic tomato plants was done according to Sun et al. (2006). Shoots were selected on solidified Murashige and Skoog medium containing 100 mg liter^{-1} kanamycin. Diploid individuals were screened in T_0 generation. Transgenic plants of T_3 generation were analysed.

For gene expression analyses, leaves and roots from 4 week-old plantlets grown in greenhouse were submerged in B5 medium with 100 μM MeJA and incubated for 24 h in the dark. Four individuals of 7 week-old plants were placed in airtight plastic containers (ca. 8.1 letters of volume), with a cotton sheet soaked with 5 ml of 100 μM MeJA. The cotton was replaced with a newly soaked one every day during the duration. Leaves detached from plants exposed to MeJA vapour for 4 d were used for metabolite analysis.

To generate the dominant suppression vectors, coding sequences of *JRE3*, *JRE4*, and *JRE5* were amplified by PCR with primers including the restriction sites and a sequence for EAR motif (5'-CGGCCGCTTGATTTGGATCTTGAACTCAGACTT GGATTTGCTTA-3'; encoding LDLDLELRLGFA; Hiratsu et al., 2003) and inserted into the *Xba*I and *Sac*I sites on pBI121. To generate transgenic hairy roots, tomato hypocotyls from 7-day-old seedlings were infected with *Agrobacterium rhizogenes* strain ATCC15834 harboring a binary vector by briefly contacting one ends of hypocotyl segment (1.5 cm in length) to a bacterial colony and then standing the segments on the same agar medium with the attached ends up. Hairy roots emerging from infected sites were excised and subcultured every week twice on the solidified B5 medium containing 300 mg letter^{-1} cefotaxime for disinfection and 50 mg letter^{-1} kanamycin for drug-

resistance selection. The selected lines were maintained by subculturing every week in 125-ml glass flasks filled with 25 ml of liquid B5 medium supplemented with 2% (w/v) sucrose with shaking at 100 rpm in the dark. MeJA was directly added to 4-day-old cultures to a final concentration of 100 μM.

cDNA microarray analysis

Total RNA was isolated from leaves treated with MeJA for 24 h and hairy roots treated with MeJA for 24 h using an RNeasy kit (Qiagen). RNA integrity was checked with an Agilent 2100 Bioanalyzer (Agilent). Total RNA (500 ng) was used to generate Cyanine 3-labelled cRNA probes using a Quick Amp Labeling Kit, One-Color (Agilent). Tomato custom oligoarray with 60-mer probes of more 40,000 sequences, designed using transcript sequences of the Tomato Gene Index Version 11 (LeGI v.11; http://www.danafarber.org/), was hybridized with the labelled samples and scanned, and data were captured and processed as described (Ruiu et al. 2015). Due to poor labelling, hybridization was cancelled for sample from *JRE4-EAR* line #2.

Probes with low signal intensities (averages for the two controls <0.2) and intensities variable between the lines (differences between the two controls >2.5 folds) were excluded from the analysis. Values relative to the controls were obtained by pairwise comparisons and averaged for each construct; defined R_{ox}, R_{j3}, R_{j4}, and R_{j5} derived from data for *JRE4-OX*, *JRE3-EAR*, *JRE4-EAR*, and *JRE5-EAR* lines, respectively. For overexpression experiment, probes with R_{ox}>5 are listed in **Supplementary Table S1**. For suppression experiment, Q is defended as $Q^2=R_{j3}^2+R_{j4}^2+R_{j5}^2$ and probes with Q<0.85 are listed in **Supplementary Table S2**.

qRT-PCR

Total RNA was isolated from plant samples that had been ground in liqid nitrogen using RNeasy kit (Qiagen) and then converted to frist-strand cDNA using ReverTra Ace qPCR RT Master Mix (Toyobo) with oligo(dT) primer. The cDNA templates were amplified using a LightCycler 96 (Roche) with SYBR Premix Ex Taq (Takara) according to Shoji et al. (2010). The primer sequences are given in **Supplementary Table S9**. *EF1α* (Solyc05g005060) was used as a reference gene. Each assay was repeated at least three times. Based on amplifications from equal molar quantities of cloned amplicons, amplifications from different primer pairs were normalized.

Metabolite analysis

For measurement of SGAs, freeze-dried samples (2 mg) were extracted with 250 μl (for hairy root samples) or 500 μl (for leaf samples) of 80% (v/v) methanol containing 2.5 μM lidocaine and 2.5 μM 10-camphor sulfonic acid using a mixer mill with zirconia beads for 7 min at 18 Hz and 4 °C. After centrifugation for 10 min at 12,000×g, the supernatant was filtered using an HLB μElution plate (Waters). The extracts (1 μl) were analyzed using LC-QTOF-MS (LC, Waters Acquity UPLC system; MS, Waters Xevo G2 Q-Tof). Positive ion mode was used and analytical conditions were as follows: LC column, acquity bridged ethyl hybrid (BEH) C18 (1.7 μm, 2.1 mm×100 mm, Waters); solvent system, solvent A (water including 0.1% formic acid) and solvent B (acetonitrile including 0.1% formic acid); gradient program, 99.5% A/0.5% B at 0 min, 99.5% A/0.5% B at 0.1 min, 20% A/80% B at 10 min, 0.5% A/99.5% B at 10.1 min, 0.5% A/99.5% B at 12.0 min, 99.5% A/0.5% B at 12.1 min and 99.5% A/0.5% B at 15.0 min; flow rate, 0.3 ml min^{-1} at 0 min, 0.3 ml min^{-1} at 10 min, 0.4 ml min^{-1} at 10.1 min, 0.4 min min^{-1} at 14.4 min and 0.3 ml min^{-1} at 14.5 min; column temperature, 40°C; MS detection: capillary voltage, +3.0 keV, cone voltage, 25.0 V, source temperature, 120°C, desolvation temperature, 450°C, cone gas flow, 50 l h^{-1}; desolvation gas flow, 800 l h^{-1}; collision energy, 6 V; mass range, m/z 50–1,500; scan duration, 0.1 s; inter-scan delay, 0.014 s; data acquisition, centroid mode; Lockspray (leucine enkephalin): scan duration, 1.0 s; inter-scan delay, 0.1 s. MS/MS data were acquired in ramp mode using the following analytical conditions: (i) MS: mass range, m/z 50–1,500; scan duration, 0.1 s; inter-scan delay, 0.014 s; data acquisition, centroid mode; polarity, positive/negative; and (ii) MS/MS: mass range, m/z 50–1,500; scan duration, 0.02 s; inter-scan delay, 0.014 s; data acquisition, centroid mode; polarity, positive/negative collision energy, ramped from 10 to 50 V. In this mode, MS/MS spectra of the top 10 ions (>1,000 counts) in an MS scan were automatically obtained. If the ion intensity was <1,000, MS/MS data acquisition was not performed and moved to the next top 10 ions. Chemical assignment of SGAs was performed using the MS/MS spectra reported in Itkin et al. 2011 (Itkin et al. 2011). All SGA levels were calculated based on a calibration curve of α-tomatine (Tokyo Chemical Industry Co., Ltd.), assuming the same molar responses of SGAs.

For measurement of triterpenes, the extraction of plant tissues with added standards ([25,26,26,26,27,27,27-$^{2}H_{7}$]cholesterol (98% D, Cambridge Isotope

Laboratories, Inc.) or synthesized [3,28,28,28-$^2H_4$]β-amyrin, [28,28,28-$^2H_3$]α-amyrin and 28,28,28-$^2H_3$)lupeol; Ohyama et al. 2007) was carried out using the method previously described (Tsukagoshi et al. 2016). Quantification of triterpenes except for lanosterol and squalene using GC-MS analysis was performed as described previously (for sterols, Choi et al. 2014; for triterpenols, Ohyama et al. 2007). Lanosterol amounts were calculated using the peak area ratio of the fragment ion (m/z: 393) of trimethylsilylated lanosterol and that (m/z: 336) of the standard (TMS derivative of the labeled cholesterol). Quantification of squalene was performed using the standard calibration curve with coefficients of determination, $r^2 > 0.9996$. The curves were constructed using the peak area value of TIC (total ion chromatogram).

Transactivation assay

The 5'-flanking regions of *HMGR1*, *DWF7*, *DWF5, GAME6, GAME1* and *GAME4* were amplified by PCR from tomato genomic DNA with primers attached with the restriction sites and cloned into the *Hin*dIII and *Bam*HI sites on pBI121 to generate the *GUS* reporter constructs. For mutant effector and reporter constructs, before cloning the fragments into pBI121, PCR-based mutagenesis (Hemsley et al. 1989) was adapted to substitute the nucleotides in the cloned sequences; nucleotide substitutions for promoter sequences introduced are shown in **Fig. 14a**. *pGBW17* was used as empty-vector controls for effector plasmids. The binary vectors, *p19s* for P19 silencing suppressor (Voinnet et al. 2003) and *p35S-GFP* for *GFP* reference gene, were used.

Transient gene expression was performed in tomato fruits according to an agroinjection protocol (Orzaez et al. 2006). Briefly, *Agrobacteriun tumefaciens* strain EHA105 with a binary vector was grown overnight in YEB medium supplemented with 20 μM acetosyringone and appropriate antibiotics and recovered by centrifugation at 4,000 *g* for 20 min. The cells were re-suspended in infiltration buffer (10 mM MES, 10 mM $MgCl_2$, 200 μM acetosyringone, pH 5.7) by adjusting optical density at 600 nm to 0.25, and then incubated for at least 2 h at room temperature in the dark. The bacterial suspensions for reporter and effector vectors plus those for *p19s* and *p35S-GFP* vectors were combined, and the resultant solution (200 to 300 μl per fruit) was injected into mature green fruits (1 to 1.5 cm in size) using a 1 ml plastic syringe attached with a 27-gauge needle. Gene expression was analyzed by qRT-PCR using the fruits harvested 3 d after the injection.

EMSA

Bacterial expression and purification of recombinant fusion proteins of JRE4, called Sl1g90340 in Shoji et al. (2013), were done as described (Shoji et al. 2013). In the pET32b-based expression vector, a portion, but not full-length, of *JRE4* (corresponding to 40-219 amino acid residues) was placed downstream of a sequence for N-terminal tags, a thioredoxin, an S-tag, and a His-tag (Shoji et al. 2013). The proteins only with the tag portion from empty pET32b were purified and used as the controls.

Sequences of sense and antisense oligonucleotides used are given in **Supplementary Table S10**. Probe preparation, DNA-protein-binding assays, gel separation, and detection of the reaction products were carried out as described (Shoji et al. 2010).

Analysis of GUS reporter activity

For histochemical staining, transgenic hairy root lines were incubated with GUS staining solution (0.5 mM 5-bromo-4-chloro-3-indosyl-b-D-glucoronide cyclohexylamine (X-gluc), 10 mM sodium phosphate buffer (pH 7.0), 0.5 mM potassium ferricyanide, 0.5 mM potassium ferrocyanide and 0.1%(v/v) Triton X-100) at 37°C for 24 h. Stained tissues were cleared with 70% ethanol twice before observation with light microscope (Olympus MVX10) attached with camera (Olympus DP70) (Olympus, Japan).

GUS enzymatic activities in plant tissues were measured according to Shoji et al. (Shoji et al. 2008) with minor modifications. Soluble proteins were extracted with GUS extraction buffer (0.1 M potassium phosphate (pH7.8), 1 mM EDTA, 5% (v/v) glycerol and 0.1% (v/v) Triton X-100). Plant extracts were incubated with 25 mM 4-methyl umbeliferyl glucoronide (MUG, Sigma) in GUS extraction buffer at 37°C for 30 min.

Computational analysis

I used Regulatory Sequence Analysis Tools (RSAT; Turatsinze et al. 2008, http://rsat.ulb.ac.be/rsat/) to search putative JRE binding elements in the query genomic sequences by weight matrix scoring. Weight matrices for P box, CS1 box, and GCC box used (Shoji et al. 2013) are given in **Supplementary Table S1**. All parameters were used in the default setting. The elements with score higher than 7.0 were adapted except

for G2 in *GAME4*. Genes with putative JRE-binding elements in the examined regions were counted. Significant differences of the values against those of group W including all tomato protein coding genes was determined by one-sided Fisher's exact test (a=0.05) using the fisher test function of R (V. 3.2.2).

Based on sequences predicted as the JRE-binding elements by RSAT in the regions (-300 to -1) of group R genes, position-specific probability matrices of P, CS1, and GCC boxes (**Supplementary Table S1**) were generated by MEME software (v. 4. 10. 2., Bailey et al. 2006) with option settings; '2' for '-nmotif', '10' for '-minw' and applying '-revcomp'. To retrieve the sequences commonly found in the queries, MEME was used with option settings; '10' for '-nmotif', '7' for '-minw' and applying '-revcomp'. Match scores representing the similarities between a pair of the retrieved sequence and the JRE-binding box (P, CS1, or GCC) were calculated using position-specific probability matrices of the pairs. When a pair of sequences with lengths of L1 and L2 were aligned with the overlapping length of L3, the alignment length Le was defined as Le=L1+L2-L3. Differences between 1 and normalized vector distances were summed for overlapping positions and divided by Le to give scores for the alignments. The alignment scores were calculated for all possible alignments with no gap in both orientations for a sequence pair, and the highest alignment score was adapted as match score for the pair.

Results

JRE genes in tomato genome

In tomato, there is a gene cluster (spanning about 100 kb) with five clade 2 *ERF* genes of group IXa on chromosome I and one additional *ERF* gene of this clade also resides as a singleton on chromosome V (**Fig. 5a**). Since all of the six *ERF* genes were inducible by jasmonate (**Fig. 6**) and *JRE5* respectively correspond to *GAME9-like1*, *GAME9-like2*, *GAME9-like3*, *GAME9*, and *GAME9-like4* in a recent study (Cárdenas et al. 2016).

Based on multiple alignments of amino acid sequences of a conserved DNA-binding domain, a phylogenetic tree including JREs from tomato and related ERF proteins from Arabidopsis, *Catharanthus roseus*, and tobacco, was generated to examine the evolutionary relationships among the members (**Fig. 5b**). As defined previously (Shoji et al. 2013), clade 2 is divided into 4 subgroups; JRE3 and JRE4 are in clade 2-2b, and the remaining four JREs in clade 2-3 (**Fig. 5b**).

Expression patterns of *JRE* genes

The expression patterns of *JRE* genes along with SGA biosynthetic *HMGR1*, *SMO2*, and *GAME1* genes in tomato tissues were examined with qRT-PCR (**Fig. 6** and numerical values in **Supplementary Table S2**). Transcript levels of *JRE*s were expressed relative to that of house-keeping *EF1α*. *JRE* and SGA biosynthesis genes were expressed in organs from 7 week-old plants and no apparent organ specificity was observed. *JRE4* was most predominantly expressed among *JRE*s in nearly all examined tissues, though in a few cases like roots from plants and fruits in certain stages, the dominances of *JRE4* were relatively diminished (but still *JRE4* transcript is major in most), mainly due to decreased *JRE4* expression in the tissues. Toxic SGAs, such as a predominant α-tomatine, as well as their production drastically decrease during fruit ripening in parallel with increased catabolism of toxic SGAs to less toxic forms (Iijima et al. 2009). In accordance with such changes, expression of SGA biosynthesis genes and some members of *JRE*s, *JRE1*, *JRE2*, and *JRE4*, progressively decreased, when fruits were maturing. Except for *HMGR1* of which expression downed clearly at the breaker stage, decreases of the SGA biosynthesis and *JRE* gene expression were most evident during green fruit stages, where fruits are rapidly enlarging, rather than during later color-changing stages.

Expression levels of *JRE*s in cultured hairy roots were comparative or sometime higher than those in tissues from greenhouse-grown plants, suggesting the usefulness of the cultured material in studies on *JRE*s and SGA biosynthesis. Like in other tissues (see below), MeJA coordinately induced SGA biosynthesis genes in tomato hairy roots (**Fig. 6c**). As reflected to their naming, all *JRE*s were induced by MeJA treatment in tomato hairy roots, but induction kinetics in terms of magnitudes and timings were varied among the members; *JRE4* and *JRE6* were gradually induced during the 24-h duration, while acute and strong induction within 30 min followed with sharp decline was characteristic to *JRE1*, *JRE2*, and *JRE3* and induction of *JRE5* peaked at 4 h after the start of the treatment.

Transgenic tomato lines with altered *JRE* function

To study impact of altered *JRE* function on gene expression and metabolism in tomato, stable transgenic tomato lines of plants and hairy roots were generated by *Agrobacterium*-mediated transformation. Two *JRE4* overexpression (*JRE4-OX*) lines of plants, OX1 and OX12, were established by introducing *JRE4* cDNA under the control of cauliflower mosaic virus (CaMV) 35S promoter. Because of dominance of its transcript in tomato tissues among *JRE*s according to Tomato eFP (http://bar.utoronto.ca/efp_tomato/cgi-bin/efpWeb.cgi), which had been known when I started the experiment and was lately confirmed (see above), *JRE4* was chosen as a target gene for overexpression. In leaves of the *JRE4-OX* lines, high expression of *JRE4* transcript was confirmed, not significantly changing with MeJA treatment, while MeJA induced endogenous *JRE4* gene in wild-type controls (**Fig. 7a**). No visible abnormality was found in the *JRE4*-OX plants (**Fig. 7b**).

Dominant suppression strategy was taken to compromise the *JRE* function, since there are closely related *JRE* genes, which may have overlapping function. Three JREs, JRE3, JRE4, and JRE5, were attached with ERF-associated amphiphilic repression (EAR) motif at their C termini, which are known to dominantly suppress the gene expression targeted by the transcription factors (Hiratsu et al. 2003). The EAR-attached fusions *JRE-EAR*s were overly expressed with CaMV35S promoter in transgenic tomato hairy roots. Two independent lines for each construct were selected and analyzed. Overexpression of the introduced *JRE* genes were confirmed in *JRE-EAR* lines with qRT-PCR (**Fig. 8a**). Reflecting different expression levels of endogenous *JRE* genes (see above), degrees of overexpression shown relative to vector controls were varied among

lines with different fusion constructs. There were significant reductions of off-target *JRE* gene expression in certain combinations, suggesting the down-regulation of the *JRE*s by transformed *JRE-EAR* fusions. There were slight variations of growth and morphology among the lines (**Fig. 8b**), but they seemed within the range normally observed for hairy root cultures.

Transcript profiling in overexpression and dominant-suppression lines of *JRE*s

To clarify the regulatory function of JRE transcription factors in tomato, I investigated the impacts of altered *JRE* function on transcriptome to reveal genes targeted by *JRE*s. Comparative transcript profiling was carried out using the transgenic lines and a tomato custom oligoarray representing over 40,000 transcripts (Ruiu et al. 2015). Total RNA from each line was labeled and hybridized to the array. Two control samples for each comparison, wild-type plants for overexpression and vector control lines for suppression, were included. To examine the profiles in distinct types of tissues and those after JA elicitation, leaves treated with MeJA for *JRE4-OX* lines and hairy roots treated with MeJA for suppression lines were used.

Probes representing genes up-regulated in *JRE4-OX* lines and down-regulated in *JRE-EAR* lines, are given in **Supplementary Table S3** and **Table S4**, respectively; list of the genes included is available in **Supplementary Table S5**. A large number of probes for metabolic genes involved in SGA biosynthesis are among the *JRE*-regulated genes; 24 genes regulated in either *JRE4-OX* or *JRE-EAR* lines and corresponding probes with their signal intensities are shown in **Fig. 9** (values available in **Supplementary Table S6**). Nearly all probes indicated in **Fig. 9**, whether they satisfied or not the both listing criteria (indicated with asterisks), showed trends of signal increases in *JRE4-OX* lines as well as decreases in *JRE-EAR* lines. The *JRE*-regulated metabolic genes are involved in nearly all branches of the entire pathway leading to SGAs from upstream mevalonate pathway to cholesterol synthesis and downstream aglycone formation and its glycosylation steps (**Fig. 9**). Reflected in intense coloring in the maps, extents of regulation generally seemed greater for later steps, especially those after cholesterol (**Fig. 9**); top parts of **Supplementary Table S3** and **Table S4** are enriched with probes for *GAME* genes. All of the biosynthesis genes were similarly suppressed by *JRE3-EAR*, *JRE4-EAR*, or *JRE5-EAR*, and such tendency was corroborated with unbiased distribution of probes for SGA biosynthesis genes in a Venn diagram (**Fig. 10**).

To validate the results of microarray analyses, transcript levels of SGA biosynthesis genes were analyzed in *JRE4-OX* and *JRE4-EAR* lines by qRT-PCR. In leaves from wild type and *JRE4-OX* plants, MeJA-dependent inductions were clearly observed for examined SGA genes except for *acetyl-CoA C-acetyltransferase* (*ACAA*) (**Fig. 11a**). Increased expression of the genes, except *ACAA*, was observed in leaves of *JRE4-OX* lines relative to wild-type controls in both MeJA-treated and mock-treated conditions (**Fig 11a**). Consistent with the trend found in microarray analysis, degrees of up-regulation in *JRE4-OX* lines were greater for genes involved in later parts of the SGA pathway (**Fig. 11a**). I also found clear up-regulation of *SMO2* and *GAME1* but not *HMGR1* of mevalonate pathway in roots from *JRE4-OX* plants (**Fig. 12**). In transgenic hairy roots with *JRE4-EAR*, all of the examined SGA biosynthesis genes were suppressed to 28 to 70% levels relative to the controls (**Fig. 11b**).

Metabolic impact of altered *JRE4* function

To clarify how altered *JRE4* function affected SGA and related metabolisms in tomato, I next examined metabolite levels in select transgenic samples, leaves from *JRE4-OX* plants exposed to MeJA vapor (**Fig. 13a**) and hairy roots of a *JRE4-EAR* line treated with MeJA (**Fig. 13b**). SGAs, including a predominant α-tomatine, were extracted and measured using LC-qTOF-MS, whereas more hydrophilic substances, including pathway intermediates and other sterols and triperpenoids, were done using GC/MS. In a *JRE4-OX* line (line OX1), level of α-tomatine increased 2.1 folds relative to wild-type controls, while in a *JRE4-EAR* line (line #1), clear reductions of α-tomatine to 47 % level of controls was observed. Similar changes were observed for other SGAs (**Supplementary Table. S7**). Cholesterol, a sterol precursor of SGAs, increased 1.5 folds in the *JRE4-EAR* line and slightly, but not significantly, decreased in the *JRE4-OX* line. Phytosterols, campesterol and stigmasterol, did not show any significant changes except for 32 % decrease of stigmasterol in the *JRE4-OX* line. Cycloartenol and lanosterol, first tetracyclic triperpenoid intermediates, markedly decreased in the *JRE4-OX* line to 9 and 15 % levels, respectively, while 3.3-fold increase of cycloartenol and 2.9-fold of lanosterol were observed in the *JRE4-EAR* line. Triterpenoids, α-amyrin, β-amyrin, and lupeol, were increased 1.3 to 1.5 folds in the *JRE4-OX* line and decreased to 14 to 80 % levels of the controls in the *JRE4-EAR* line. Squalene decreased to 48 % level of the control in the *JRE4-OX* line and did not significantly change in the *JRE4-*

EAR line.

JRE4 activate transcription of SGA biosynthesis genes by binding to GCC box-like promoter elements

To study whether *JRE4* activates the transcriptions of SGA biosynthesis genes *in vivo* through their 5'-flanking regions, transient transactivation assays were performed in tomato fruits by adapting *Agrobacterium*-mediated infection, or agroinjection, for gene deliveries. To be expressed transiently, *β-glucuronidase* (*GUS*) reporter placed downstream of 5'-flanking regions of *sterol reductase* (*DWF5*) (-1500 to 1; counted from first ATG, only shorter version was shown in the figure) and *GAME4* (-1500 to 1) (**Fig. 14a**) and a CaMV 35S promoter-driven *JRE4* effector were co-delivered into tomato fruits by agroinjection along with a CaMV 35S promoter-driven *green fluorescent protein* (*GFP*) reference gene. The expression levels of the *GUS* reporter genes were analyzed by qRT-PCR and normalized with respect to that of the reference *GFP* gene (**Fig. 14b**). *DWF5* and *GAME4*-driven *GUS* reporter genes were clearly up-regulated 3.8 and 8.2 folds by *JRE4* overexpression, respectively, indicating the *JRE4*-mediated gene activation dependent on the included regions. I succeeded to delimitate the 1,500-bp region of *DWF5* to a relatively short region (-285 to -1) without losing reporter responsiveness (10.6 fold) (**Fig. 14b**) and basal activity, indicating the functional importance of this proximal region.

JRE4 recognizes two different but structurally related, elements, GCC box-like P box and GCC box (Shoji et al. 2013, **Supplementary Table S1**). P box and GCC box elements were computationally predicted within 1,500 bp-long 5'-flanking regions of DWF5 and GAME4 which were activated by JRE4 in transient transactivation assays; adapting cutoff score of 7.0, D5-1 (-110 to -101 with score 7.4 for P) and D5-2 (-228 to -219 with score 11.2 for P) for the shorter version of *DWF5*, and G4-1 (-248 to -239 with score 10.1 for P, including -246 to -239 hit with score 6.1 for P) in *GAME4* were predicted (**Fig. 14a**).

To clarify the requirements of the predicted elements for the *JRE4*-dependent reporter activations, nucleotides within the elements were substituted (**Fig. 14a**) and the resultant mutant reporters were subjected to transient transactivation assays (**Fig. 14b**). For *DWF5*, mutation in D5-2 completely cancelled the *JRE4*-dependent activation of the reporter driven by the short region (-285 to 1), while mutations in D5-1, which resides in

5'-untranslated region rather than promoter, did not have major influences on the inductions, indicating the requirement of functional D5-2 element but not of D5-1. Since *GAME4* activation dependent on the 1,500-bp region did not change much with mutations only in G4-1, the presence of additional elements indispensable for the promoter induction was assumed. Based on such assumption, lowering the cutoff value, I found the G4-2 element (-1166 to -1157) with a score of 6.1 for P box (**Fig. 14a**) and included in the assays. Whereas mutations at G4-2 were not much effective like those at G4-1, promoter double-mutated at both G4-1 and G4-2 did not positively respond to *JRE4* effector, pointing the involvement of functionally redundant G4-1 and G4-2 in the *GAME4* activation.

To validate *in vitro* binding of the elements to JRE4 proteins, Electrophoretic Mobility Shift Assay (EMSA) was carried out with oligonucleotide probes with sequences of the elements (**Supplementary Table S10**). When incubated with recombinant JRE4 proteins, fusion proteins of a truncated JRE4 (corresponding to 40 to 219 amino acids) with N-terminal thioredoxin and other short tags, but not with the control proteins with only tag portion, DNA-protein complexes were detected as intense shifted bands of triplet for D5-2 and G4-1 probes and as similarly patterned but fainter bands for D5-1 and G4-2 probes (**Fig. 14c**); intensities of the shifted bands were correlated with the scores of the elements. The bindings were completely abolished when mutated probes (**Fig. 14a**) were used, confirming the specific bindings of the wild-type probes.

In addition to those of *DWF5* and *GAME4*, 5'-flanking regions (-1500 to -1) of other SGA biosynthetic genes, *HMGR1*, *DWF7*, *GAME1* and *GAME6*, were placed upstream of GUS reporter gene (**Fig. 15a**). The *GUS* reporters were up-regulated by *JRE4* overexpression;12.7 fold for *HMGR1*, 8.3 fold for *DWF7*, 4.7 fold for *GAME1* and 13.2 fold for *GAME6* (**Fig. 15b**). A number of P box and GCC box elements were predicted in the flanking regions (**Fig. 15a**).

Promoter analysis of *GAME4* gene

To further study the transcriptional regulation of *GAME4* gene, GUS reporter genes driven with *GAME4* promoter (-1500 to -1) (GAME4-GUS) and its derivative mutated at JRE4-binding G4-1 and G4-2 elements (mGAME4-GUS) were introduced into tomato to generate transgenic hairy root lines (**Fig. 16a**). GUS activities of the independent lines

were measured for each construct. Though variable among the lines, the activities of *GAME4-GUS*-transformed lines were much higher than those of *mGAME4-GUS* lines, indicating the importance of the JRE4-binding elements for the basal *GAME4* promoter activity (**Fig. 16b**). To observe the tissue specific expression patterns of the *GAME4-GUS* reporters, transgenic hairy root lines were treated with DMSO or 100 μM MeJA for 24 h and were subjected to histochemical GUS staining. GUS signals were consistently observed in primordia of lateral roots and root tips in the transgenic hairy root lines and the signal intensities were more intense in samples treated with MeJA. No signals were observed in *mGAME4-GUS* lines (**Fig. 16c**). To analyze the effects of JA treatment, one line with the highest GUS activity for each reporter were chosen, and treated with MeJA before measuring GUS activities. While *GAME*4-*GUS* reporter was significantly induced 5.4 times, no significant induction was observed for the mGAME4-GUS line, suggesting the requirement of the binding elements for the JA-mediated reporter induction (**Fig. 16d**).

Putative JRE-binding elements found in proximal promoter regions of *JRE*-regulated genes

The JRE4-binding elements found in proximal promoter regions (**Fig. 14a and 15a**), prompted me to examine whether genes with such JRE-binding elements in promoter regions were enriched among a group of *JRE*-regulated genes. In addition to P box and GCC box targeted by clade 2-2b JRE4, related CS1 box, which could be recognized by clade 2-3 JREs (**Fig. 17a**), was included in the analysis; all the examined boxes are represented as weighted matrices (**Supplementary Table S1**). With the help from Dr. Kudo, we computationally searched P, CS1, or GCC boxes with a cut-off score of 7.0 in promoter regions (up to -800; counted from first ATG) of *JRE*-regulated genes (group R) (180 genes in **Supplementary Table S5**) and of *JRE*-regulated SGA biosynthesis genes, (group SR) (24 genes in **Fig. 9**), a subset of group R genes. The corresponding regions of all protein coding genes annotated in a tomato reference genome (group W) (34,725 genes) were retrieved and analyzed as controls. The genes predicted with the elements in each group were counted and significant differences of the values against group W controls were statistically determined. The 800 bp-long regions were searched with a window size of 100 bp (**Fig. 17b**). The values even for group W were slightly variable

among examined regions, possibly reflecting biased GC-contents or other genomic features in promoter regions. We detected the increases of genes with P box in -200 to -100 region for both R (2.1 fold) and SR groups (5.8 folds) and of genes with CS1 box in -300 to -1 region for group R (2.2 to 2.7 folds) and in -300 to -200 region for group SR (5.7 folds), along with other likely, but no significant, increases around the regions.

To examine whether sequences related to P, CS1, and GCC boxes could be retrieved by non-targeted ways, the 5'-flanling sequences (-1500 to -1) of group R and SR genes were subjected to MEME (Multiple Em for Motif Elicitation) analysis (Bailey et al. 2006), retrieving the sequences commonly found among the queries. Multiple sequences with similarities to the JRE-binding boxes were retrieved (**Supplementary Table S8**); match scores representing the similarities were calculated using position-specific probability matrices of P, CS1, and GCC boxes based on sequences retrieved from 5'-flanking regions (-300 to -1) of group R genes (**Supplementary Table S1**).

Discussion

Impacts of altered *JRE* function on SGA biosynthesis

Transgenic approaches, overexpression and dominant suppression (Hiratsu et al. 2003), were taken to elucidate the regulatory functions of JRE transcription factors, close cousins of alkaloid-regulating ORCA3 from *C. roseus* (van der Fits and Memelink 2001) and ERF189 from tobacco (Shoji et al. 2010), in tomato. Based on microarray analyses, I have succeeded to identify a large number of *JRE*-regulated metabolic genes involved in SGA biosynthesis, including all clustered *GAME* genes, except *GAME2*, constituting a core pathway after cholesterol (Itkin et al. 2011, Itkin et al. 2013), genes for cholesterol synthesis, including *SSR2* (Sawai et al. 2014), and flux-controlling *HMGR* (Narita and Gruissem 1989) and others involved in mevalonate pathway, demonstrating the *JRE*-mediated transcriptional regulation of the entire SGA pathway. The regulation of the upstream pathways, far up to the isoprenoid-producing branch, may be required to meet the metabolic demands for downstream SGA production without disturbing homeostasis of other metabolites derived from highly branched terpenoid pathways. Relatively small changes of essential phytosterols (Boutté and Grebe 2009), campesterol and stigmasterol, in the transgenics support the point. Although the pathway was generally coordinated, I also noticed that expression levels of genes involved in later steps, such as *GAME*s, had changed much more in the transgenic lines than the upstream genes (**Fig. 9**, **Fig. 11a**, **Fig. 12, Supplementary Table S3**, **Supplementary Table S4, Supplementary Table S5**). Such differential regulation between distinct parts of the pathway was corroborated with the changes of metabolites; changes of SGAs and upstream intermediates, cholesterol, cycloartenol, lanosterol, and squalene, showed opposite trends in both overexpression and suppression lines (**Fig. 13**), presumably reflecting imbalances between the early and late parts. To explain the metabolic changes of triterpenoids, α-amyrin, β-amyrin, and lupeol, which showed a trend opposite to cycloartenol and lanosterol (**Fig. 13**), I should scrutinize the regulation of *oxidosqualene cyclase* genes, none of which were screened by the microarray analysis.

The microarray-based approach screening genes possibly involved in a *JRE*-controlled regulon, seems a promising strategy not only to point known structural genes (**Fig. 9**) but also to mine novel metabolic and transport genes required for complex SGA

and related metabolisms. In this regard, it is quite stimulating that a bunch of uncharacterized genes annotated as glucosyltransferases, cytochrome P450 enzymes, and peptide transporters are included in the list (**Supplementary Table S5**). Similar transgenic approach combined with transcript profiling is considered applicable in other species producing SGAs to reveal the molecular bases of chemically diverse metabolites of this group (Friedman 2002, Friedman 2006, Iijima et al 2013). I believe that identification of a series of *JRE*-regulated metabolic genes also gave new insights on cholesterol formation, which have been relatively unexplored in plants compared to other organisms (Sawai et al. 2013).

To understand the regulation in the context of a greater metabolic network, I need to address the coordination of the *JRE*-mediated regulation with other mechanisms operating at transcriptional and post-transcriptional levels (Pollier et al. 2013, Van Moerkercke et al. 2015, Mertens et al. 2016). As discussed below, it is still an open question whether all parts of the pathway are similarly subjected to the transcriptional regulation by *JRE*s. It is worth to point that a gene encoding a RING-finger E3 ubiquitin ligase, a homolog of MAKIBISH1 (MKB1) from *Medicago truncatula* that controls HMGR enzyme activity (Pollier et al. 2013), was identified as a gene regulated by *JRE*s (**Supplementary Table S5**). In addition to structural genes, molecular factors important for the pathway regulation could be included in the *JRE*-regulated genes. I believe that the studies on tomato *JRE*s or *GAME9* (Cárdenas 2016, this study), along with recent studies on a group of related bHLH transcription factors (Van Moerkercke et al. 2015, Mertens et al. 2016), open a new chapter of research on the regulation of terpenoid pathways, which had been remained unexplored until recent days.

Transcriptional regulation of SGA biosynthesis genes

JRE4 directly activates the transcription of SGA genes by recognizing the GCC-like elements in their promoter regions (**Fig. 14 and 15**). All of the three elements in *DWF5* and *GAME4* validated experimentally, are present in similarly distanced proximal regions (-248 to -63) (**Fig. 14a and 15a**). This finding is corroborated with previous reports on ORCA3- and ERF189-recognizing elements present in similar regions of the targeted genes (van der Fits and Memelink 2000, Shoji et al. 2010, Shoji and Hashimoto 2011a) and also with the computational predictions of the elements in the *JRE*-regulated genes (**Fig. 17**), suggesting a common mechanistic feature among transcription factors of this

group. The promoter-based regulation of *GAME4* in a two-gene metabolic cluster (**Fig. 14**) gives insights on the regulation of such cluster, which has been proposed to occur at chromosomal level (Wegel et al. 2009).

Even though, my transient transactivation assays, computational prediction of JRE-binding sites and EMSA indicated that JRE4 could directly bind to the JRE-binding sites in the SGA promoter regions (**Fig. 14, Fig. 15, Fig. 17**). It has remained to be addressed whether all *JRE*-regulated SGA biosynthesis genes, including clustered *GAME*s, are regulated directly by *JRE*s in a similar manner as demonstrated for the genes examined. Considering a large number of regulated steps and the differential regulation observed as mentioned, I cannot exclude the possibilities of the involvement of additional mechanisms, such as indirect regulation through other transcription factors or metabolite-mediated feedback regulation. As demonstrated for regulation of nicotine biosynthesis genes by ERF189 and a JAZ-interacting bHLH transcription factor MYC2 (Shoji and Hashimoto 2011b), it is also plausible that *JRE*s regulate the downstream genes in cooperation with other transcription factors. Nevertheless, the significant enrichments of genes bearing P or CS1 box in proximal promoters in the *JRE*-regulated gene sets (**Fig. 17**) and complementary results of MEME analysis (**Supplementary Table S8**) suggest that *JRE4* and possibly other *JRE*s, including clade 2-3 members that can recognize CS1 box, participate in the transcriptional regulation of many, but not necessarily all, of the genes by binding to the predicted elements. The frequent occurrences of the JRE-binding elements in the regulated genes support a notion that genes acting downstream are recruited into regulons under the controls of transcription factors, which are more conservative in nature than binding-element nucleotides, through acquisitions of functional *cis*-elements in appropriate promoter regions (Shoji and Hashimoto 2011a, Moghe and Last 2015).

The results of the promoter-related analyses (**Fig. 14, Fig. 15, Fig. 17**, **Supplementary Table S8**), all point the possible importance of GCC-like P rather than canonical GCC box for *JRE*-mediated regulation, although all JREs presumably have substantial *in vitro* binding abilities to GCC box (**Fig. 17a**, Shoji et al. 2013). As proposed for tobacco ERF189 that exclusively target P box (Shoji et al. 2013), such preference to the GCC-like box of JREs may allow the *JRE*-controlled regulon to be free from influence by a large number of GCC box-recognizing ERFs.

Regulatory function of multiple *JRE* genes

Gene clustering is common to *JRE*s (**Fig. 5a**) and related *ERF*s (Shoji et al. 2013); in tobacco, *ERF189* is clustered with related genes on a nicotine-controlling *NIC2* locus and the *NIC2*-locus cluster was found to be deleted in a low-nicotine mutant (Shoji et al. 2010), while *ORCA3* was found to reside on a same genomic contig with a similar gene in *C. roseus* (Kellner et al. 2015). When overexpressed in a low-nicotine mutant, *ERF189* recovered nicotine accumulation to the wild-type levels, and thus *ERF189* has been considered to work most effectively as a regulator of nicotine biosynthesis among the clustered *ERF*s (Shoji et al. 2010). As the *NIC2*-locus cluster in tobacco, tomato *JRE* cluster includes members of different clades, clade 2-2b and 2-3 (**Fig. 5b**). Dominant suppression of either clade 2-2b *JRE3*, 2-2b *JRE4*, or 2-3 *JRE5* similarly repressed the expression of SGA biosynthesis genes (**Fig. 9, Fig. 10**), suggesting overlapping functions of the three *JRE*s: of course, the effects of ectopic expression of the dominant repressive forms should be interpreted carefully. As pointed above, the involvement of clade 2-3 *JRE*s in SGA regulation was also supported by the frequent occurrences of CS1 box in promoters of the regulated gene. In addition to overexpression (**Fig. 9, Fig. 11, Supplementary Table S3**) and promoter binding (**Fig. 14 and 15**) analyses, as performed for *JRE4*, knock-out or knock-down experiment for individual member is required to confirm the *in planta* contributions of each *JRE* to SGA regulation.

Expression patterns strongly support the role of *JRE4* in SGA regulation (**Fig. 6**). *JRE4* is expressed most predominantly among *JRE*s at transcript level and, as pointed in Itkin et al. (2013), its expression is clearly coordinated with SGA biosynthesis genes in various samples (**Fig. 6**). In fruits, progressive decreases of expression were evident for *JRE4* and *SMO2* and *GAME1* during green fruit stages (**Fig. 6b**), indicating that SGA formation mainly declines during the green stages rather than later color-changing stages (Iijima et al. 2009). In hairy roots, all *JRE*s were clearly induced by MeJA treatment, but their induction patterns were variable between the members (**Fig. 6c**). Again gradual induction of *JRE4* was well paralleled with those of SGA biosynthesis genes during the 24-h duration. The similar differential responses to MeJA had been demonstrated for the clustered *ERF*s in tobacco and as in the case of tomato *JRE4*, *ERF189* was gradually induced up to 24 h along with nicotine biosynthesis genes in tobacco hairy roots treated with MeJA (Shoji et al. 2010). In tobacco, though nicotine biosynthesis was not much altered with salt stress, salt-induced expression was

demonstrated for most of the clustered *ERF* genes but not *ERF189*, further supporting a role of *ERF189* in nicotine regulation (Shoji and Hashimoto 2015). To distinguish multiple *JRE*s, it is interesting to analyze how *JRE* genes respond to external elicitors other than MeJA in tomato. According to the co-expression and other evidences, I can infer that one or few select members, such as tomato *JRE4*, tobacco *ERF189*, and possibly *C. roseus ORCA3*, play a predominant role in regulation of targeted metabolic pathways in each species. Beside of these expression differences, even though the DNA-binding domains are highly conserved, the activation domain in N-termini and the portion of protein in C-termini of JREs are totally diverged. Especially clade 2-2b JRE3 and JRE4, I detected high acidic activation domain in the N-terminal and serine-rich region in C-terminal of JRE4 (**Supplementary Fig. 1**), which possibly give JRE4 a unique function. I need to further understand functional redundancy and divergence among the multiple *ERF* members to address why these *ERF* genes are maintained in a form of gene clusters during plant evolution.

SGAs as defense chemicals in tomato

Plants usually adapt particular classes of metabolites for chemical defense. A variety of compounds, including SGAs, methyl ketones, and sesquiterpenes, are considered to mediate the herbivore resistance in *Solanum* species (Antonious et al. 2014). SGAs are a group of bioactive compounds with abilities to bind to cholesterol, disrupt cellular membranes, and inhibit cholinesterases (Friedman 2015). Based on the toxic and pharmacological properties, SGAs has been proposed to be involved in plant host resistance against a wide range of biotic agents, such as bacteria, fungi, virus, insects and animals (Friedman 2002, Friedman 2006). A series of gene encoding biosynthetic enzymes and transcription factors involved in SGA biosynthesis, were induced by MeJA treatment in tomato tissues (**Fig. 6c, Fig. 11a, Fig. 12, Fig. 16**). The JA-induced expression of the genes and engagement of tomato homologs of *ORCA3* and *ERF189* in the induction underline the committed roles of SGAs and JA signaling in induced chemical defense in tomato, as in the case of nicotine in tobacco (Baldwin 1998, Shoji and Hashimoto 2013). Although induced significantly after elicitation, SGAs and nicotine are substantially produced even at basal levels and the amounts of SGA and nicotine accumulation in the tissues seem in a similar range (in orders of mg per g dry weight), indicating the similarities of the two alkaloid groups with analogous regulatory

mechanisms. As previously discussed, drastic declines of expression of SGA biosynthetic and regulatory *JRE* genes during early fruit development in tomato (**Fig. 6b**) is considered an example of developmental regulation of defense chemical pathways, which may operate more generally, ensuring the removal of toxic substances from seed-bearing mature fruits to allow seed dispersals assisted by fruit-eating herbivores.

One of the focusing points in tomato and potato breeding is the removal of toxic and anti-nutritional SGAs, which are considered not required for plant protection during normal cultivation and occasionally causing poisoning. The removal of SGAs become critically required, when considering the introduction of desirable genetic traits into cultivated species from counterparts in wild that usually produce SGAs at higher levels (Iijima et al. 2013). Identification of the transcriptional regulators of SGA pathway provides us a promising molecular tool applicable for the generation of the crops with low-SGA contents.

References

Antonious, G.F., Kamminga, K., Snyder, J.C. (2014) Wild tomato leaf extracts for spider mite and cowpea aphid control. *J. Environ. Sci. Health B*. 49: 527-531.

AbuQamar, S., Luo, H., Laluk, K., Mickelbart, M.V. and Mengiste, T. (2009) Crosstalk between biotic and abiotic stress responses in tomato is mediated by the AIM1 transcription factor. *Plant Journal* 58: 347-360.

Bailey, T.L., Williams, N., Misleh, C. and Li, W.W. (2006) MEME: discovering and analyzing DNA and protein sequence motifs. *Nucleic Acids Res*. 34: W369-373.

Baldwin, I.T. (1998) Jasmonate-induced responses are costly but benefit plants under attack in native populations. *Proc. Natl. Acad. Sci. USA*. 95: 8113-8118.

Bednarek, P. and Osbourn, A. (2009) Plant-microbe interactions: chemical diversity in plant defense. *Science* 324: 746-748.

Betz, J.M., (1999) Plant toxins. *J. AOAC Int*. 82: 781-784.

Boutté, Y. and Grebe, M. (2009) Cellular processes replying on sterol function in plants. *Curr. Opin. Plant Biol*. 12: 705-713.

Boycheva, S., Daviet, L., Wolfender, J.L. and Fitzpatrick, T.B. (2014) The rise of operon-like gene clusters in plants. *Trends in Plant Sci*. 19: 447-459.

Cárdenas, P.D., Sonawane, P.D., Heinig, U., Bocobza, S.E., Burdman, S. and Aharoni, A. (2015) The bitter side of the nightshades: genomics drives discovery in Solanaceae steroidal glycoalkaloid metabolism. *Phytochemistry* 113: 24-32.

Cárdenas, P.D., Sonawane, P.D., Pollier, J., Bossche, R.V., Dewangan, V., weithorn, E., Tal, L., Meir, S., Rogachev, I., Malitsky, S., Giri, A.P., Goossens, A., Burdman, S. and Aharoni, A. (2016) GAME9 regulates the biosynthesis of steroidal alkaloids and upstream isoprenoids in the plant mevalonate pathway. *Nat. Comm*. 7:10654.

Chowański, S., Adamski, Z., Marciniak, P., Rosiński, G., Büyükgüzel, E., Büyükgüzel, K., Falabella, P., Scrano, L., Ventrella, E., Lelario, F. and Bufo, S. A. (2016) A Review of Bioinsecticidal Activity of *Solanaceae* Alkaloids. *Toxins*. 8: 1-28.

Crooks, G.E., Hon, G., Chandonia, J.M. and Brenner, S.E. (2004) WebLogo: a sequence logo generator. *Genome Res*. 14: 1188-1190.

De Geyter, N., Gholami, A., Goormachtig, S. and Goossens, A. (2012) Transcriptional machineries in jasmonate-elicited plant secondary metabolism. *Trends Plant Sci*. 17: 349-359.

Fonseca, S., Chini, A., Hamberg, M., Adie, B., Porzel, A., Kramell, R., Miersch, O., Wasternack, C. and Solona, R. (2009) (+)-7-iso-jasmonoyl-L-isoluecine is the

endogenous bioactive jasmonate. *Nature Chem. Biol*. 5: 344-350.

Friedman, M. (2002) Tomato glycoalkaloids: role in the plant and in the diet. *J. Agric. Food Chem*. 50: 5751-5780.

Friedman, M. (2006) Potato glycoalkaloids and metabolites: roles in the plant and in the diet. *J. Agric. Food Chem*. 54: 8655-8681.

Friedman, M. (2015) Chemistry and anticarcinogenic mechanisms of glycoalkaloids produced by eggplants, potatoes, and tomatoes. *J. Agric. Food Chem*. 63: 3323-3337.

Frey, M., Schullehner, K., Dick, R., Fiesselmann, A. and Gierl, A. (2009) Benzoxazinoid biosynthesis, a model for evolution of secondary metabolic pathways in plants. *Phytochemistry*. 70: 1645-1651.

Hemsley, A., Amheim, N., Toney, M.D., Cortpassi, G. and Galas, D.J. (1989) A simple method for site-directed mutagenesis using the polymerase chain reaction. *Nucleic Acids Res*. 17: 6547-6551.

Hiratsu, K., Mitsuda, N., Matsui, K. and Ohme-Takagi, M. (2003) Dominant repression of target genes by chimeric repressors that include the EAR motif, a repression domain, in Arabidopsis. *Plant J*. 34: 733-739.

Iijima, Y., Fujiwara, Y., Tokita, T., Ikeda, T., Nohara, T., Aoki, K. and Shibata, D. (2009)

Involvement of ethylene in the accumulation of esculeoside A during fruit ripening of tomato (*Solanum lycopersicum*). *J. Agric. Food Chem.* 57: 3247-3252.

Iijima, Y., Watanabe, B., Sasaki, R., Takenaka, M., Ono, H., Sakurai, N., Umemoto, N., Suzuki, H., Shibata, D. and Aoki, K. (2013) Steroidal glycoalkaloid profiling and structures of glycoalkaloids in wild tomato fruit. *Phytochemistry* 95: 145-157.

Itkin, M., Heinig, U., Tzfadia, O., Bhide, A.J., Shinde, B., Cárdenas, P., Bocobza, S.E., Unger, T., Malitsky, S., Finkers, R., Tikunov, Y., Bovy, A., Chikate, Y., Singh, P., Rogachev, I., Beekwilder, J., Giri, A.P. and Aharoni, A. (2013) Biosynthesis of antinutritional alkaloids in Solanaceous crops is mediated by clustered genes. *Science* 341: 175-179.

Itkin, M., Rogachev, I., Alkan, N., Rosenberg, T., Malitsky, S., Masini, L., Meir, S., Iijima, Y., Aoki, K., de Vos, R., Prusky, D., Burdman, S., Beekwilder, J. and Aharoni, A. (2011) GLYCOALKALOID METABOLISM1 is required for steroidal alkaloid glycosylation and prevention of phytotoxicity in tomato. *Plant Cell* 23: 4507-4525.

Kellner, F., Kim, J., Clavijo, B.J., Hamilton, J.P., Childs, K.L., Vaillancourt, B., Cepela, J., Habermann, M., Steuernagel, B., Clissold, L., McKay, K., Buell, C. R. and O'Connor, S.E. (2015) Genome-guided investigation of plant natural product biosynthesis. *Plant J.* 82: 680-692.

Kimura, S. and Sinha, N (2008) Tomato (*Solanum lycopersicum*): a model fruit-bearing crop. *Cold Spring Harb. Protoc.* doi: 10.1101/pdb.emo105.

Mennela, G., Lo Scalzo, R., Fibiana, M., D'Alessandro, A., Francese, G., Toppino, L., Acciarri, N., de Almeida, A.E. and Rotino, G.L. (2012) Chemical and bioactive quality traits during fruit ripening in eggplant (*S. melangena* L.) and allied species. *J. Agric. Food. Chem.* 60: 11821-11831.

Mertens, J., Pollier, J., Vanden Bossche, R., Lopez-Vidriero, I., Franco-Zorrilla, J.M. and Goossens, A. (2016) The bHLH transcription factors TSAR1 and TSAR2 regulate triterpene saponin biosynthesis in *Medicago truncatula*. *Plant Physiol.* 170: 194-210.

Moghe, G.D. and Last, R.L. (2015) Something old, something new: conserved enzymes and the evolution of novelty in plant specialized metabolism. *Plant Physiol.* 169: 1512-1523.

Moriyama, S., Suemori, K., Moriwaki, J., Taura, K., Tanaka, H., Aso, M., Tanaka, M., Suemune, H., Shimohigashi, Y. and Shoyama, Y. (2001) Morphine metabolism in the opium poppy and its possible physiological function. Biochemical characterization of the morphine, bismorphine. *J. Biol. Chem.* 276: 38179-38184.

Nakano, T., Suzuki, K., Fujimura, T. and Shinshi, H. (2006) Genome-wide analysis of the ERF gene family in Arabidopsis and rice. *Plant Physiol.* 140: 411-432.

Narita, J.O. and Gruissem, W. (1989) Tomato hydroxymethylglutaryl-CoA reductase is required early in fruit development but not during ripening. *Plant Cell* 1: 181-190.

Ohyama, K., Suzuki, M., Masuda, K., Yoshida, S. and Muranaka, T. (2007) Chemical phenotypes of the hmg1 and hmg2 mutants of Arabidopsis demonstrate the in-planta role of HMG-CoA reductase in triterpene biosynthesis. *Chem. Pharm. Bull.* 55: 1518–1521.

Orzaez, D., Mirabel, S., Wieland, W.H. and Granell, A. (2006) Agroinjection of tomato fruits. A tool for rapid functional analysis of transgenes directly in fruit. *Plant Physiol*. 140: 3-11.

Osbourn, A.E. (1996) Preformed antimicrobial compounds and plant defense against fungal attack. *Plant cell* 8:1821-1831.

Osbourn, A.E. (2010a) Secondary metabolic gene clusters: evolutionary toolkits for chemical innovation. *Trends Genet*. 26: 449-457.

Osbourn, A.E. (2010b) Gene clusters for secondary metabolic pathways: an emerging theme in plant biology. *Plant Physiol*. 154: 531-535.

Ososio, S., Alba, R., Damasceno, Cynthia M.B., Lopez-Casado, G., Zanor, M.I., Tohge, T., Usadel, B., Rose, J.K.C., Fei, Z., Giovannoni, J.J. and Fernie, A.R. (2011) Systems biology of tomato fruit development: combined transcript, protein, and metabolite analysis of tomato transcription factor (nor, rin) and ethylene receptor (Nr) mutants reveals novel regulatory interactions. *Plant Physiol*. 157: 405-425.

Pauwels, L. and Goossens, A. (2011) The JAZ proteins: a crucial interface in the jasmonate signaling cascade. *Plant cell* 23: 3089-3100.

Pollier, J., Moses, T., González-Guzmán, M., De Geyter, N., Lippens, S., Vanden Bossche, R., Marhavý, P., Kremer, A., Morreel, K., Guérin, C.J., Tava, A., Oleszek, W., Thevelein, J.M., Campos, N., Goormachtig, S. and Goossens, A. (2013) The protein

quality control system manage plant defense compound synthesis. *Nature* 504: 148-152.

Ruiu, F., Picarella, M.E., Imanishi, S. and Mazzucato, A. (2015) A transcriptomic approach to identity regulatory genes involved in fruit set of wild-type and perthenocarpic tomato genotypes. *Plant Mol. Biol.* 89: 263-278.

Samach, A. and Lotan, H. (2007) The transition of flowering in tomato. *Plant Biotechnol.* 24: 71-82.

Sawai, S, Ohyama, K., Yasumoto, S., Seki, H., Sakuma, T., Yamamoto, T., Takebayashi, Y., Kojima, M., Sakakibara, H., Aoki, T., Muranaka, T., Saito, K. and Umemoto, N. (2014) Sterol side chain reductase 2 is a key enzyme in the biosynthesis of cholesterol, the common precursor for toxic steroidal glycoalkaloids in potato. *Plant Cell* 26: 3763-3774.

Seymour, G.B., Ostergaard, L., Chapman, N.H., Knapp, S. and Martin, C. (2013) Fruit development and ripening. *Annal. Rev. Plant Biol.* 64: 219-241.

Shikata, M. and Ezura, H. (2016) Micro-Tom as an alternative plant model system: mutant collection and efficient transformation. *Methods Mol. Biol.* 1363: 47-55.

Shoji, T. and Hashimoto, T. (2011a) Recruitment of a duplicated primary metabolism gene into the nicotine biosynthesis regulon in tobacco. *Plant J.* 67: 949-959.

Shoji, T. and Hashimoto, T. (2011b) Tobacco MYC2 regulates jasmonate-inducible nicotine biosynthesis genes directly and by way of the NIC2-locus ERF genes. *Plant Cell Physiol*. 52: 1117-1130.

Shoji, T. and Hashimoto, T. (2015) Stress-induced expression of NICOTINE2-locus genes and their homologs encoding Ethylene Response Factor transcription factors in tobacco. *Phytochemistry* 113: 33-40.

Shoji, T., Inai, K., Yazaki, Y., Sato, Y., Takase, H., Shitan, N., Yazaki, K., Goto, Y., Toyooka, K., Matsuoka, K. and Hashimoto, T. (2009) Multidrug and toxic compound extrusion-type transporters implicated in vacuolar sequestration of nicotine in tobacco roots. *Plant Physiol*. 149; 708-718.

Shoji, T., Kajikawa, M. and Hashimoto, T. (2010) Clustered transcription factor genes regulate nicotine biosynthesis in tobacco. *Plant Cell* 22: 3390-3409.

Shoji, T., Mishima, M. and Hashimoto, T. (2013) Divergent DNA-binding specificities of a group of ETHYLENE RESPONSE FACTOR transcription factors involved in plant defense. *Plant Physiol*. 162: 977-990.

The tomato genome consortium. (2012) The tomato genome sequence provides insights into fleshy fruit evolution. *Nature* 485: 635-641.

Turatsinze, J.V., Thomas-Collier, M., Defrance, M. and van Helden, J. (2008) Using RSAT to scan genome sequences for transcription factor binding sites and cis-regulatory modules. *Nat. Protoc*. 3: 1578–1588.

UGA Extension. (2014) Commercial tomato production handbook. http://extension.uga.edu/publications/files/pdf/B%201312_5.PDF.

USDA National Agricultural Statistics Service. (2015) 2015 California Processing tomato report. https://www.nass.usda.gov/Statistics_by_State/California/Publications/Vegetables/201508ptom.pdf.

Van der Fits, L. and Memelink, J. (2000) ORCA3, a jasmonate-responsive transcriptional regulator of plant primary and secondary metabolism. *Science* 289: 295-297.

Van Moerkercke, A., Steensma, P., Schweizer, F., Pollier, J., Gariboldi, I., Payne, R., Vanden Bossche, R., Miettinen, K., Espoz, J., Purnama, P.C., Kellner, F., Seppänen-Laakso, T., O'Connor, S.E., Rischer, H., Memelink, J. and Goossens, A. (2015) The bHLH transcription factor BIS1 controls the iridoid branch of the monoterpenoid indole alkaloid pathway in *Catharanthus roseus*. *Proc. Natl. Acad. Sci. USA* 112: 8130-8135.

Voinnet, O., Rivas, S., Mestre, P. and Baulcombe, D. (2003) An enhanced transient expression system in plants based on suppression of gene silencing by the p19 protein of tomato bushy stunt virus. *Plant J.* 33: 949-956.

Wasternack, C. and Hause, B. (2013) Jasmonates: biosynthesis, perception, signal transduction and action in plant stress response, growth and development. An update to the 2007 review in Annals of Botany. *Ann. Bot.* 111: 1021-1058.

Wegel, E., Koumproglou, R., Shaw, P. and Osbourn, A. (2009) Cell type-specific

chromatin decompensation of a metabolic gene cluster in oats. *Plant Cell* 21: 3926-3936.

Yamanaka, T., Vincken, J.P., Zuilhof, H., Legger, A., Takada, N. and Gruppen, H. (2009) C22 isomerization in α-tomatine-to-esculeoside A conversion during tomato ripening is driven by 27 hydroxylation of triterpenoidal skeleton. *J. Agric. Food Chem.* 57: 3786-3761.

Yukimune, Y., Tabata, H., higashi, Y. and Hara, Y. (1996) Methyl jasmonate-induced overproduction of paclitaxel and baccatin III in Taxus cell suspension cultures. *Nat. Biotechnol.* 14: 1129-1132.

Zhang, H., Hedhili, S., Montiel, G., Zhang, Y., Chatel, G., Pré, M., Gantet, P. and Memelink, J. (2011) The basic helix-loop-helix transcription factor CrMYC2 controls the jasmonate-responsive expression of the ORCA genes that regulate alkaloid biosynthesis in *Catharanthus roseus*. *Plant J.* 67: 61-71.

Zhang, F., Yao, J., Ke, J., Zhang, L., Lam, V.Q., Xin, X., Zhou, Z.E., Chen, J., Brunzella, J., Griffin, P.R., Zhou, M., Xu, H.E., Melcher, K and He, S.Y. (2015) Structural basis of JAZ repression of MYC transcription factors in jasmonate signaling. *Nature* 525: 269-273.

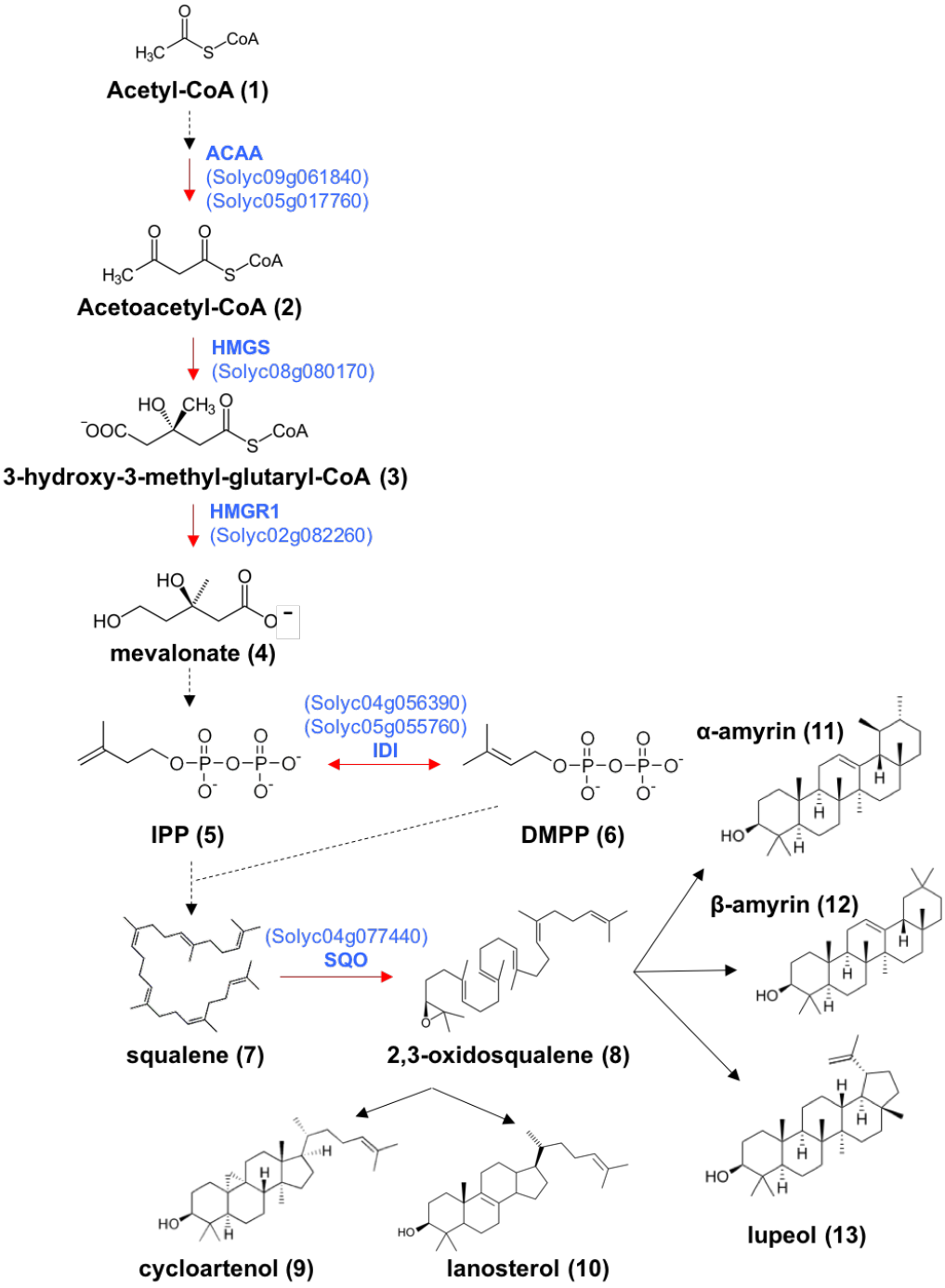

Figure 1. Aglycone formation in tomato

Isopentenyl diphosphate e.g. IPP (5), previously synthesized from the conversion of mevalonate (4), is the precursor for the formation of squalene terpenoid (7). Squalene is further oxidized by squalene monooxygenase (SQO) to form the oxidosqualene (8), an important intermediate for the biosynthesis of plant sterol like amyrins (11 and 12), lupenol (13), campesterol and stigmasterol (15 and 16), and the formation of a substrate in cholesterol biosynthesis like cycloartenol (9) and lanosterol (10). The reaction catalyzing by enzyme discovered in this study is indicated by the red arrow. Multiple enzymatic reactions involved in the formation of a chemical are indicated by dashed arrow. The gene for the enzyme is indicated by colored letter and number in the bucket represents the Gene ID in tomato genomes. ACAA, acetyl-CoA *C*-acetyltransferase; HMGS, hydroxymethylglutaryl-CoA synthase; HMGR, 3-hydroxy-3-methylglutaryl CoA reductase: IDI, isopentenyl-diphosphate D-isomerase; SQO, squalene monooxygenase. DMPP (6) is dimethylallyl diphosphate.

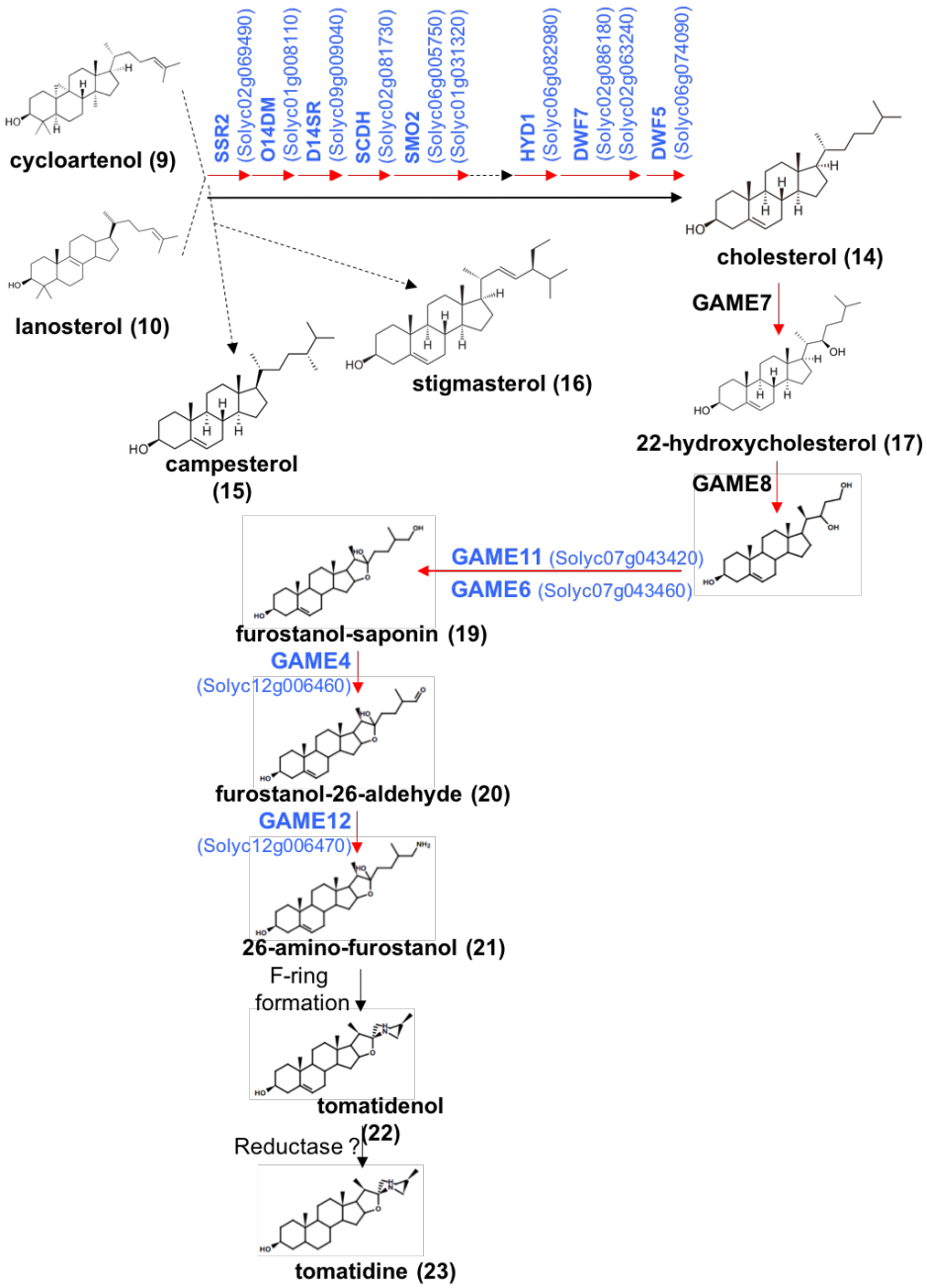

Figure 1. Aglycone formation in tomato (continued)
Cycloartenol (9) and lanosterol (10) are consumed by to synthesize the cholesterol backbone (14) of SGAs. Cycloartenol or lanosterol is converted to the cholesterol by multistep reactions of side-chain sterol reductase 2 (SSR2, obtusifoliol 14-alpha demethylase (O14DM), delta14-sterol reductase (D14SR), sterol-4a-carboxylate 3-dehydrogenase (SCDH), 3b-hydroxysteroid-D8D7-isomerase (HYD1), sterol 4a-methyl oxidase 2 SMO2, sterol C-5 desaturase (DWF7), and finally BY sterol reductase (DWF5). Plant alkyl sterols like campesterol and stigmasterol are also synthesized by multiple enzymatic reactions by using cycloartenol and lanosterol as the substrate. Metabolic enzymes encoded by the clustered *GLYCOALKALOID METABOLISM* (*GAME*) genes Then catalyze the formation of steroidal aglycones by using cholesterol as the building block. GAME7 and GAME8 subsequently hydroxylate the cholesterol at C22 and C26 to form 22,26-dihydroxycholesterol (18). However, the coupled enzymatic reaction of GAME 11 and GAME6 differently catalyzes the conversion 22,26-dihydroxycholesterol to the furostanol-saponin (19) in tomato. GAME4 oxidizes furostanol-saponin (19) to furostanol aldehyde (20) which is later transaminated by GAME12 to form amino-furostanol (21). Aminol-furostanol is cyclized to tomatidenol (22) and reduced to form the tomatidine aglycone (23). The reaction catalyzing by enzyme discovered in this study is indicated by the red arrow. Multiple enzymatic reactions involved in the formation of a chemical are indicated by dashed arrow. The gene for the enzyme is indicated by colored letter and number in the bucket represents the Gene ID in tomato genomes.

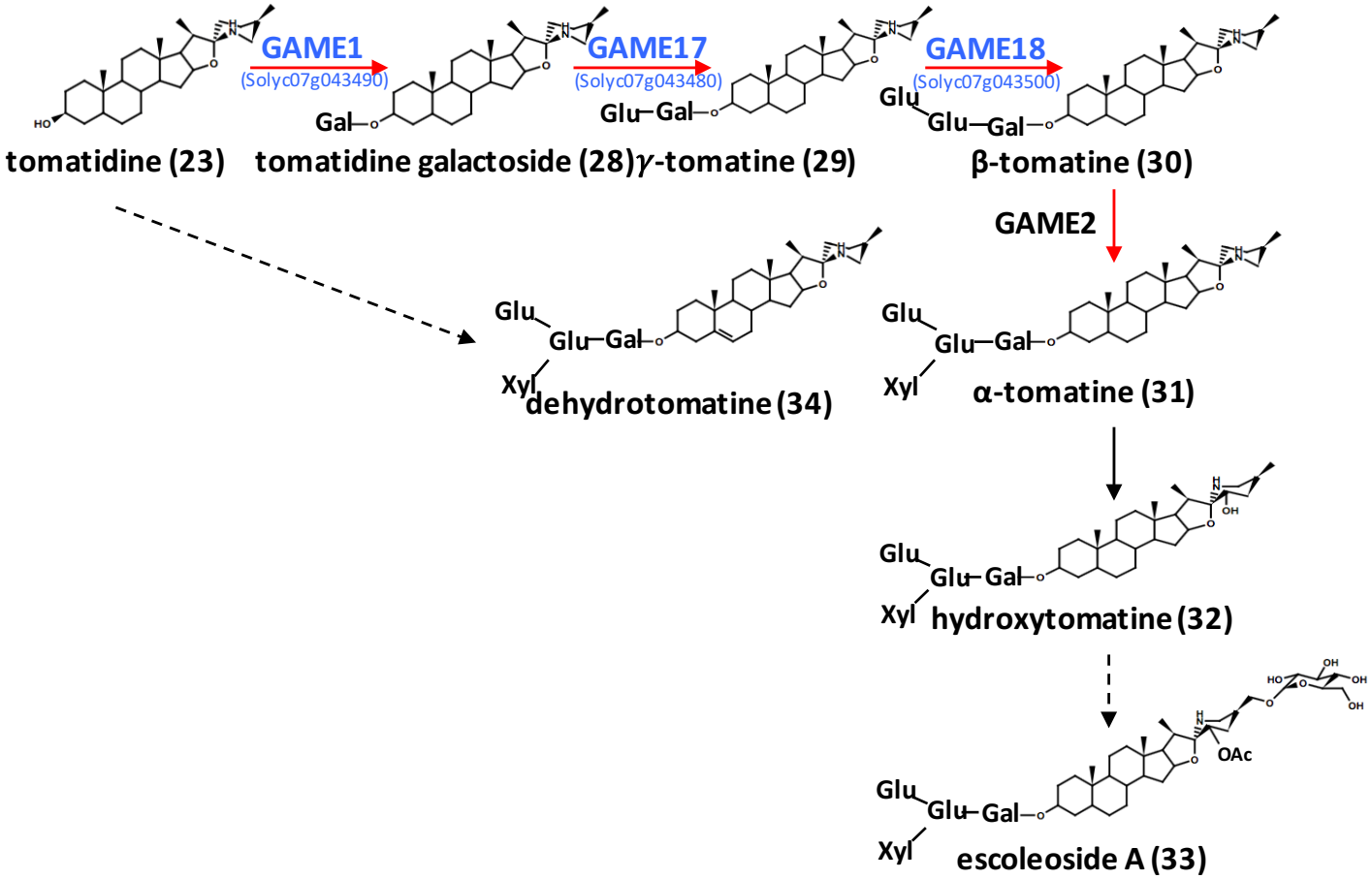

Figure 2. SGA biosyntheses from steroidal aglycones in tomato

(a) Four sugar moieties are attached to the tomatidine aglycone (23) by a series of UDP-glycosyltrasferases to form α-tomatine (31) in tomato. GAME1 (a UDP-galactosyltransferase) attaches galactoside sugar moiety to tomatidine to form tomatidine galactoside (28). GAME17 and GAME18 with their glucosyltransferase activities forms γ-tomatine (29) and β-tomatine (30), respectively. The finally step of α-tomatine (31) formation is catalyzed by GAME2 (xylosyltransferease). However, the toxic α-tomatine is further catabolized into least toxicity and human health benefit compound lycoesculeosides, e.g. esculeoside A (33), by C22 isomerase and a glycosyltransferase. The reaction that catalyzed by enzyme discovered in this study is indicated by the red arrow. Multiple enzymatic reactions involved in the formation of a chemical are indicated by dashed arrow. The gene for the enzyme is indicated by colored letter and number in the bucket represents the Gene ID in tomato genomes. GAME, *GLYCOALKALOID METABOLISM* gene.

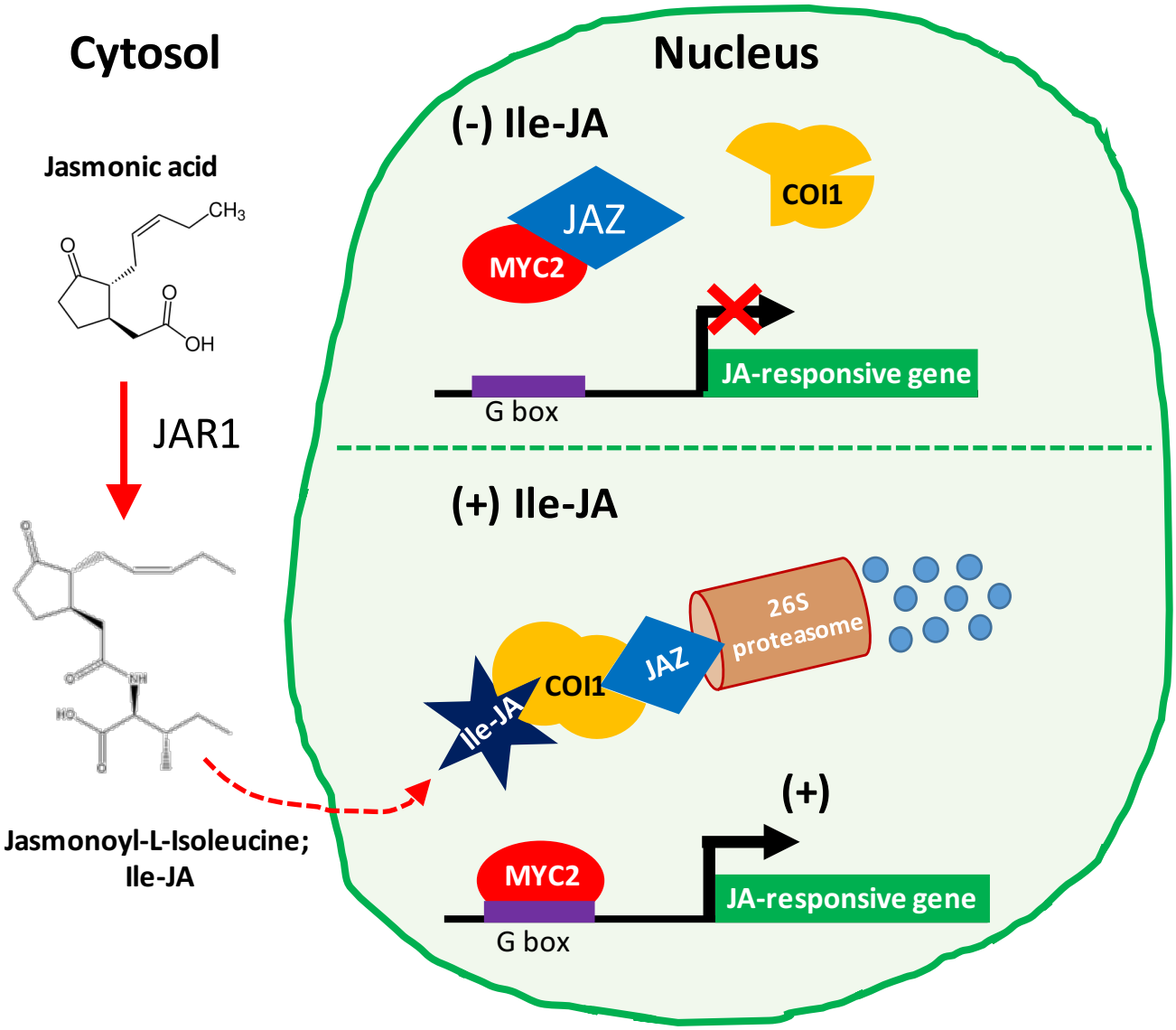

Figure 3. General JA-mediated transcriptional activation in plant
Jasmonic acid, priory synthesized in the cytoplasm of plant cell, is converted into more stability, mobile and functional effective form, jasmonoyl-L-isoleucine; Ile-JA, by JAR1 (JASMONATE RESISTANT 1 protein). During plant developmental processes and environmental stress responses, the level of Ile-JA rises due to the activation of JA biosynthesis pathway. Ile-JA can be recognized by COI1 and causes COI1-conformational change. This leads to the substantial recognition of COI1 with transcription factor - interacting JAZ protein (e.g. beta-helix-loop-helix (bHLH)-family MYC2) and the degradation of JAZ repressor protein by 26S proteasome complex. MYC2 transcription factor, released from JAZ repressor protein, then activates the transcription of JA-responsive genes by recognizing with G-box consensus sequence 5'-CTCGAG-3' in the promoters. COI1, CORONATINE INSENSITIVE 1 protein; JAZ, JASMONATE ZIM-DOMAIN protein; MYC2, beta-Helix-Loop-Helix family MYC2 transcription factor;

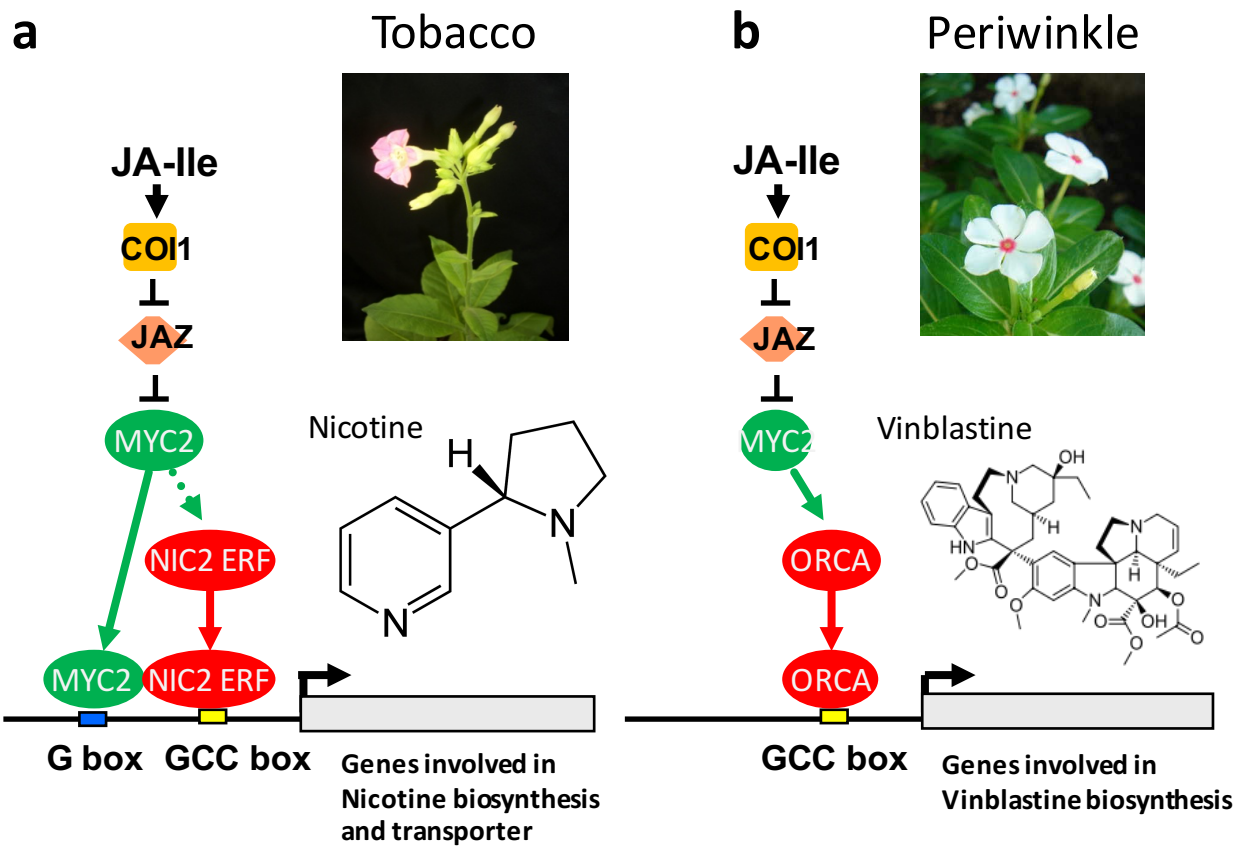

Figure 4. Regulation of alkaloid biosynthesis in tobacco and periwinkle (*Catharanthus roseus*) by JA signaling cascade

JA-induced formation of ornithine-derived nicotine is regulated by ERF189 in tobacco (a) whereas JA-inducible ORCA3 controls the JA-dependent production of monoterpenoid indole alkaloid vinblastine (b) by recognizing specific GCC box-like elements found in promoters of the targeted. JA-inducible expression of *ORCA3* and *ERF189* is regulated by a basic helix-loop-helix (bHLH)-family MYC2 transcription factor which is involved in the regulation of a wide range of JA downstream responses. COI1; Coronatine-Insensitive 1 protein, JAZ; Jasmonate ZIM-domain protein. JA-Ile; Isoleucine-conjugated jasmonate.

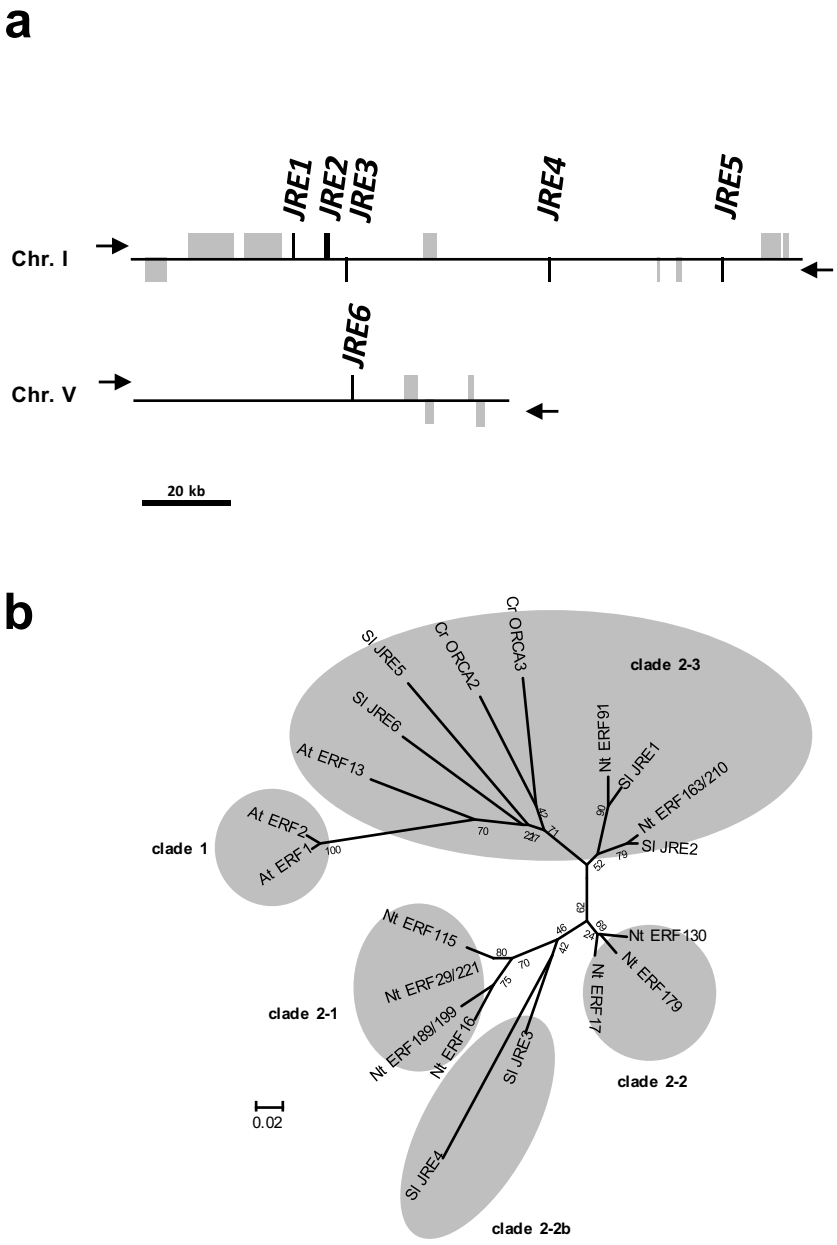

Figure 5. **Tomato *JRE* genes**

(a) Schematic presentation of a gene cluster of five *JRE* genes on chromosome I and *JRE6* gene on chromosome V. *JRE* and other genes are represented as black and gray boxes. Strands on which each gene resides are indicated with arrowheads.

(b) A phylogenetic tree of tomato JREs and related ERF proteins from Arabidopsis, *Catharanthus roseus*, and tobacco. Two clade 1 ERF genes of group IXa, AtERF1 and AtERF2 are included as genes of an outer group. Amino acid sequences of a DNA-binding domain were aligned with ClustalW (Thompson et al. 1994). An unrooted phylogenetic tree was constructed using the neighbor-joining algorithm with MEGA6 (Tamura et al. 2013). Bootstrap values are indicated at branch nodes, and the scale bar indicates the number of amino acid substitution per site. According to species, names are denoted with prefixes. At, Arabidopsis; Cr, *C. roseus*; Nt, tobacco; Sl, tomato.

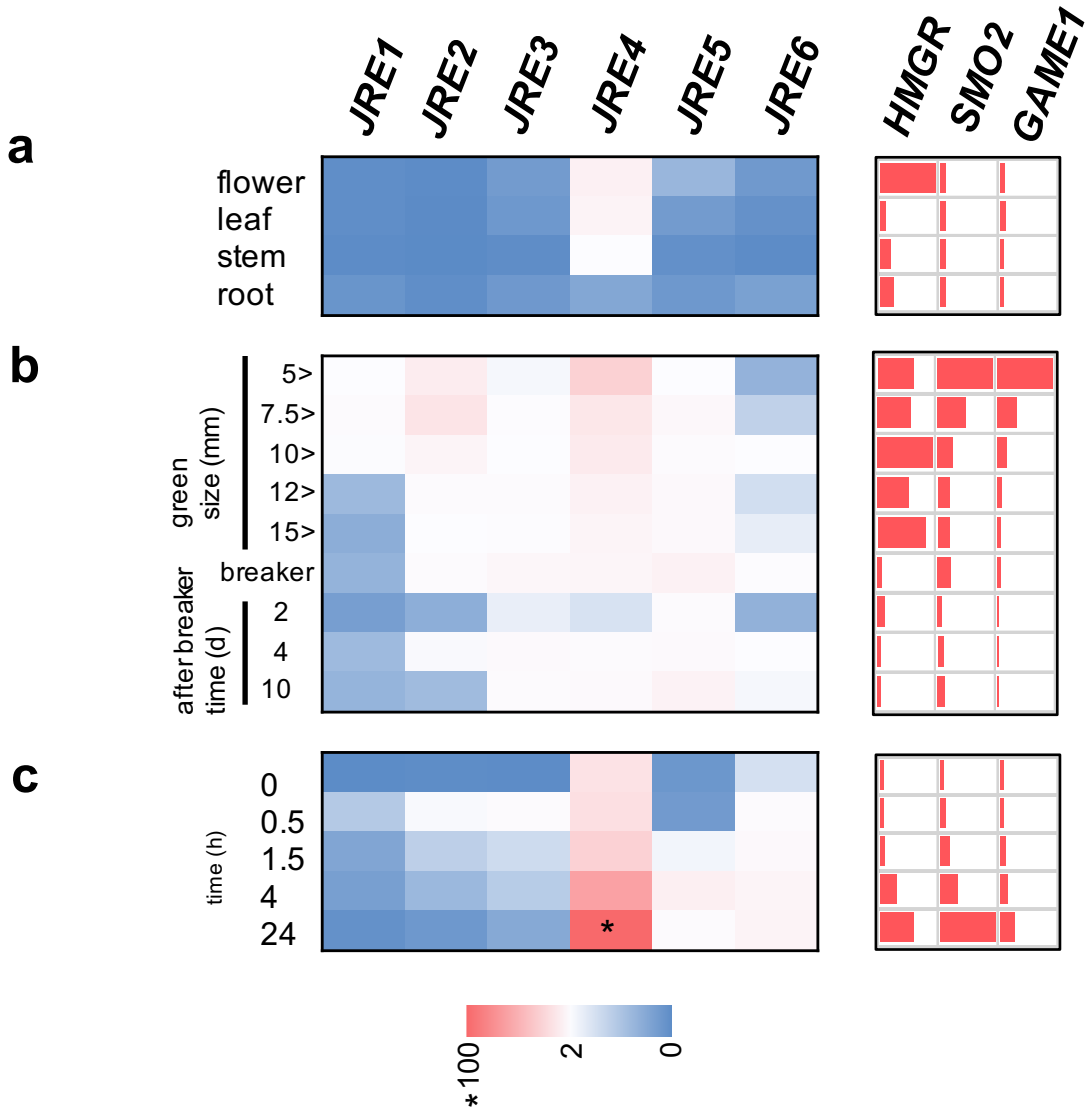

Figure 6. Expression patterns of *JRE* genes in tomato

Tomato organs (a), flower, leaf, stem, and root, and fruits of different ripening stages (b) were examined. Wild-type tomato hairy roots were treated by 100mM MeJA for 0, 0.5, 1.5, 4, and 24h (c). Transcript levels were analyzed by qRT-PCR. Heat maps are drawn using average values of three biological replicates. For *JRE*s, values are calculated relative to those of *EF1α*, and are shown as relative levels against the value (set to 100, marked with asterisk) of *JRE4* in hairy roots treated by MeJA for 24 h. For *HMGR1*, *SMO1*, and *GAME1*, levels are shown relative to those in leaf, in fruit at stages with highest expression for each, or in hairy roots at 0 h

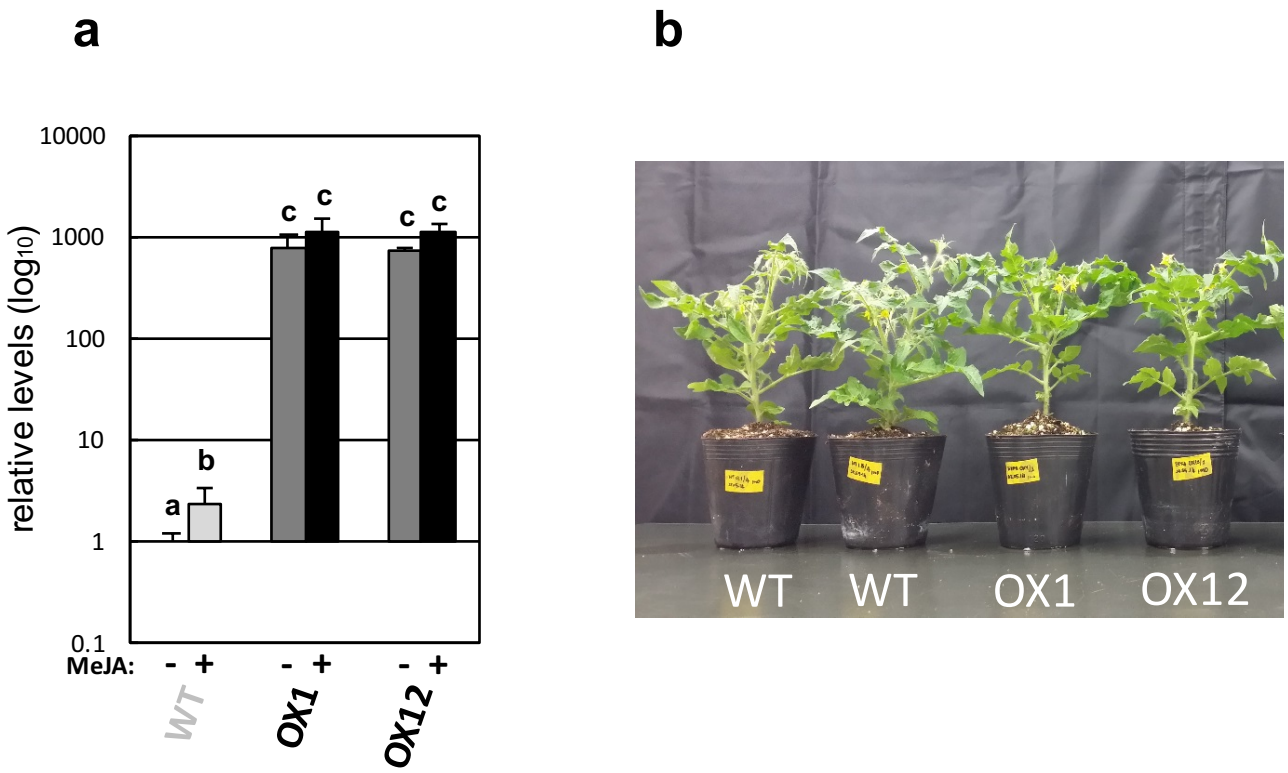

Figure 7. Transgenic JRE4-OX tomato plants
(a) Expression levels of *JRE4* in leaves analyzed by qRT-PCR. Leaves were treated with 100 mM MeJA (+) or mock-treated (-) for 24 h. The error bars indicate the SD for three biological replicates. Significant differences at $P<0.05$ were determined by one-way analysis of variance (ANOVA) followed by the Tukey-Kramer test and are indicated by different letters.
(b) Images of 7-week-old plants of wild-type (WT) and JRE4-OX lines (OX1 and OX12).

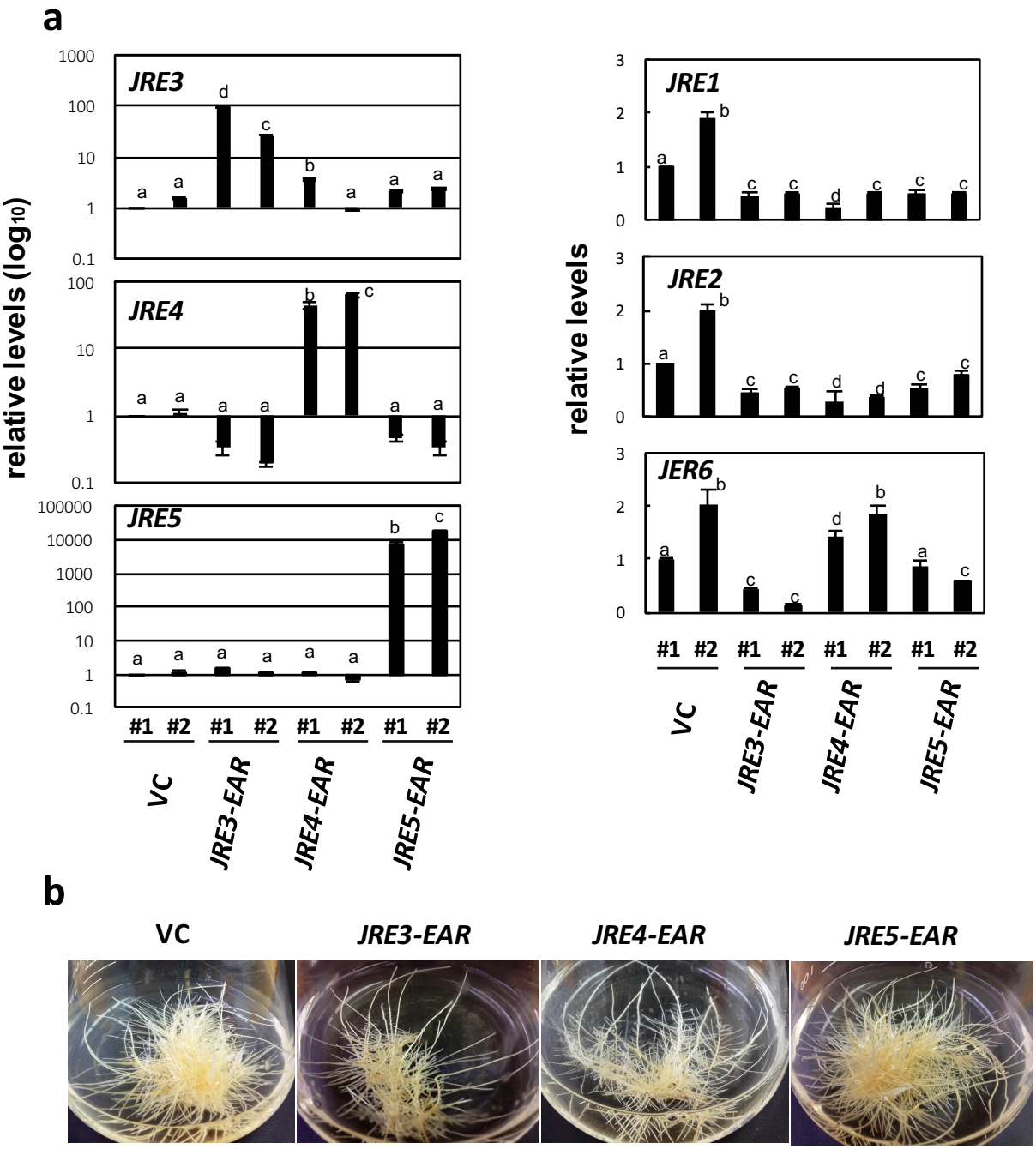

Figure 8. Expression levels of *JRE* genes in transgenic JRE-EAR hairy root lines

(a) The hairy root lines were treated by 100 mM MeJA for 24 h. Expression levels were analyzed by qRT-PCR and are shown relative to levels in a vector control line VC #1 for each *JRE* gene. Significant differences at $P<0.05$ among the lines were determined by one-way analysis of variance (ANOVA) followed by the Tukey-Kramer test and are indicated by different letters.

(b) Characteristics of transgenic JRE-EAR and vector control (VC) hairy root lines cultured in liquid media for 7 days.

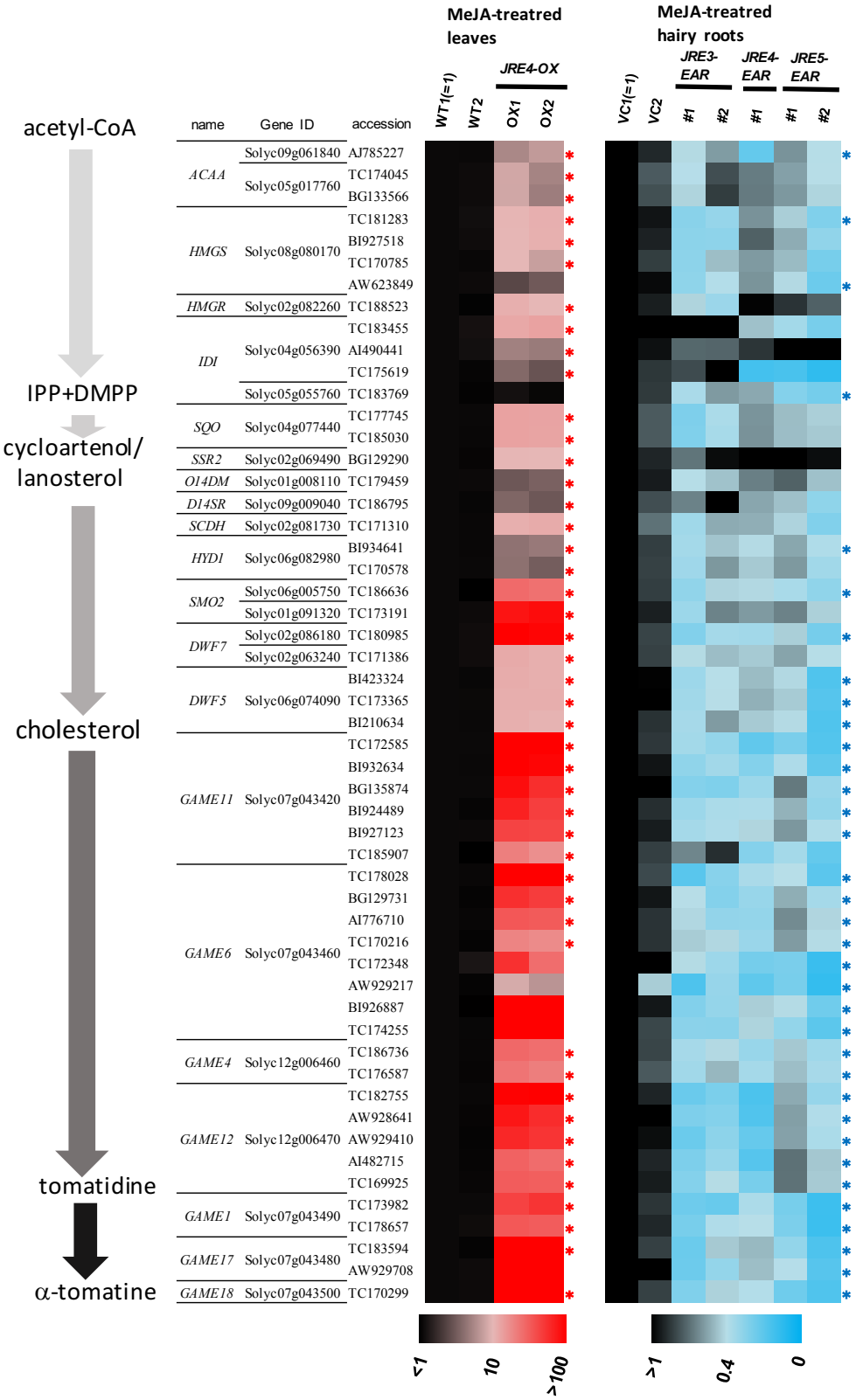
acetyl-CoA
IPP+DMPP
cycloartenol/
lanosterol
cholesterol
tomatidine
α-tomatine
name
Gene ID
accession
MeJA-treatred
leaves
WT1(=1)
WT2
JRE4-OX
OX1
OX2
MeJA-treatred
hairy roots
VC1(=1)
VC2
JRE3-
EAR
JRE4-
EAR
JRE5-
EAR
#1
#2
<1
10
>100
>1
0.4
0

Figure 9. *JRE*-regulated SGA biosynthesis genes identified by cDNA microarray analysis
Probes corresponding to SGA biosynthesis genes up-regulated by *JRE4* overexpression or down-regulated by dominant suppression of *JRE*s are shown. Signal intensities relative to those of one of the controls (WT1 or VC1) are represented as heat maps. Probes with R_{ox}>5 and Q<0.85 are marked with red and blue asterisks, respectively. Schematic view of SGA biosynthesis pathway is on the left. ACAA, acetyl-CoA *C*-acetyltransferase; HMGS, hydroxymethylglutaryl-CoA synthase; HMGR, 3-hydroxy-3-methylglutaryl CoA reductase: IDI, isopentenyl-diphosphate D-isomerase; SQO, squalene monooxygenase; SSR2, sterol side chain reductase 2; O14DM, obtsuifoliol 14a-demethylase; D14SR, D14-sterol reductase; SCDH, sterol-4a-carboxylate 3-dehydrogenase; HYD1, 3b-hydroxysteroid-D8D7-isomerase; SMO2, sterol 4a-methyl oxidase 2; DWF7, sterol C-5 desaturase; DWF5, sterol reductase; GAME, glycoalkaloid metabolism; IPP, isopentenyl pyrophosphate; DMPP, dimethylallyl pyrophosphate.

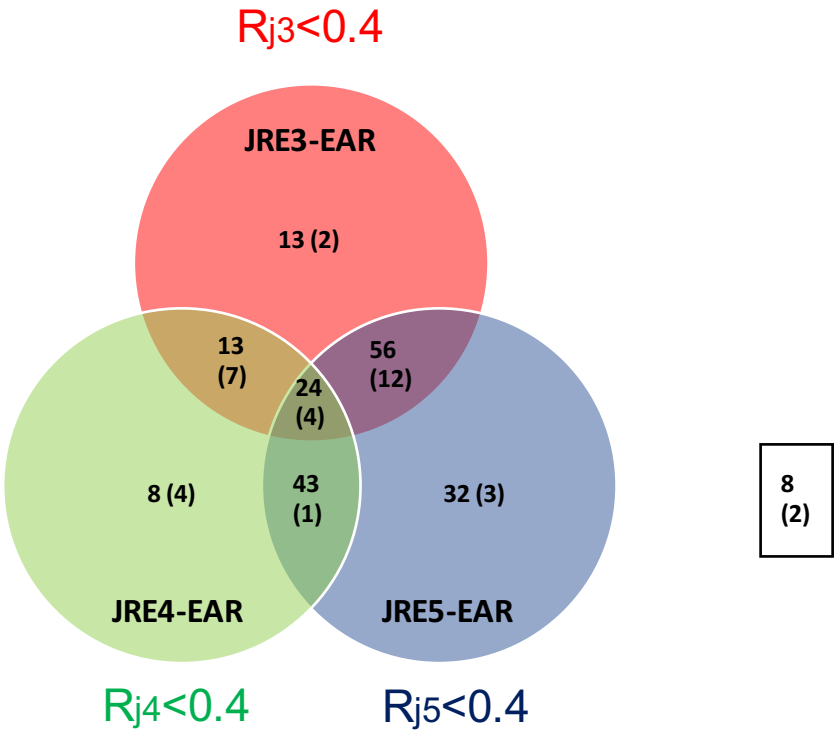

Figure 10. Venn diagram showing numbers of the probes down-regulated by each *JRE-EAR*.
All probes with Q<0.85 are divided according to Rj values. Eight probes without Rj values higher than 0.4 are not included in the diagram but in a square. Numbers of SGA biosynthesis gene in each group are bracketed. (Rj3<0.4 for JRE3-EAR, Rj4<0.4 for JRE4-EAR, Rj5<0.4 for JRE5-EAR)

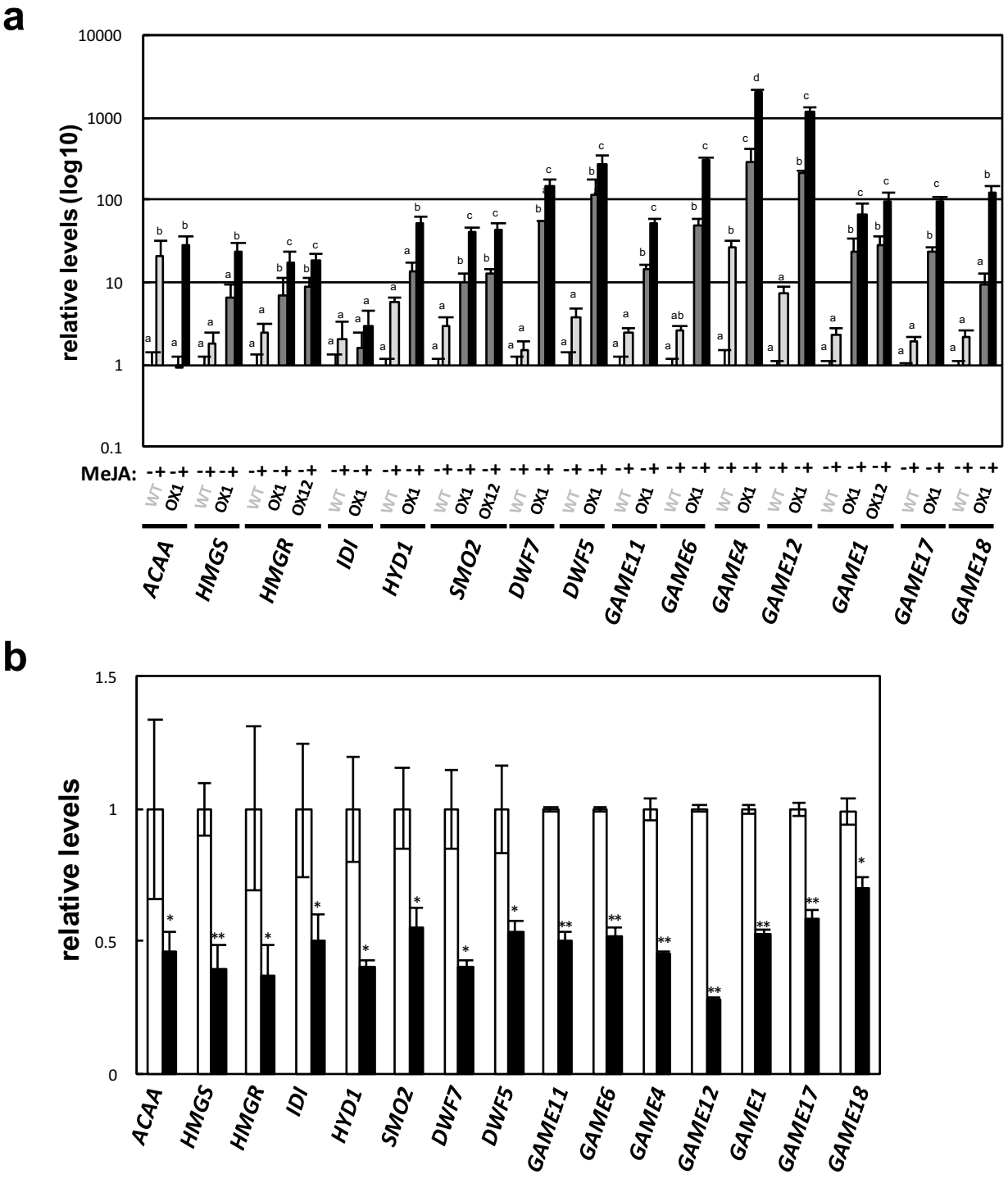

Figure 11. Expression levels of SGA biosynthesis genes in transgenic tomato *JRE4-OX* plant and *JRE4-EAR* hairy root lines

Transcript levels were analyzed by qRT-PCR. The error bars indicate the SD for three biological replicates. Levels are shown relative to the controls. See legend of **Fig. 9** for abbreviations of gene names.

(a) Levels in leaves from *JRE4-OX* plant lines treated with MeJA for 24 h.

(b) Levels in hairy roots of *JRE4-EAR* (line #1) treated with MeJA for 24 h.

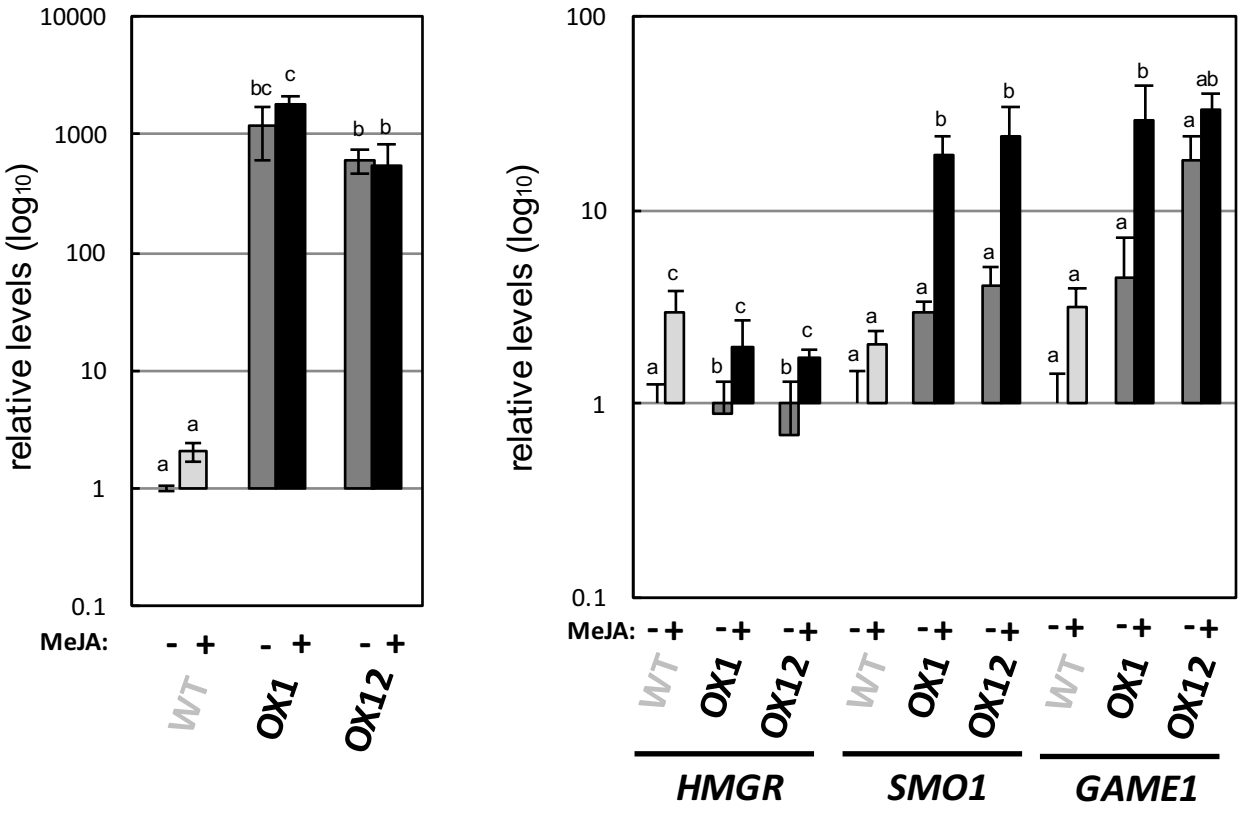

Figure 12. Gene expression in roots of transgenic *JRE4-OX* tomato plants
Transcript levels were analyzed by qRT-PCR. The error bars indicate the SD for three biological replicates. Roots were immersed in 100mM MeJA for 24h for the treatment. Significant differences at $P<0.05$ among the samples for each gene were determined by one-way analysis of variance (ANOVA) followed by the Tukey-Kramer test and are indicated by different letters. (a) Levels of *JRE4*. (b) Levels of *HMGR1*, *SMO1*, and *GAME1*. HMGR, 3-hydroxy-3-methylglutaryl CoA reductase; SMO2, sterol 4a-methyl oxidase; GAME, glycoalkaloid metabolism.

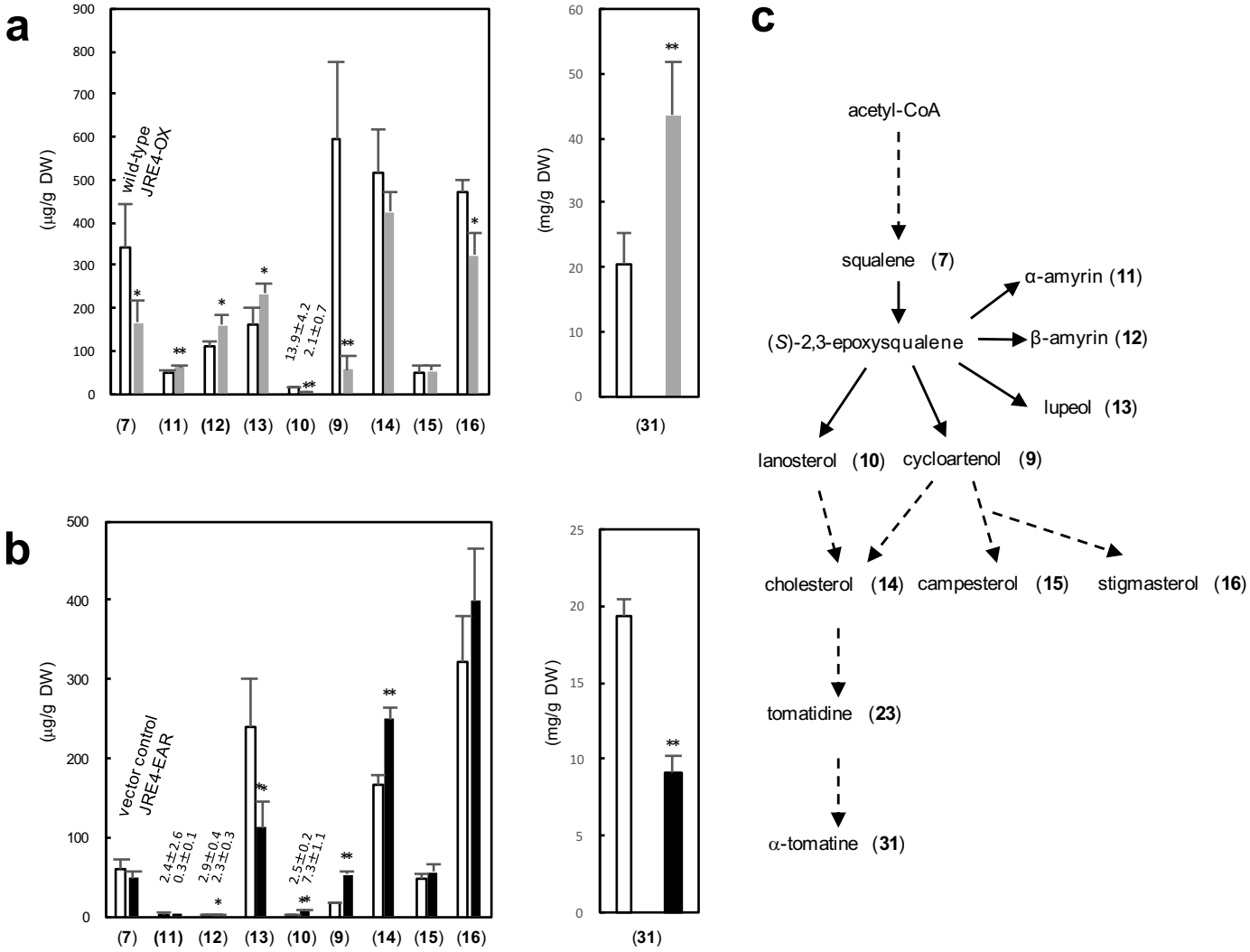

Figure 13. Metabolite levels in transgenic tomato *JRE4-OX* plant and *JRE4-EAR* hairy root lines
Metabolite levels were analyzed by LC-QTOF-MS for a-tomatine and by GC/MS for others. The error bars represent SD from four (for a) or five (for b) biological replicates.
(a) Levels in leaves from *JRE4-OX* plants (line OX1) exposed to MeJA vapor for 4 d.
(b) Levels in hairy roots of *JRE4-EAR* (line #1) treated with MeJA for 4 d.
(c) Metabolites are schematically indicated in SGA biosynthesis pathway. Number in bucket relates to the chemical structure in **Fig. 1 and 2**.

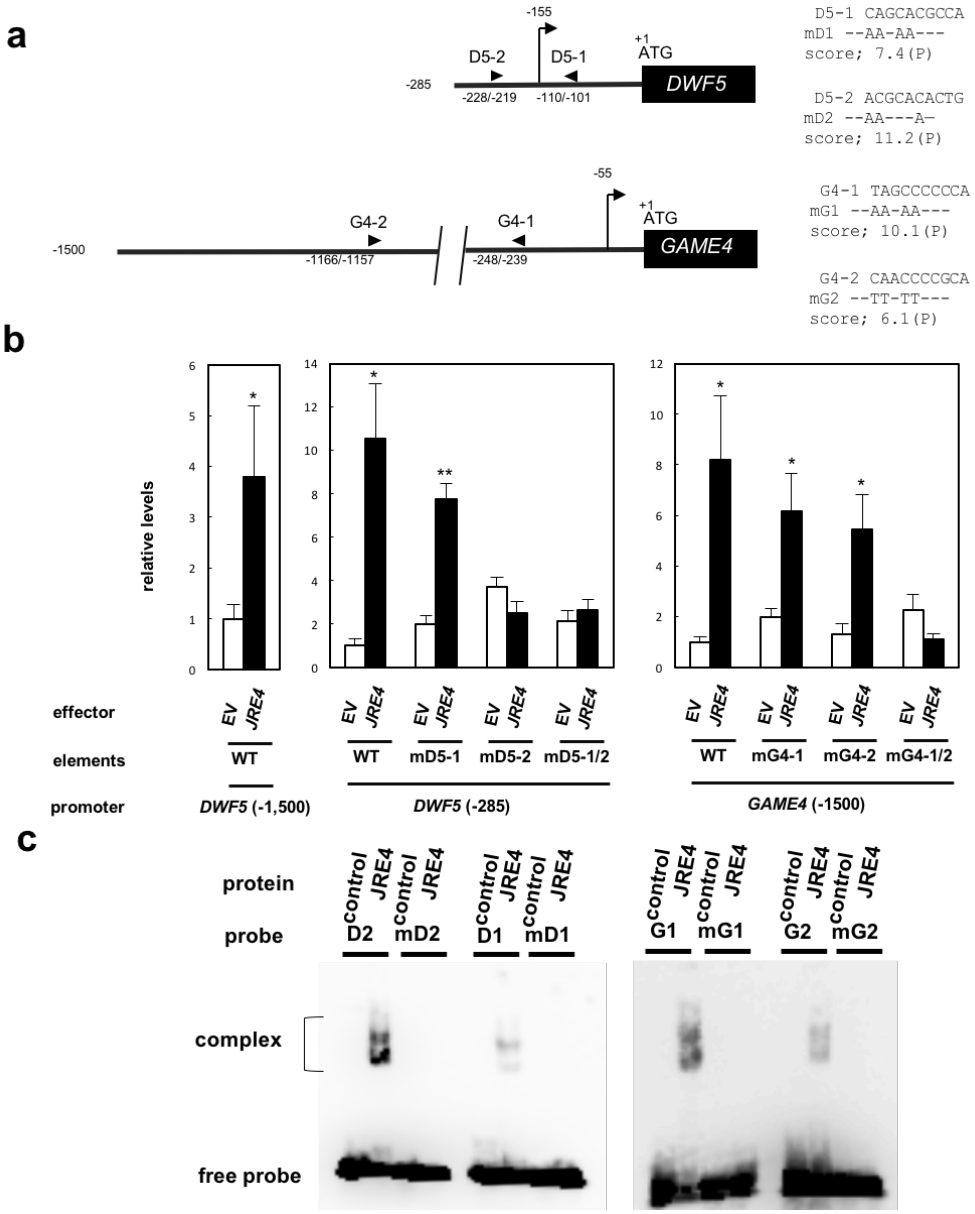

Figure 14. JRE4-mediated activation of *DWF5* and *GAME4* dependent on JRE-binding elements found in the promoter regions

(a) Schematic representation of 5'-flanking regions of *DWF5* and *GAME4*. The positions of JRE-binding elements (arrowheads) and transcriptional start sites (arrows with vertical lines) are shown. On the right, nucleotide sequences of the elements are shown, while only the substituted nucleotides are indicated in mutated versions.

(b) Transient transactivation assays in tomato fruits. *GUS* reporter gene fused with 5'-flanking regions of *DWF5* (-1,500 to 1 or -285 to 1; counted from first ATG) and *GAME4* (-1,500 to 1) or their mutated versions, were delivered into tomato fruits by agroinjection with *JRE4* effector plasmid or empty vector (EV) and *GFP* reference plasmid. Expression levels of *GUS* reporter gene are divided with those of *GFP* reference gene, and are shown as relative values against the values of each wild-type reporter with EV. The bars indicate SD from four independent experiments. Significant differences between EV and *JRE4* effector for each reporter were determined by Student's *t*-test: **P*<0.05; ***P*<0.01.

(c) *in vitro* binding of recombinant JRE4 to the predicted elements. Probes were incubated with proteins from empty vector control or recombinant JRE4.

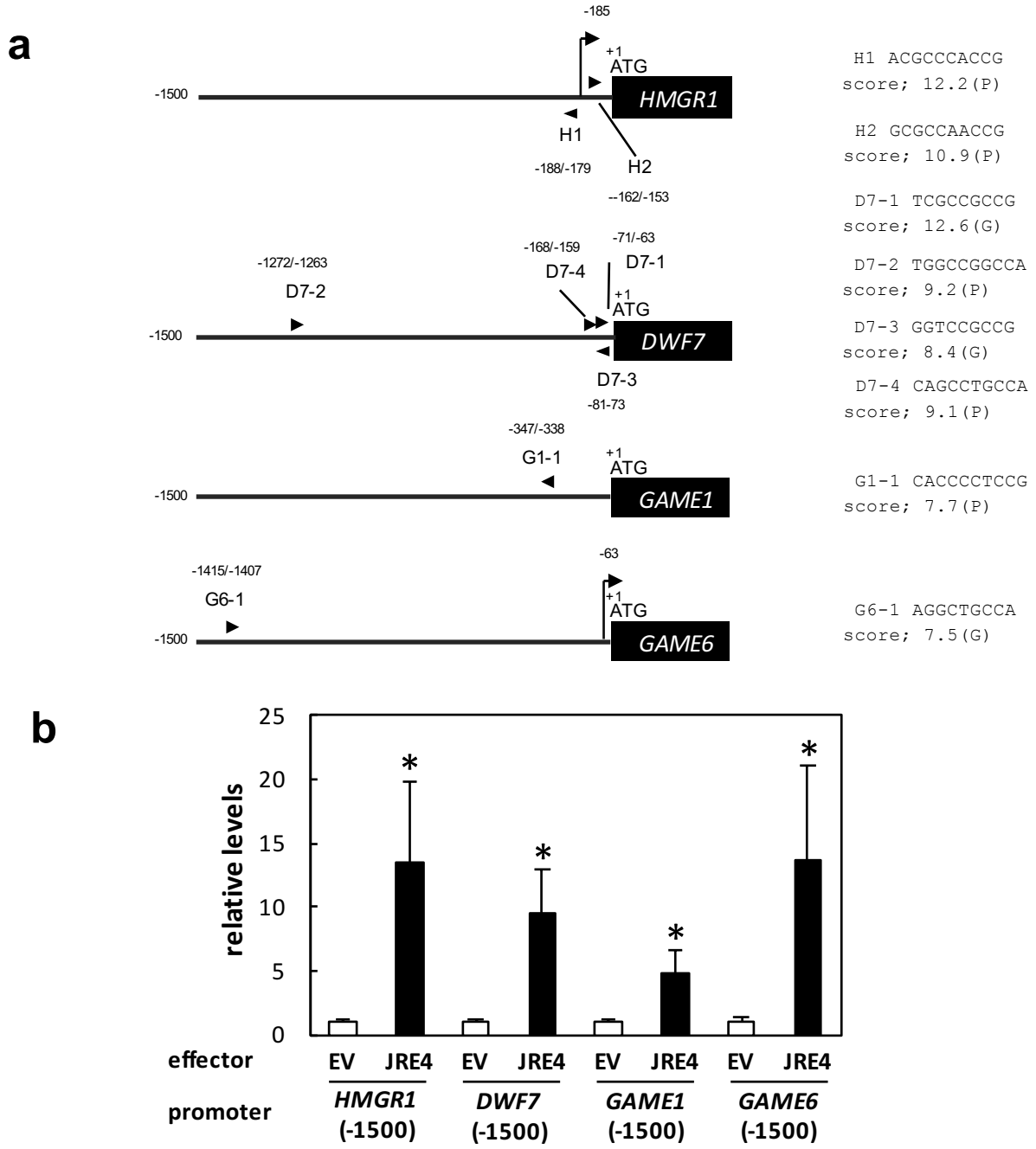

Figure 15. JRE4-mediated activation of *SGA* genes

(a) Schematic representation of 5'-flanking regions of *HMGR1*, *DWF7*, *GAME1*, and *GAME6*. The positions of JRE-binding elements (arrowheads) and transcriptional start sites (arrows with vertical lines) are shown. On the right, nucleotide sequences of the elements are shown and the RSAT PWM score for each predicted JRE4-binding elements are represented.

(b) Transient transactivation assays in tomato fruits. *GUS* reporter gene fused with 5'-flanking regions of *HMGR1*, *DWF7*, *GAME1*, *GAME6* (-1500 counted from first ATG), were delivered into tomato fruits by agroinjection with *JRE4* effector plasmid or empty vector (EV) and *GFP* reference plasmid. Expression levels of *GUS* reporter gene are divided with those of *GFP* reference gene, and are shown as relative values against the values of each wild-type reporter with EV. The bars indicate SD from four independent experiments. Significant differences between EV and *JRE4* effector for each reporter were determined by Student's *t*-test: **P*<0.05.

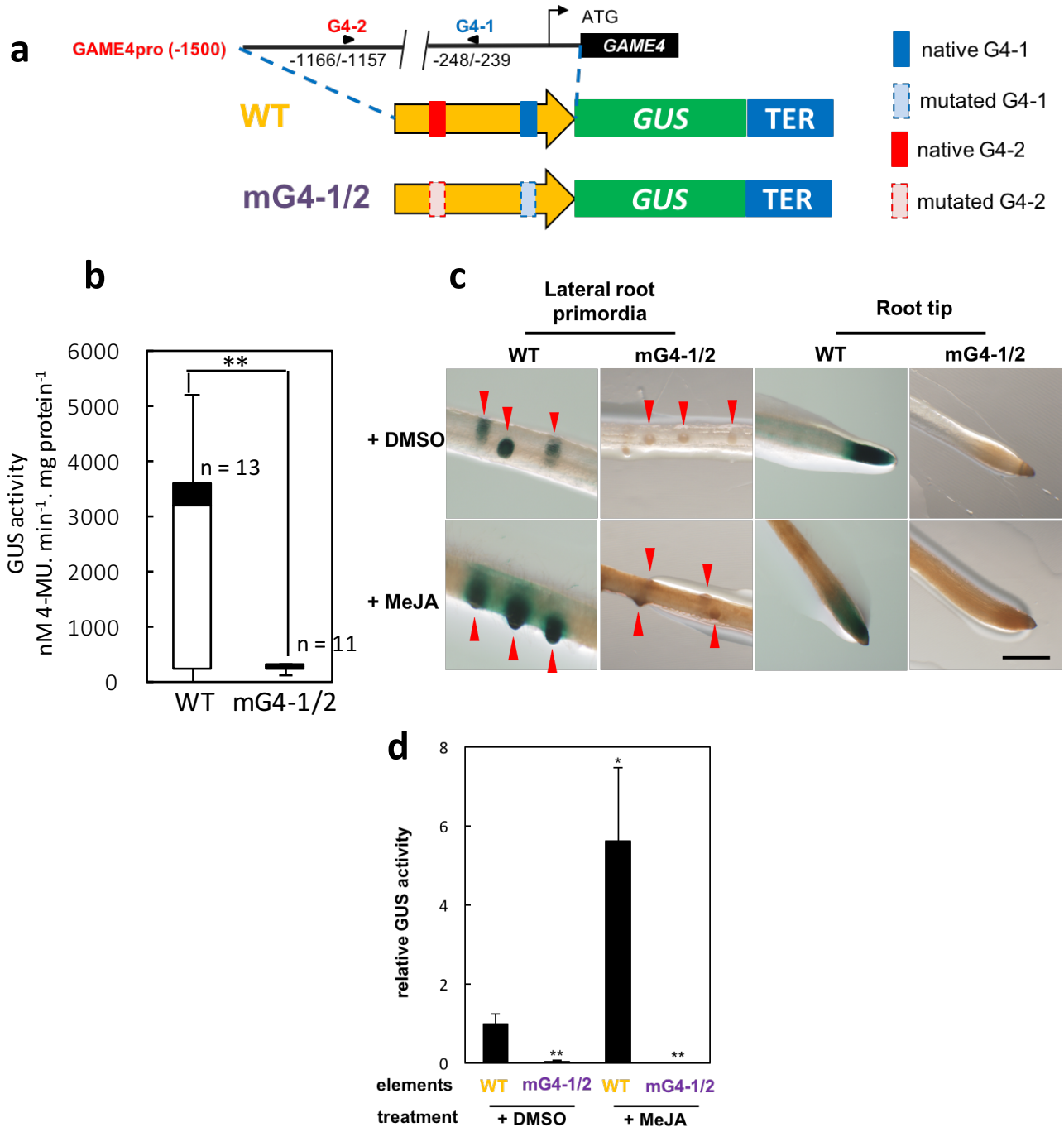

Figure 16. Activation and localization of 5'-flanking regions-driven GUS reporter in transgenic tomato hairy root lines

(a) GAME4-GUS and mGAME4-GUS expression cassettes.

(b) Promoter activity in more than 10 transgenic lines for each construct was determined by GUS activity assay. White- and black-column represent the GUS activity in individual that is distributed in Quartile 1 (25%) and Quartile 3 (75%), respectively. Error bars represent the minimum- and maximum GUS activity in the lowest- and highest-GUS expressers.

(c) Localization of GUS reporter at lateral root primordia and root tip in transgenic GAME4-GUS reporter after MeJA and DMSO treatment. Red arrows indicate the lateral root primordia stained with X-gluc solution. Bar = 1 mm.

(d) Relative GUS activity in GAME4-GUS transgenic lines after MeJA treatment. Gus activity in GAME4-GUS (WT) and mGAME4-GUS (mG4-1/2) transgenic hairy root lines treated with MeJA were compared with that in GAME4-GUS reporter transgenic line treated with DMSO (set as 1). The bars indicate SD from three independent experiments. Significant differences between MeJA-treated and DMSO-treated samples were determined by Student's *t*-test: **P*<0.05, ***P*<0.01).

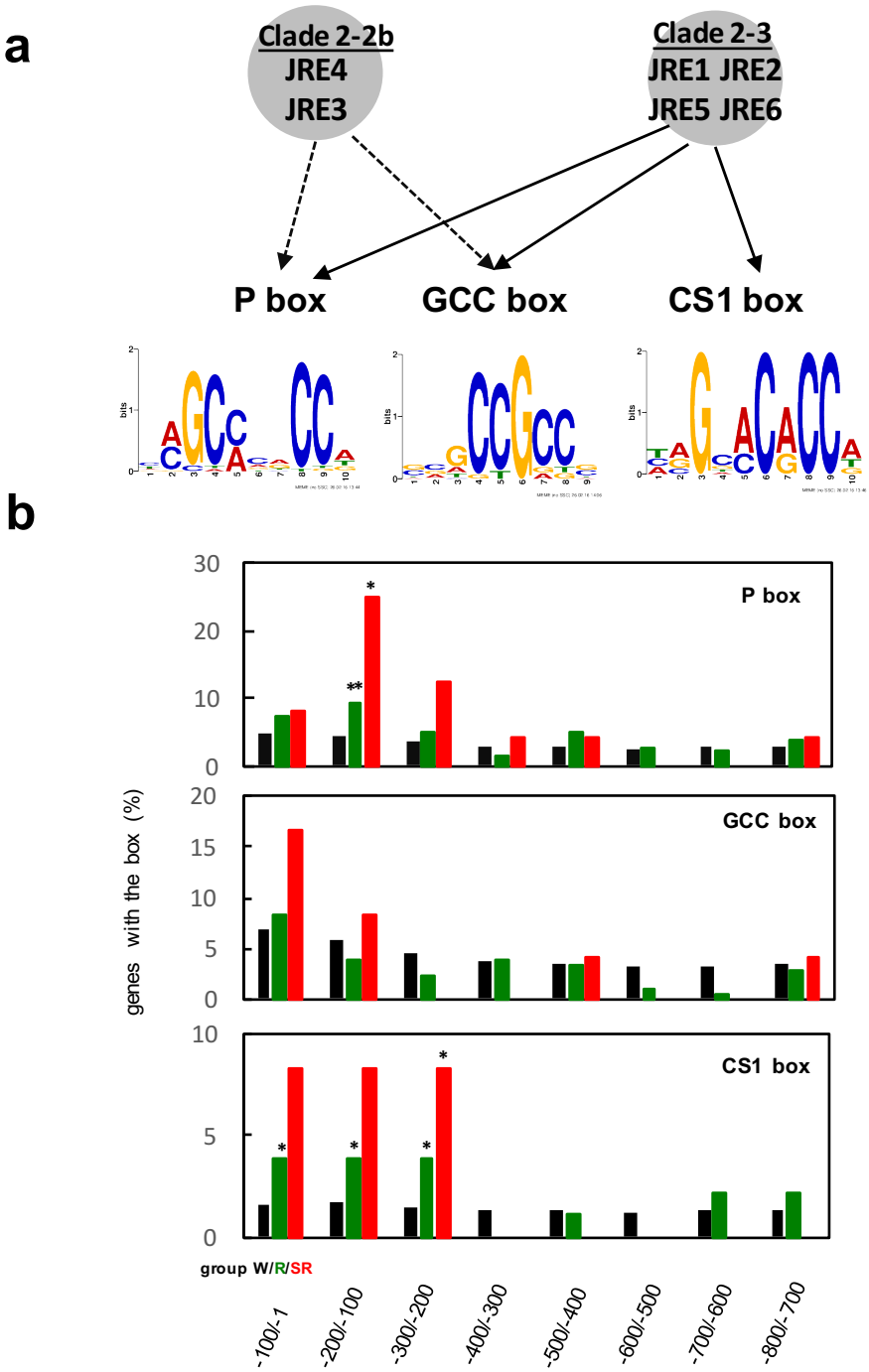

Figure 17. Computational prediction of putative JRE-binding elements in promoter regions of genes regulated by *JRE*s

(a) Presumed binding elements of JREs. The binding of JRE4 to P and GCC boxes was experimentally validated (Shoji et al. 2013), while those for other JREs are based on the assumption that binding specificities are common among the clade members. Sequence logos representing P , CS1 , and GCC boxes were generated by WebLogo (Crooks et al. 2004) based on position-specific probability matrices, which were determined using the sequences predicted in the 5'-flanking regions (-300 to -1) of group R genes.

(b) Genes predicted with JRE-binding elements (scores>7.0) for indicated region in group W (black), R (light blue) and SR (blue). The genes of group R (180 *JRE*-regulated genes) and of group SR (*JRE*-regulated 24 SGA biosynthesis genes) are given in **Supplementary Table S3** and **Fig. 9**, respectively. Significant differences of values (shown in %) against those for group W (all 34,725 protein coding genes in tomato genome) were determined by one-sided Fisher's exact test; **P*<0.05, ***P*<0.01.

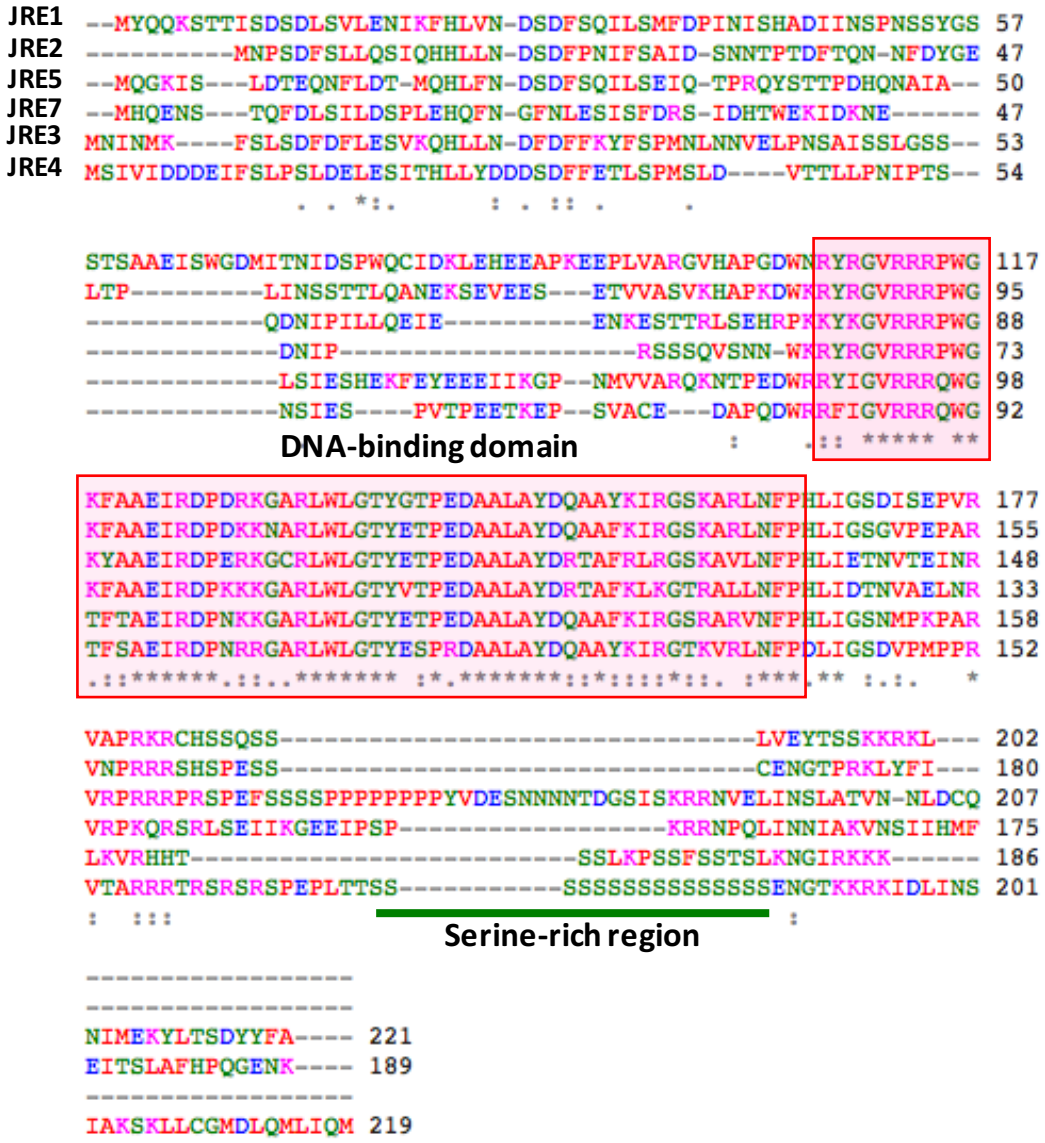

Supplementary figure 1. Multiple sequence alignment of JRE proteins in tomato
Amino acid sequences of JRE transcription factors found in tomato were aligned by ClustalW (Thompson et al. 1994). Amino acids with similar functional group were indicated as the same color and gaps between the multiple alignment were indicated by dash line. Residues shaded by pink box represent the DNA-binding domain of JREs. Green line indicates the serine-rich region specifically found in JRE4. Dot and asterisk represent similar and homologous amino acid found in particular position of JREs.

Table S1 Matrices for P box, CS1 box, and GCC box

Values of position weight matrices used to predict JRE-binding elements in **Fig. 5** and **6** and of position-specific probability matrices used for MEME analysis in **Supplementary Table S8** are included. The weight matrices had been obtained based on DNA-bindind experiment using recombinant ORCA3 in Shoji et al. (2013). The probability matrices were generated based on sequences predicted as JRE-binding elements in the 5'-flanking regions (-300 to -1) of group R genes. GCC box, a 7-mer element, is shorter than 10-mer P and CS1 boxes.

position weight matrices

		position									
box name	nucleotite	1	2	3	4	5	6	7	8	9	10
P	A	83	81	0	1	79	32	77	9	2	99
	C	97	100	3	100	100	100	15	100	100	2
	G	67	15	100	0	0	36	100	0	9	100
	T	100	0	0	2	0	12	54	5	7	32
CS1	A	100	100	0	39	100	0	11	0	0	100
	C	12	24	0	100	21	100	0	100	100	12
	G	3	79	100	71	0	0	100	0	0	25
	T	34	4	0	64	1	0	0	0	0	38
GCC	A	88	9	10	9	3	14	0			
	C	100	14	100	100	7	100	100			
	G	45	100	2	17	100	5	8			
	T	14	17	5	26	1	21	12			

position-specific probability matrices

		position									
box name	nucleotite	1	2	3	4	5	6	7	8	9	10
P	A	0.15625	0.5	0	0.03125	0.40625	0.21875	0.40625	0	0	0.5
	C	0.40625	0.46875	0.0625	0.9375	0.59375	0.5	0.09375	0.96875	0.9375	0.03125
	G	0.125	0.03125	0.9375	0	0	0.15625	0.34375	0	0.03125	0.21875
	T	0.3125	0	0	0.03125	0	0.125	0.15625	0.03125	0.03125	0.25
CS1	A	0.3125	0.5	0	0.125	0.6875	0	0.6875	0	0	0.5625
	C	0.3125	0.1875	0	0.5625	0.3125	1	0	1	1	0
	G	0	0.3125	1	0.1875	0	0	0.3125	0	0	0.1875
	T	0.375	0	0	0.125	0	0	0	0	0	0.25
GCC	A	0.272727	0.181818	0	0	0	0.090909	0			
	C	0.409091	0.045455	0.954545	0.909091	0	0.818182	0.818182			
	G	0.272727	0.636364	0.045455	0	1	0.090909	0.090909			
	T	0.045455	0.136364	0	0.090909	0	0	0.090909			

Table S2 Transcript levels of *JRE* genes and SGA biosynthesis genes in tomato tissues.
Values used to draw heat maps in **Fig. 7** are included. Values used as references are in gray.

Experiment		*JRE* genes						SGA biosynthesis genes		
	organ	*JRE1*	*JRE2*	*JRE3*	*JRE4*	*JRE5*	*JRE6*	*HMGR*	*SMO2*	*GAME1*
a; tomato organs	flower	0.083429	0.041808	0.318882	10.35039	0.794887	0.278367	8.227297	0.947391	0.578763
	leaf	0.082189	0.033217	0.250233	8.372414	0.315435	0.137625	1	1	1
	stem	0.040959	0.022219	0.065472	2.35766	0.123873	0.045245	1.534438	0.922072	0.451969
	root	0.199191	0.078051	0.265529	0.522541	0.257967	0.408984	2.090229	0.790903	0.496819
b; fruit developmental stages	stage									
	green (-5mm)	2.297509	13.08707	1.945406	31.34299	2.51415	0.727022	0.659754	1	1
	green (-7.5mm)	3.605178	18.12703	3.340516	16.68027	5.579248	1.274622	0.607097	0.510506	0.339151
	green (-10mm)	2.01401	7.727867	2.265879	14.32111	3.580276	2.042123	1	0.264255	0.167241
	green (-12mm)	0.840938	3.605178	3.784417	9.781604	5.205622	1.494922	0.574349	0.225313	0.083043
	green (-15mm)	0.627286	2.281639	3.317442	7.516552	4.790149	1.765492	0.864537	0.223756	0.062068
	breaker (Br)	0.730383	3.630254	6.190565	7.26051	9.781601	3.317439	0.072293	0.248273	0.042986
	Br+2d	0.368585	0.641744	1.790138	1.569245	3.387147	0.702257	0.129408	0.07911	0.014579
	Br+4d	0.858607	1.986282	4.112658	3.410707	4.469367	2.234683	0.054409	0.115023	0.025737
	Br+10d	0.747461	0.876648	4.000197	4.141263	8.815673	1.945404	0.061214	0.129408	0.029564
c; time course of MeJA-dependent induction	time (h)									
	0	0.036141	0.058305	0.04982	19.60129	0.235849	1.528742	1	1	1
	0.5	1.12638	1.982222	3.717122	21.43408	0.300988	3.582051	0.726667	1.651079	1.027304
	1	0.493462	1.238889	1.443543	30.73955	1.907755	5.130776	1.19	2.453237	1.542662
	4	0.37546	0.820764	1.172878	62.70096	10.88798	7.618728	4.803333	5.381295	1.962457
	24	0.13302	0.255676	0.559373	100	3.716678	8.542967	9.586667	16.07194	4.1843

Table S3 Probes up-regulated in *JRE4-OX* lines

Top 132 probes up-regulated in *JRE4-OX* lines (Rox>5.0) are ordered according to Rox values. Signal intensities are shown relative to levels in wild-type control (WT1). The sequences corresponding to the probes were searched against reference tomato genes with BLASTN at SOL Genome Network (https://solgenomics.net/). Matches with e-values smaller than 1e-40 are considered significant. Probes corresponded to same genes are marked with numbered asterisks. SGA biosynthesis genes are highlighted in yellow.

					Relative signal intensities (WT1=1)				
Rank	Probe ID	Accession	Descriptions	Gene ID	WT1	WT2	OX1	OX2	Rox value
1	TowgeN_I_21108	TC180917	JRE4	Solyc01g090340	1	1.689113	2771.988	2764.927	2203.713
2	TowgeN_I_23098	TC182907	Cellulose synthase family protein	Solyc07g043390	1	0.655643	324.3317	307.0789	398.6127
3	TowgeN_I_21638	TC181447	Heme-binding protein 2	Solyc07g061800	1	0.535549	119.6318	154.4387	196.4567
4	TowgeN_I_23785	TC183594	GAME17	Solyc07g043480	1	0.735856	161.7173	170.0751	195.6715
5	TowgeN_I_18219	TC178028	GAME6	Solyc07g043460 (*15)	1	0.923118	170.0818	178.4329	181.5139
6	TowgeN_I_14564	TC174373		no hit	1	0.901094	120.4624	114.2756	123.8103
7	TowgeN_I_12776	TC172585	GAME11	Solyc07g043420 (*14)	1	1.011034	110.1742	112.8818	110.9194
8	TowgeN_I_10490	TC170299	GAME18	Solyc07g043500	1	1.066581	108.0615	112.6339	106.9035
9	TowgeN_I_22946	TC182755	GAME12	Solyc12g006470 (*22)	1	0.931718	99.04693	106.2098	106.389
10	TowgeN_I_35805	BI932634	GAME11	Solyc07g043420 (*14)	1	0.955715	108.8269	98.0142	105.8167
11	TowgeN_I_32491	CO751218		no hit	1	1.269192	115.9369	102.373	97.5792
12	TowgeN_I_21176	TC180985	Sterol C-5 desaturase (DWF7)	Solyc02g086180	1	1.184102	110.5292	97.59696	95.9733
13	TowgeN_I_46317	AW928641	GAME12	Solyc12g006470 (*22)	1	0.830709	89.24932	78.52043	92.43234
14	TowgeN_I_25298	TC185107	Unknown Protein	Solyc07g043400	1	0.654201	70.36507	72.51037	90.31809
15	TowgeN_I_46071	AW929410	GAME12	Solyc12g006470 (*22)	1	0.764771	81.02268	74.86666	89.93184
16	TowgeN_I_13382	TC173191	Sterol 4-alpha-methyl-oxidase 2 (SMO2)	Solyc01g091320	1	1.065271	90.66405	94.39727	89.69591
17	TowgeN_I_48635	BG129731	GAME6	Solyc07g043460 (*15)	1	0.736299	77.12106	70.66887	87.1275
18	TowgeN_I_34639	BI924489	GAME11	Solyc07g043420 (*14)	1	0.791274	83.94899	69.74382	86.98183
19	TowgeN_I_33484	BG135874	GAME11	Solyc07g043420 (*14)	1	1.008802	93.73397	77.98379	85.48433
20	TowgeN_I_30837	TC190646		no hit	1	2.23399	98.12319	123.9436	80.36763
21	TowgeN_I_11758	TC17156	Hydrolase	Solyc03g123390	1	0.756827	73.4723	63.33477	79.39276
22	TowgeN_I_14173	TC173982	GAME1	Solyc07g043490 (*16)	1	1.002708	67.80652	74.71268	71.16339
23	TowgeN_I_34758	BI927123	GAME11	Solyc07g043420 (*14)	1	1.032108	67.46698	66.19639	65.79216
24	TowgeN_I_26827	TC186636	Sterol 4-alpha-methyl-oxidase 2 (SMO2)	Solyc06g005750	1	0.563219	48.24578	45.12938	64.7909
25	TowgeN_I_38909	AI776710	GAME6	Solyc07g043460 (*15)	1	0.852484	57.49373	55.93754	61.62276
26	TowgeN_I_24433	TC184242	RING finger protein 5	Solyc10g008410	1	0.853673	61.66979	47.33241	59.1721
27	TowgeN_I_10116	TC169925	GAME12	Solyc12g006470 (*22)	1	0.858323	55.10971	53.90769	59.00739
28	TowgeN_I_26929	TC186738	Peptide transporter	Solyc04g005070 (*4)	1	0.93377	57.63536	54.02363	57.80941
29	TowgeN_I_50870	AI482715	GAME12	Solyc12g006470 (*22)	1	0.794899	52.24999	47.22228	56.15262
30	TowgeN_I_18848	TC178657	GAME1	Solyc07g043490 (*16)	1	1.141792	57.31623	55.01481	52.6781
31	TowgeN_I_38770	AI772072	Chlorophyll a/b binding protein	Solyc02g070940	1	0.983357	52.7928	50.70956	52.18913
32	TowgeN_I_24107	TC183916		no hit	1	0.984379	50.76197	51.68613	51.6305
33	TowgeN_I_23243	TC183052	UDP-glucosyltransferase	Solyc11g066670	1	0.760126	42.7825	45.93134	51.35581
34	TowgeN_I_26927	TC186736	GAME4	Solyc12g006460 (*21)	1	0.878452	49.28353	46.21897	51.05481
35	TowgeN_I_26098	TC185907	GAME11	Solyc07g043420 (*14)	1	0.52248	38.23898	30.52259	50.09193
36	TowgeN_I_23288	TC183097	Carboxyl methyltransferase	Solyc04g055260	1	1.099929	41.56453	53.94358	45.58481
37	TowgeN_I_16778	TC176587	GAME4	Solyc12g006460 (*21)	1	0.822708	43.35172	38.7919	45.49727
38	TowgeN_I_29104	TC188913	Peptide transporter	Solyc04g005070 (*4)	1	0.834656	43.4623	37.49733	44.4893
39	TowgeN_I_23322	TC183131	Cytochrome P450	Solyc04g078340	1	0.997599	49.90408	32.27187	41.13741
40	TowgeN_I_10407	TC170216	GAME6	Solyc07g043460 (*15)	1	0.736903	35.61379	32.24015	39.98344
41	TowgeN_I_37213	AI485590	Blue copper protein	Solyc11g01230	1	0.983011	37.86071	35.62674	37.06124
42	TowgeN_I_13451	TC173260		no hit	1	0.982472	33.6434	32.45062	33.3418
43	TowgeN_I_44783	DN172298	POT family domain containing protein	Solyc09g075230 (*19)	1	0.947783	24.75103	28.88855	27.5586
44	TowgeN_I_28413	TC188222	POT family domain containing protein	Solyc09g075230 (*19)	1	0.875001	23.06841	26.58935	26.60235
45	TowgeN_I_34881	BI931323	Retinol dehydrogenase 12	Solyc03g025390 (*3)	1	0.817564	21.62777	26.21773	26.59188
46	TowgeN_I_12024	TC171833		no hit	1	0.807087	20.40921	25.41738	25.65171
47	TowgeN_I_14360	TC174169	GAME11	Solyc07g043420 (*14)	1	0.992136	23.04043	21.46408	22.34045
48	TowgeN_I_17936	TC177745	Squalene monooxygenase	Solyc04g077440 (*6)	1	0.951095	21.17192	20.32349	21.28112
49	TowgeN_I_25221	TC185030	Squalene monooxygenase	Solyc04g077440 (*6)	1	0.93081	20.93639	19.88298	21.16825
50	TowgeN_I_23742	TC183551		no hit	1	0.974911	20.56864	20.18244	20.63772
51	TowgeN_I_13925	TC173734	UDP-glucuronosyltransferase	Solyc12g009930 (*24)	1	0.958886	15.80649	21.62175	19.11532
52	TowgeN_I_20707	TC180516	Primary amine oxidase	Solyc05g013440 (*8)	1	0.982007	19.35083	17.43896	18.56342
53	TowgeN_I_37174	BG643837		no hit	1	0.912023	17.38037	15.67612	17.32543
54	TowgeN_I_28189	TC187998	Solute carrier family 15 member 4	Solyc05g005940	1	0.870566	17.40185	14.70677	17.24777
55	TowgeN_I_25626	TC185435		no hit	1	0.931117	15.61143	17.16208	16.99289
56	TowgeN_I_23646	TC183455	Isopentenyl-diphosphate delta-isomerase (IDI)	Solyc04g056390 (*5)	1	1.390309	17.961	21.13118	16.80245
57	TowgeN_I_11501	TC171310	Sterol-4-alpha-carboxylate 3-dehydrogenase	Solyc02g081730	1	0.895681	14.49682	16.75199	16.53429
58	TowgeN_I_46480	BI423324	Sterol reductase (DWF5)	Solyc06g074090 (*11)	1	0.888223	16.06357	14.5303	16.25944
59	TowgeN_I_36651	AW648952	Aldehyde dehydrogenase	Solyc12g099290 (*25)	1	0.944719	12.66776	18.68283	16.13392
60	TowgeN_I_27928	TC187737	Aldehyde dehydrogenase	Solyc12g099290 (*25)	1	0.966704	12.48227	18.67159	15.84519
61	TowgeN_I_28714	TC188523	3-hydroxy-3-methylglutaryl CoA reductase (HMGI	Solyc02g082260	1	0.686731	14.51534	10.96161	15.64395
62	TowgeN_I_13556	TC173365	Sterol reductase (DWF5)	Solyc06g074090 (*11)	1	0.986297	15.21924	15.18812	15.3093
63	TowgeN_I_11577	TC171386	Sterol C-5 desaturase (DWF7)	Solyc02g063240	1	1.189806	16.94733	14.45596	14.44923
64	TowgeN_I_24001	TC183810	Transporter major facilitator family	Solyc01g096740	1	0.843265	10.4495	15.81152	14.35077
65	TowgeN_I_48216	BI210634	Sterol reductase (DWF5)	Solyc06g074090 (*11)	1	0.943085	14.71237	12.89597	14.22071
66	TowgeN_I_26293	TC186102	Uncharacterized oxidoreductase	Solyc01g073640 (*2)	1	1.102391	13.96008	14.85704	13.73942
67	TowgeN_I_15136	TC174945	CONSTANS-like protein	Solyc07g006630	1	2.054864	12.6743	22.26906	12.98714
68	TowgeN_I_45452	BG135198	POT family domain containing protein	Solyc09g075260	1	1.164083	12.13972	15.08554	12.65325
69	TowgeN_I_29333	TC189142	Sterol 3-beta-glucosyltransferase	Solyc09g061860	1	1.002106	12.33329	12.53934	12.42325
70	TowgeN_I_26651	TC186460		no hit	1	0.788361	11.73767	10.16155	12.41935
71	TowgeN_I_48283	BG129290	Sterol side chain reductase (SSR2)	Solyc02g069490	1	0.817671	11.22924	10.93802	12.31937
72	TowgeN_I_50155	AW649246	Glucosyltransferase	Solyc12g009920 (*23)	1	1.123188	11.12459	14.76172	12.23338
73	TowgeN_I_37530	AW096562	Glucosyltransferase	Solyc12g009920 (*23)	1	0.882016	10.10337	12.06406	11.82503
74	TowgeN_I_11977	TC171786		no hit	1	0.724027	9.750402	10.0535	11.78908
75	TowgeN_I_21474	TC181283	Hydroxymethylglutaryl-CoA synthase (HMGS)	Solyc08g080170 (*18)	1	1.257646	11.70824	14.42098	11.72637
76	TowgeN_I_34723	BI927518	Hydroxymethylglutaryl-CoA synthase (HMGS)	Solyc08g080170 (*18)	1	1.15215	11.05402	13.94774	11.67546
77	TowgeN_I_12379	TC172188	UDP-glucuronosyltransferase	Solyc11g066680 (*20)	1	1.062691	11.11228	12.90784	11.6558
78	TowgeN_I_27831	TC187640	UDP-glucuronosyltransferase	Solyc12g009930 (*24)	1	0.769342	10.52727	9.717909	11.64003
79	TowgeN_I_17082	TC176891	Retinol dehydrogenase 12	Solyc03g025390 (*3)	1	0.790908	9.433715	11.03458	11.58695
80	TowgeN_I_47212	AW092719	UDP-glucuronosyltransferase	Solyc11g066680 (*20)	1	1.063743	11.6714	11.83319	11.40018
81	TowgeN_I_18368	TC178177	Retinol dehydrogenase 12	Solyc03g025390 (*3)	1	0.851295	10.02847	10.71544	11.27785
82	TowgeN_I_26437	TC186246	Aldehyde dehydrogenase	Solyc12g099290 (*25)	1	0.870972	10.13055	9.760124	10.682
83	TowgeN_I_17516	TC177325	Cytochrome P450	Solyc07g062510	1	0.988221	10.21418	10.4187	10.37792
84	TowgeN_I_10976	TC170785	Hydroxymethylglutaryl-CoA synthase (HMGS)	Solyc08g080170 (*18)	1	0.905634	9.976382	8.744177	9.847946
85	TowgeN_I_41668	BP878201	Primary amine oxidase	Solyc05g013440 (*8)	1	0.748579	9.347942	6.742412	9.396224
86	TowgeN_I_17234	TC177043	Homeobox-leucine zipper-like protein	Solyc02g085630	1	0.528995	5.065472	7.877862	9.352776
87	TowgeN_I_25824	TC185633	Cytochrome P450	Solyc07g062520	1	0.895544	9.433805	7.811068	9.125297
88	TowgeN_I_43878	BP907947	Unknown protein	Solyc01g007700	1	1.100131	9.235928	9.458151	8.921669
89	TowgeN_I_21613	TC181422	Primary amine oxidase	Solyc05g013440 (*8)	1	1.116369	9.755058	8.768644	8.779127
90	TowgeN_I_34577	AJ785227	Acetyl-CoA C-acetyltransferase (ACAA)	Solyc09g061840	1	0.961648	7.550433	8.483722	8.176944
91	TowgeN_I_14236	TC174045	Acetyl-CoA C-acetyltransferase (ACAA)	Solyc05g017760 (*9)	1	1.104596	9.138964	7.339797	7.84928
92	TowgeN_I_36136	BE449289	UDP-sugar pyrophosphorylase	Solyc06g051080	1	1.066818	7.732636	8.296935	7.763792
93	TowgeN_I_45198	BG133566	Acetyl-CoA C-acetyltransferase (ACAA)	Solyc05g017760 (*9)	1	1.120552	9.130856	7.004796	7.633846
94	TowgeN_I_14602	TC174411	S8-RNase	Solyc07g006570 (*13)	1	0.887054	6.818756	7.464331	7.596198
95	TowgeN_I_19214	TC179023	Potassium/sodium hyperpolarization-activated cycl	Solyc01g010080	1	1.23385	9.257945	7.449244	7.561972
96	TowgeN_I_30480	TC190289	Solute carrier family 15 member 4	Solyc05g005950 (*7)	1	1.177781	7.831979	8.280844	7.448372
97	TowgeN_I_44324	DN169009	Obtsuifoliol 14-alpha-demethylase	Solyc01g008110 (*1)	1	0.987602	6.770321	7.507322	7.183631
98	TowgeN_I_15656	TC175465	Cytochrome P450	Solyc01g109150	1	0.940176	7.907063	5.723926	7.032332
99	TowgeN_I_48201	BI208050	Epoxide hydrolase	Solyc05g054320 (*10)	1	0.822562	7.883914	4.618313	6.92534
100	TowgeN_I_35925	BI934641	3-beta-hydroxysteroid-Delta8 Delta7-isomerase	Solyc06g082980 (*12)	1	0.917078	6.429609	6.799937	6.913826
101	TowgeN_I_11461	TC171270	Epoxide hydrolase	Solyc05g054320 (*10)	1	0.862593	8.143655	4.53331	6.843327
102	TowgeN_I_27133	TC186942		no hit	1	0.85069	7.833133	4.466387	6.689451
103	TowgeN_I_16523	TC176332	Solute carrier family 15 member 2	Solyc05g005990	1	0.99856	6.811128	6.390174	6.605412
104	TowgeN_I_37354	AI487581	S8-RNase	Solyc07g006570 (*13)	1	0.979697	6.470813	6.537188	6.571394
105	TowgeN_I_25685	TC185494	Solute carrier family 15 member 4	Solyc05g005950 (*7)	1	0.88075	6.30264	5.852207	6.488854
106	TowgeN_I_37439	AI490441	Isopentenyl-diphosphate delta-isomerase (IDI)	Solyc04g056390 (*5)	1	1.300929	7.192049	6.867939	6.216909
107	TowgeN_I_29077	TC188886		no hit	1	0.914268	5.957346	5.666428	6.084381
108	TowgeN_I_15810	TC175619	Isopentenyl-diphosphate delta-isomerase (IDI)	Solyc04g056390 (*5)	1	0.803331	5.952957	4.840635	6.057408
109	TowgeN_I_10769	TC170578	3-beta-hydroxysteroid-Delta8 Delta7-isomerase	Solyc06g082980 (*12)	1	0.952229	6.360481	5.341404	5.997705
110	TowgeN_I_27212	TC187021	Glutathione S-transferase	Solyc09g007150	1	0.913117	6.201449	5.208203	5.976233
111	TowgeN_I_26986	TC186795	Delta14-sterol reductase	Solyc09g009040	1	0.849176	5.77837	5.032411	5.885421
112	TowgeN_I_34165	AJ784448	Acyltransferase-like protein	Solyc08g075210 (*17)	1	1.23362	6.120897	6.779872	5.839604
113	TowgeN_I_21818	TC181627	Acid phosphatase	Solyc06g062370	1	0.604345	4.358563	4.264321	5.722758
114	TowgeN_I_14942	TC174751	Acyltransferase-like protein	Solyc08g075210 (*17)	1	0.884256	6.327367	4.379528	5.703814
115	TowgeN_I_10895	TC170704	Proline-rich protein	Solyc12g009650	1	0.837182	5.785768	4.556331	5.673892
116	TowgeN_I_37269	AI487895	Peptide transporter	Solyc05g005970	1	0.755706	5.028022	4.606354	5.595806
117	TowgeN_I_26399	TC186208	Unknown Protein	Solyc12g038560	1	1.077277	5.686488	5.845262	5.559073
118	TowgeN_I_36020	AW037915	Solute carrier family 15 member 4	Solyc05g005950 (*7)	1	1.068135	5.298306	6.055183	5.49569
119	TowgeN_I_40469	BF114271	Unknown Protein	Solyc03g096410	1	1.375104	9.100518	3.56368	5.468457
120	TowgeN_I_35390	AW735923	Solute carrier family 15 member 4	Solyc05g005950 (*7)	1	0.960841	5.04883	5.613617	5.439861
121	TowgeN_I_15190	TC174999		no hit	1	1.323967	6.64918	5.692655	5.415925
122	TowgeN_I_48902	BG643145	Uncharacterized oxidoreductase	Solyc01g073640 (*2)	1	1.06726	5.346034	5.721188	5.359243
123	TowgeN_I_46083	AW929606	Calmodulin-binding heat-shock protein	Solyc05g051280	1	0.989592	4.456981	6.166027	5.339435
124	TowgeN_I_42566	BP890544	Scarecrow transcription factor family protein	Solyc01g008910	1	1.590919	6.040993	7.06125	5.334472
125	TowgeN_I_19889	TC179698	Uncharacterized oxidoreductase	Solyc01g073640 (*2)	1	0.989864	5.300505	5.225368	5.289882
126	TowgeN_I_14445	TC174254	Erg28 like protein	Solyc04g077150	1	0.996772	5.906556	4.523234	5.22334
127	TowgeN_I_19650	TC179459	Obtsuifoliol 14-alpha-demethylase	Solyc01g008110 (*1)	1	1.032319	5.034661	5.56824	5.218463
128	TowgeN_I_17855	TC177664	Light regulated protein-like protein	Solyc09g092110	1	1.296216	6.304732	5.375814	5.172953
129	TowgeN_I_10212	TC170021	Pyruvate kinase	Solyc04g008740	1	0.769138	5.211178	3.683388	5.114724
130	TowgeN_I_49800	BP051890	CONSTANS-like zinc finger protein	Solyc07g045180	1	0.823676	3.780276	5.357312	5.057814
131	TowgeN_I_12104	TC171913	Seed specific protein	Solyc06g072840	1	1.284891	6.183491	5.141932	5.034931
132	TowgeN_I_30069	TC189878		no hit	1	1.04893	4.497647	5.77595	5.01699

Table S4 Probes down-regulated in *JRE-EAR* lines.
Top 197 probes down-regulated in *JRE-EAR* lines (Q<0.85) are ordered according to Q values. Signal intensities are shown relative to levels in vector control line (VC1). The sequences corresponding to the probes were searched against reference tomato genes with BLASTN at SOL Genome Network (https://solgenomics.net/). Matches with e-values smaller than 1e-40 are considered significant. Probes corresponded to same genes are marked with numbered asterisks. SGA biosynthesis genes are highlighted in yellow

					Relative signal intensities (VC1=1)							
Rank	Probe ID	Accession	Description	Gene ID	VC1	VC2	*JRE3-EAR#1*	*JRE3-EAR#2*	*JRE4-EAR#1*	*JRE5-EAR#1*	*JRE5-EAR#2*	Q value
1	TowgeN_I_28346	TC188155	1-aminocyclopropane-1-carboxylate oxidase 2	Solyc09g066320	1	1.710358	0.067722	0.12913	0.025413	0.028995	0.030285	0.083898
2	TowgeN_I_19546	TC179355	Auxin response factor 17	Solyc11g013470	1	0.799505	0.10866	0.057351	0.038054	0.050948	0.069064	0.122965
3	TowgeN_I_12330	TC17213	Peptide transporter	Solyc03g113430	1	0.493011	0.192244	0.065541	0.152063	0.190661	0.012146	0.338645
4	TowgeN_I_39680	BI208342	Pol polyprotein	Solyc03g115130	1	1.006727	0.234743	0.437144	0.166934	0.054661	0.080931	0.379937
5	TowgeN_I_24433	TC184242	RING finger protein 5	Solyc10g008410	1	0.954066	0.17844	0.401116	0.082519	0.319321	0.143528	0.389064
6	TowgeN_I_25914	TC185723	Unknown Protein	Solyc05g024190	1	2.022265	0.110932	0.920137	0.139006	0.05547	0.056541	0.401179
7	TowgeN_I_47669	AW616373	Germacrene-D synthase	Solyc12g006570 (*23)	1	0.888727	0.262309	0.266536	0.012821	0.358005	0.185367	0.403085
8	TowgeN_I_36480	BE458680	Cytochrome P450	Solyc00g247300	1	1.751781	0.323874	0.269432	0.139984	0.16447	0.646046	0.409501
9	TowgeN_I_13567	TC173376	Beta-1 3-glucanase	Solyc01g008620 (*1)	1	0.436974	0.12523	0.135522	0.207219	0.089196	0.092517	0.42937
10	TowgeN_I_21829	TC181638	Sentrin specific protease 1b	Solyc11g072220	1	1.726634	0.214073	0.122326	0.308265	0.433585	0.427222	0.438602
11	TowgeN_I_23243	TC183052	UDP-glucosyltransferase	Solyc11g066670	1	0.93958	0.273999	0.197313	0.292261	0.248938	0.163301	0.442065
12	TowgeN_I_31436	TC191245	Xyloglucan endotransglucosylase/hydrolase 7	Solyc07g055990	1	0.887257	0.385065	0.282973	0.240087	0.055949	0.065484	0.442227
13	TowgeN_I_44756	DN172257	Beta-1 3-glucanase	Solyc01g008620 (*1)	1	0.503878	0.186998	0.209991	0.197664	0.081493	0.129539	0.446706
14	TowgeN_I_46846	AW615961	Wax synthase isoform 3	Solyc11g012200 (*20)	1	1.316171	0.273424	0.263301	0.429915	0.200724	0.155934	0.472728
15	TowgeN_I_12539	TC172348	GAME6	Solyc07g043460 (*12)	1	1.079942	0.410767	0.343589	0.257287	0.268776	0.12797	0.479382
16	TowgeN_I_41766	BP879276	Chalcone synthase 2	Solyc05g053550	1	0.575327	0.092147	0.180371	0.069515	0.125587	0.505254	0.479935
17	TowgeN_I_37259	AI489767		no hit	1	0.46222	0.25522	0.165528	0.16732	0.073415	0.25019	0.496255
18	TowgeN_I_12776	TC172585	GAME11	Solyc07g043420 (*11)	1	0.852349	0.357757	0.324873	0.212764	0.267048	0.183102	0.500813
19	TowgeN_I_24615	TC184424	Ethylene responsive transcription factor 2a	Solyc06g063070	1	0.40273	0.249872	0.249598	0.075704	0.17176	0.091671	0.509073
20	TowgeN_I_19557	TC179366	Auxin-responsive family protein	Solyc06g053260	1	1.358814	0.166188	0.200412	0.549923	0.126804	0.094595	0.512225
21	TowgeN_I_46990	BI926443	Dihydroflavonol 4-reductase family	Solyc01g094070	1	1.069321	0.414773	0.203221	0.233462	0.403827	0.338165	0.51892
22	TowgeN_I_14173	TC173982	GAME1	Solyc07g043490 (*14)	1	0.858718	0.242186	0.229215	0.376808	0.261688	0.134485	0.526627
23	TowgeN_I_47770	AW979806	Serine/threonine-protein kinase receptor	Solyc10g005630	1	0.763689	0.468679	0.256203	0.270121	0.057437	0.11414	0.531281
24	TowgeN_I_39474	BI206806	NAC domain protein	Solyc01g102740	1	0.880924	0.074583	0.37701	0.433367	0.147561	0.065648	0.533959
25	TowgeN_I_47207	AW092214	Alcohol dehydrogenase zinc-containing	Solyc09g059040	1	2.00001	0.540929	0.396506	0.470879	0.342351	0.217756	0.540756
26	TowgeN_I_35805	BI932634	GAME11	Solyc07g043420 (*11)	1	0.946928	0.316201	0.355442	0.289269	0.381599	0.213353	0.548761
27	TowgeN_I_26929	TC186738	Peptide transporter	Solyc04g005070 (*8)	1	1.193336	0.368775	0.456101	0.284557	0.399107	0.263107	0.551939
28	TowgeN_I_22946	TC182755	GAME12	Solyc12g006470 (*22)	1	0.904166	0.231805	0.270111	0.167338	0.540936	0.32899	0.557367
29	TowgeN_I_22522	TC182331	Pectate lyase	Solyc03g111690	1	1.056693	0.605289	0.392802	0.275321	0.089929	0.05569	0.559173
30	TowgeN_I_36034	AW040345	Transcription factor CYCLOIDEA	Solyc12g014140 (*24)	1	0.73995	0.289547	0.131685	0.407155	0.098102	0.161485	0.560143
31	TowgeN_I_36023	AW037628	Transcription factor CYCLOIDEA	Solyc12g014140 (*24)	1	0.83236	0.403629	0.179717	0.397806	0.106238	0.159295	0.562274
32	TowgeN_I_29504	TC189313	Glucose transporter 8	Solyc01g098500	1	0.707626	0.483284	0.227182	0.267587	0.140439	0.1656	0.567492
33	TowgeN_I_46317	AW928641	GAME12	Solyc12g006470 (*22)	1	1.034202	0.277494	0.289386	0.17769	0.570701	0.386981	0.574465
34	TowgeN_I_48658	BG130125	Germacrene-D synthase	Solyc12g006570 (*23)	1	0.864186	0.22558	0.219276	0.019205	0.657338	0.313862	0.57646
35	TowgeN_I_26293	TC186102	Uncharacterized oxidoreductase	Solyc01g073640 (*2)	1	0.80558	0.30086	0.435077	0.278172	0.313465	0.142992	0.576758
36	TowgeN_I_34778	AW624081	Maleylacetoacetate isomerase/glutathione S-tran	Solyc01g091330	1	0.622512	0.129933	0.283662	0.111099	0.465859	0.300816	0.585795
37	TowgeN_I_18848	TC178657	GAME1	Solyc07g043490 (*14)	1	0.895963	0.262972	0.385465	0.402354	0.2718	0.132259	0.58703
38	TowgeN_I_14700	TC174509	Auxin-regulated protein	Solyc06g030470	1	0.733999	0.446452	0.217483	0.262893	0.267698	0.258213	0.588779
39	TowgeN_I_47927	BG123222	Unknown Protein	Solyc11g008080	1	1.075535	0.248935	0.340451	0.510593	0.202493	0.1421	0.592627
40	TowgeN_I_45997	BI930585	Mitogen-activated protein kinase 15	Solyc05g008020	1	0.441386	0.1021	0.102315	0.347381	0.037757	0.024306	0.59341
41	TowgeN_I_32409	CN385204		no hit	1	1.196077	0.2386	0.248138	0.549989	0.249246	0.233927	0.595011
42	TowgeN_I_37269	AI487895	Peptide transporter	Solyc05g005970	1	0.915623	0.372745	0.295173	0.435276	0.139996	0.168992	0.596229
43	TowgeN_I_46071	AW929410	GAME12	Solyc12g006470 (*22)	1	0.966394	0.235814	0.308445	0.224924	0.564927	0.374353	0.597759
44	TowgeN_I_29104	TC188913	Peptide transporter	Solyc04g005070 (*8)	1	0.895868	0.313285	0.389551	0.272287	0.4229	0.278132	0.599026
45	TowgeN_I_28112	TC187921		no hit	1	1.049714	0.350594	0.47107	0.380275	0.325666	0.18632	0.600992
46	TowgeN_I_11391	TC171200	Cinnamyl alcohol dehydrogenase-like protein	Solyc02g030480	1	0.937256	0.07785	0.116956	0.543363	0.203108	0.162859	0.601028
47	TowgeN_I_18219	TC178028	GAME6	Solyc07g043460 (*12)	1	0.803286	0.19646	0.298423	0.372377	0.401699	0.199957	0.60486
48	TowgeN_I_23098	TC182907	Cellulose synthase family protein	Solyc07g043390	1	1.274698	0.347996	0.236015	0.311711	0.677956	0.37892	0.606256
49	TowgeN_I_49024	BG644091	Transcription factor CYCLOIDEA	Solyc12g014140 (*24)	1	1.077951	0.404373	0.247345	0.50559	0.168318	0.203868	0.606866
50	TowgeN_I_49735	AW398144	Expansin B1	Solyc07g054170	1	0.943694	0.159139	0.302814	0.529596	0.141735	0.102264	0.60813
51	TowgeN_I_35023	AW929217	GAME6	Solyc07g043460 (*12)	1	0.447456	0.171542	0.330396	0.209258	0.264242	0.11471	0.610941
52	TowgeN_I_34997	AW929708	GAME17	Solyc07g043480 (*13)	1	1.082934	0.239342	0.32511	0.488201	0.397026	0.190841	0.611566
53	TowgeN_I_25911	TC185720	Glucose transporter 8	Solyc01g080680	1	2.177828	0.065393	0.127252	0.831141	0.07505	0.143006	0.615609
54	TowgeN_I_40480	BF114345		no hit	1	0.69168	0.600434	0.334038	0.163956	0.085213	0.105266	0.616628
55	TowgeN_I_48902	BG643145	Uncharacterized oxidoreductase	Solyc01g073640 (*2)	1	0.798515	0.290785	0.484389	0.286137	0.373678	0.159831	0.620163
56	TowgeN_I_35461	AW615959	Wax synthase isoform 3	Solyc11g012200 (*20)	1	0.935105	0.352406	0.279416	0.426183	0.236865	0.35799	0.629294
57	TowgeN_I_10490	TC170299	GAME18	Solyc07g043500	1	0.824651	0.280921	0.433828	0.393195	0.243955	0.175244	0.63191
58	TowgeN_I_48928	AI775787	Unknown Protein	Solyc01g111180	1	0.563066	0.267003	0.189583	0.148265	0.285784	0.455765	0.638439
59	TowgeN_I_19889	TC179698	Uncharacterized oxidoreductase	Solyc01g073640 (*2)	1	0.80858	0.313244	0.490579	0.299735	0.386847	0.164765	0.63996
60	TowgeN_I_49519	AW399026	Tubulin alpha-3 chain	Solyc04g077020 (*9)	1	0.720446	0.557827	0.503627	0.102835	0.029846	0.021265	0.646203
61	TowgeN_I_22578	TC182387	2-oxoglutarate-dependent dioxygenase	Solyc02g062460 (*3)	1	0.822352	0.376105	0.70456	0.213499	0.065974	0.045955	0.646715
62	TowgeN_I_19862	TC179671	Calmodulin-like protein	Solyc02g088090	1	0.537619	0.196821	0.253684	0.357177	0.136738	0.197693	0.649482
63	TowgeN_I_37126	AI485727	MYB transcription factor	Solyc08g082890	1	0.859388	0.398054	0.369718	0.347893	0.334116	0.272898	0.649549
64	TowgeN_I_35563	BI926887	GAME6	Solyc07g043460 (*12)	1	0.938304	0.285947	0.327803	0.444228	0.410215	0.244912	0.652275
65	TowgeN_I_14446	TC174255	GAME6	Solyc07g043460 (*12)	1	0.810316	0.303888	0.30183	0.429597	0.323383	0.202977	0.656628
66	TowgeN_I_33484	BG135874	GAME11	Solyc07g043420 (*11)	1	1.045282	0.289951	0.279333	0.341455	0.674318	0.338237	0.65915
67	TowgeN_I_21176	TC180985	Sterol C-5 desaturase (DWF7)	Solyc02g086180	1	0.818411	0.285162	0.362287	0.354693	0.442846	0.259922	0.661056
68	TowgeN_I_15693	TC175502	Arabinogalactan-protein	Solyc07g053640 (*15)	1	1.224859	0.425151	0.229572	0.618644	0.246556	0.180227	0.664561
69	TowgeN_I_48572	AI774144	Calmodulin-like protein	Solyc06g083000	1	1.308826	0.060138	0.364145	0.53457	0.774319	0.206806	0.666741
70	TowgeN_I_11530	TC171339		no hit	1	0.649898	0.098268	0.850083	0.092864	0.230134	0.194009	0.669804
71	TowgeN_I_11758	TC17156	Hydrolase	Solyc03g123390	1	0.984608	0.365212	0.562849	0.22949	0.550018	0.293059	0.672814
72	TowgeN_I_34881	BI931323	Retinol dehydrogenase 12	Solyc03g025390 (*6)	1	0.902847	0.335298	0.322989	0.332226	0.560131	0.315318	0.67502
73	TowgeN_I_48635	BG129731	GAME6	Solyc07g043460 (*12)	1	0.9421	0.402957	0.28864	0.333418	0.532272	0.362124	0.676468
74	TowgeN_I_50167	AW649575	GDSL esterase/lipase 5	Solyc06g064970	1	1.048165	0.402448	0.433607	0.514312	0.192376	0.22567	0.678982
75	TowgeN_I_42479	BP888143	UDP-glucosyltransferase family 1 protein	Solyc03g058370	1	0.701465	0.039737	0.401903	0.516755	0.017879	0.018571	0.681898
76	TowgeN_I_13072	TC172881	Cytosolic ascorbate peroxidase 1	Solyc06g005160	1	1.017599	0.513637	0.469275	0.428529	0.179376	0.265609	0.683005
77	TowgeN_I_26613	TC186422	F-box/LRR-repeat protein	Solyc10g080020	1	0.633484	0.401439	0.590077	0.166537	0.120589	0.077005	0.6862
78	TowgeN_I_32589	CO751438	Ethylene-responsive methionine synthase	Solyc10g081510 (*19)	1	2.242902	0.810636	0.771052	0.481507	0.252734	0.166482	0.686291
79	TowgeN_I_46480	BI423324	Sterol reductase (DWF5)	Solyc06g074090 (*10)	1	0.995378	0.344677	0.400557	0.493111	0.416499	0.174973	0.686764
80	TowgeN_I_22880	TC182689	Ethylene-responsive methionine synthase	Solyc10g081510 (*19)	1	0.963578	0.677296	0.459846	0.287123	0.203011	0.259356	0.690419
81	TowgeN_I_36136	BE449289	UDP-sugar pyrophosphorylase	Solyc06g051080	1	0.828436	0.378002	0.52914	0.263565	0.4201	0.262846	0.69075
82	TowgeN_I_50372	AW617326	Arabinogalactan-protein	Solyc07g053640 (*15)	1	1.166154	0.436734	0.216963	0.632749	0.282379	0.146607	0.690792
83	TowgeN_I_10200	TC170009	Uncharacterized oxidoreductase	Solyc01g073640 (*2)	1	0.803567	0.339976	0.541859	0.312504	0.417696	0.177916	0.692474
84	TowgeN_I_14602	TC174411	S8-RNase	Solyc07g006570	1	0.911568	0.622398	0.440195	0.236003	0.425966	0.209815	0.694731
85	TowgeN_I_19421	TC179230	Multidrug resistance protein ABC transporter fa	Solyc01g080640	1	1.016404	0.456107	0.291286	0.421997	0.485274	0.350674	0.696073
86	TowgeN_I_11363	TC171172	Inositol 1 4 5-trisphosphate 5-phosphatase	Solyc09g082370	1	0.753096	0.268023	0.260107	0.430181	0.327041	0.322221	0.698522
87	TowgeN_I_17682	TC177491	Expansin12	Solyc05g007830	1	0.619204	0.145038	0.434442	0.422384	0.167947	0.137841	0.698906
88	TowgeN_I_44684	DN170645	Proteinase inhibitor II	Solyc03g020040	1	0.902975	0.339902	0.595318	0.321852	0.347438	0.346114	0.700947
89	TowgeN_I_17082	TC176891	Retinol dehydrogenase 12	Solyc03g025390 (*6)	1	0.778868	0.337532	0.571781	0.335339	0.351351	0.130189	0.701291
90	TowgeN_I_16953	TC176762	F-box protein PP2-B1	Solyc05g053620	1	0.835052	0.398677	0.370743	0.462474	0.239548	0.199062	0.703535
91	TowgeN_I_15386	TC175195	Galactosyltransferase-like protein	Solyc02g092840	1	1.397534	0.672244	0.289249	0.589106	0.319252	0.319697	0.707456
92	TowgeN_I_37530	AW096562	Glucosyltransferase	Solyc12g009920	1	1.023218	0.356587	0.268314	0.574467	0.212134	0.378968	0.709485
93	TowgeN_I_28870	TC188679	Fatty acid oxidation complex subunit alpha	Solyc08g068390	1	0.88303	0.053734	0.073275	0.613562	0.413195	0.118179	0.716109
94	TowgeN_I_30803	TC190612		no hit	1	0.686588	0.433057	0.458093	0.341503	0.182452	0.135801	0.716688
95	TowgeN_I_13556	TC173365	Sterol reductase (DWF5)	Solyc06g074090 (*10)	1	1.018198	0.353582	0.402966	0.526696	0.454028	0.188592	0.717232
96	TowgeN_I_34639	BI924489	GAME11	Solyc07g043420 (*11)	1	0.876317	0.341416	0.375024	0.378231	0.519336	0.323686	0.717403
97	TowgeN_I_50870	AI482715	GAME12	Solyc12g006470 (*22)	1	0.900655	0.274536	0.333092	0.188508	0.695831	0.46265	0.718246
98	TowgeN_I_44884	BG133169	Peroxidase	Solyc10g078890	1	0.411003	0.260443	0.158743	0.340433	0.150723	0.102933	0.719942
99	TowgeN_I_21855	TC181664	Arabinogalactan-protein	Solyc07g053640 (*15)	1	1.295509	0.432712	0.219244	0.706736	0.317827	0.157158	0.720914
100	TowgeN_I_26827	TC186636	Sterol 4-alpha-methyl-oxidase 2 (SMO2)	Solyc06g005750	1	0.833555	0.318685	0.430669	0.417558	0.370759	0.315918	0.723407
101	TowgeN_I_12291	TC172100	Proline dehydrogenase	Solyc02g089620 (*5)	1	0.952981	0.192813	0.238311	0.612776	0.360631	0.197947	0.724524
102	TowgeN_I_23785	TC183594	GAME17	Solyc07g043480 (*13)	1	0.828369	0.23519	0.457681	0.502314	0.322052	0.171699	0.726435
103	TowgeN_I_20753	TC180562	N-myc downstream regulated	Solyc05g026360	1	2.434242	0.694974	0.690058	0.644542	0.439039	0.381091	0.727341
104	TowgeN_I_26927	TC186736	GAME4	Solyc12g006460 (*21)	1	0.813976	0.362929	0.414977	0.333048	0.460899	0.349059	0.727451
105	TowgeN_I_22514	TC182323	Gibberellin-regulated protein 2	Solyc12g089300 (*25)	1	1.184514	0.468178	0.479781	0.495169	0.471766	0.316333	0.729068
106	TowgeN_I_45295	BF113255	Pyrimidine 5&apos-nucleotidase	Solyc05g011880	1	0.939992	0.388224	0.538897	0.458607	0.201151	0.35064	0.730645
107	TowgeN_I_41242	BP891373	Gibberellin-regulated protein 2	Solyc12g089300 (*25)	1	1.134839	0.434697	0.513996	0.492356	0.446527	0.318328	0.736832
108	TowgeN_I_15583	TC175392	Expressed protein	Solyc10g074540 (*18)	1	1.0125	0.281514	0.198224	0.623951	0.3996	0.244648	0.737455
109	TowgeN_I_11272	TC171081	bHLH transcription factor	Solyc01g102300	1	1.498404	1.317452	0.370542	0.249686	0.138244	0.143017	0.743083
110	TowgeN_I_43382	DY523865	2-oxoglutarate-dependent dioxygenase	Solyc02g062500 (*4)	1	0.722811	0.458426	0.629069	0.294532	0.094904	0.068056	0.743336
111	TowgeN_I_21013	TC180822		no hit	1	0.729174	0.466413	0.516097	0.321197	0.26385	0.183406	0.744742
112	TowgeN_I_32705	AW031585		no hit	1	1.149605	0.31394	0.409854	0.685227	0.188474	0.185694	0.745315
113	TowgeN_I_35660	BI925836	Leucine-rich repeat receptor-like protein kinase	Solyc06g084420	1	1.18027	0.514021	0.282704	0.576506	0.370982	0.433661	0.746323
114	TowgeN_I_10116	TC169925	GAME12	Solyc12g006470 (*22)	1	0.926267	0.290273	0.408015	0.263949	0.694388	0.455231	0.751235
115	TowgeN_I_47625	AW626247	Aquaporin	Solyc06g066560	1	0.783413	0.440118	0.418601	0.447365	0.235132	0.223114	0.752425
116	TowgeN_I_47860	AW650598	Mitogen-activated protein kinase 9	Solyc04g080730	1	0.57048	0.456543	0.352752	0.28462	0.262583	0.21076	0.754872
117	TowgeN_I_24085	TC183894	Tubulin alpha-3 chain	Solyc04g077020 (*9)	1	0.767103	0.658576	0.609918	0.150337	0.061872	0.077407	0.755042
118	TowgeN_I_11897	TC171706	UDP-D-glucuronic acid 4-epimerase	Solyc12g098480	1	0.935368	0.171039	0.241406	0.640762	0.358858	0.207209	0.755442
119	TowgeN_I_19053	TC178862	Helix-loop-helix DNA-binding transcription fac	Solyc01g106460	1	1.170287	0.337725	0.362773	0.708995	0.208606	0.196488	0.756926
120	TowgeN_I_13752	TC173561	Acid phosphatase	Solyc06g062380	1	0.78197	0.626136	0.670118	0.121285	0.089854	0.076545	0.757259
121	TowgeN_I_12024	TC171833		no hit	1	0.928949	0.302266	0.289366	0.417345	0.658687	0.382644	0.757829
122	TowgeN_I_15975	TC17578	Aquaporin	Solyc08g008050	1	1.690727	0.525334	0.432592	0.812997	0.146757	0.12261	0.758457
123	TowgeN_I_50554	BF113532	Lipase-like	Solyc02g077000	1	0.916085	0.237298	0.326933	0.63812	0.238245	0.175271	0.761021
124	TowgeN_I_30455	TC190264	2-oxoglutarate-dependent dioxygenase	Solyc02g062500 (*4)	1	0.855077	0.483562	0.605141	0.380059	0.241854	0.217147	0.761976
125	TowgeN_I_36037	AW037343	Peptidyl-prolyl cis-trans isomerase	Solyc01g009990	1	0.625908	0.353442	0.534378	0.264098	0.30167	0.261708	0.764169
126	TowgeN_I_19164	TC178973	2-oxoglutarate-dependent dioxygenase	Solyc02g062460 (*3)	1	0.987818	0.534815	0.661804	0.39834	0.268582	0.236543	0.766562
127	TowgeN_I_13925	TC173734	UDP-glucuronosyltransferase 1-6	Solyc12g009930	1	0.785596	0.236608	0.180577	0.558157	0.326782	0.307792	0.767191
128	TowgeN_I_28413	TC188222	POT family domain containing protein	Solyc09g075230 (*17)	1	0.695837	0.317819	0.556995	0.292425	0.406048	0.290599	0.768916
129	TowgeN_I_50249	AW618736	LRR receptor-like serine/threonine-protein kinas	Solyc02g077630	1	0.523926	0.42726	0.160813	0.328369	0.252719	0.333549	0.769851
130	TowgeN_I_42785	BW685237		no hit	1	1.185353	0.842292	0.808893	0.089131	0.116004	0.090941	0.771386
131	TowgeN_I_11485	TC171294	Exostosin-like	Solyc12g062940	1	0.750629	0.388463	0.475748	0.443752	0.298541	0.173569	0.77294
132	TowgeN_I_47433	AW399626	Unknown Protein	Solyc08g078060	1	0.446605	0.407981	0.428982	0.172686	0.093201	0.213169	0.774027
133	TowgeN_I_48216	BI210634	Sterol reductase (DWF5)	Solyc06g074090 (*10)	1	0.866961	0.36492	0.582012	0.454865	0.412824	0.174957	0.774528
134	TowgeN_I_38909	AI776710	GAME6	Solyc07g043460 (*12)	1	0.862819	0.420381	0.321604	0.325186	0.626143	0.424811	0.778067
135	TowgeN_I_34758	BI927123	GAME11	Solyc07g043420 (*11)	1	0.924691	0.362548	0.381823	0.425863	0.593774	0.384314	0.778141
136	TowgeN_I_34820	AW623849	Hydroxymethylglutaryl-CoA synthase (HMGS)	Solyc08g080170 (*16)	1	0.975909	0.314385	0.391644	0.602467	0.413759	0.236815	0.779831
137	TowgeN_I_16219	TC176028	Cytochrome P450	Solyc02g090340	1	0.743955	0.368822	0.650456	0.162362	0.342943	0.44853	0.779855
138	TowgeN_I_18579	TC17838	Aquaporin	Solyc06g075650	1	0.796776	0.365798	0.390902	0.574519	0.133212	0.075963	0.784553
139	TowgeN_I_34437	BG627279	Proline dehydrogenase	Solyc02g089620 (*5)	1	1.474689	0.208012	0.10059	0.838436	0.471237	0.299534	0.785001
140	TowgeN_I_34577	AJ785227	Acetyl-CoA C-acetyltransferase (ACAA)	Solyc09g061840	1	0.893444	0.413002	0.580993	0.21976	0.604076	0.404397	0.785527
141	TowgeN_I_26099	TC185908	Major allergen Mal d 1	Solyc09g090990	1	1.022738	0.253756	0.166403	0.703499	0.447524	0.173953	0.788385
142	TowgeN_I_44783	DN172298	POT family domain containing protein	Solyc09g075230 (*17)	1	0.68633	0.31702	0.534949	0.306332	0.429163	0.31524	0.790303
143	TowgeN_I_51039	BF098248		no hit	1	0.805728	0.509469	0.2076	0.528637	0.313173	0.291033	0.791775
144	TowgeN_I_20589	TC180398	MtN3-like protein	Solyc03g097870 (*7)	1	2.149928	0.229098	0.560559	0.932105	0.518918	0.25569	0.793986
145	TowgeN_I_21474	TC181283	Hydroxymethylglutaryl-CoA synthase (HMGS)	Solyc08g080170 (*16)	1	0.946085	0.300229	0.329895	0.606184	0.44482	0.280459	0.795492
146	TowgeN_I_24273	TC184082	NBS-LRR	Solyc11g071430	1	0.750858	0.844371	0.218159	0.34227	0.243282	0.271992	0.795697
147	TowgeN_I_47630	AW626306	Pistil extensin like protein	Solyc12g098780	1	0.589093	0.242976	0.324345	0.498541	0.1226	0.155426	0.796034
148	TowgeN_I_22794	TC182603	Senescence-associated protein	Solyc07g006280	1	0.883559	0.480734	0.496115	0.475888	0.281572	0.327861	0.79613
149	TowgeN_I_36139	BE449307	Expressed protein	Solyc10g074540 (*18)	1	1.042082	0.330333	0.234929	0.651495	0.483214	0.312741	0.797634
150	TowgeN_I_16807	TC176616	Non-specific lipid-transfer protein	Solyc06g054070	1	1.286596	0.53235	0.48943	0.683026	0.436685	0.131376	0.798874
151	TowgeN_I_10407	TC170216	GAME6	Solyc07g043460 (*12)	1	0.864562	0.449834	0.419811	0.338007	0.581559	0.410132	0.799114
152	TowgeN_I_37174	BG643837		no hit	1	0.73642	0.322709	0.614493	0.388428	0.375022	0.224657	0.799929
153	TowgeN_I_45620	AW033607	Whitefly-induced gp91-phox	Solyc03g117980	1	0.733269	0.649851	0.488207	0.293658	0.180925	0.266914	0.801736
154	TowgeN_I_33810	AI896082	Calmodulin-binding protein	Solyc01g100240	1	1.092894	0.593843	0.191437	0.54787	0.320916	0.674766	0.802346
155	TowgeN_I_22590	TC182399	Proline dehydrogenase	Solyc02g089620 (*5)	1	1.016179	0.178624	0.258586	0.713853	0.406732	0.219906	0.803211
156	TowgeN_I_15800	TC175609	Receptor-like kinase	Solyc01g067510	1	0.408876	0.339971	0.54554	0.135392	0.076066	0.046969	0.804687
157	TowgeN_I_48772	AI776612	Peptidoglycan-binding LysM domain-containing	Solyc03g026360	1	1.031115	0.262792	0.509384	0.548192	0.291696	0.6427	0.804892
158	TowgeN_I_23980	TC183789	Aquaporin-like protein	Solyc03g096290	1	1.062728	0.858009	0.549247	0.387432	0.213634	0.199966	0.804956
159	TowgeN_I_43378	DY523815	1-aminocyclopropane-1-carboxylate oxidase oxy	Solyc11g010410	1	0.934554	0.123184	0.603364	0.689846	0.057177	0.059569	0.809209
160	TowgeN_I_44225	BP911078	Subtilisin-like serine protease	Solyc07g008900	1	1.112698	0.689292	0.520153	0.492647	0.30242	0.390231	0.810205
161	TowgeN_I_19749	TC179558	Phospholipid diacylglycerol acyltransferase	Solyc03g121960	1	1.07722	0.949509	0.49223	0.333215	0.272774	0.28258	0.811148
162	TowgeN_I_31810	AJ832101		no hit	1	0.633357	0.601509	0.571601	0.140175	0.157599	0.220829	0.815005
163	TowgeN_I_40201	AW622134	Serine/threonine kinase receptor	Solyc04g077270	1	1.012499	0.329816	0.332946	0.721581	0.19736	0.214452	0.815235
164	TowgeN_I_13849	TC173658	Unknown Protein	Solyc05g013780	1	0.954492	0.577342	0.938808	0.229761	0.059196	0.105327	0.815374
165	TowgeN_I_47390	AW040353	MtN3-like protein	Solyc03g097870 (*7)	1	1.893593	0.224848	0.320565	0.981925	0.368234	0.267128	0.81559
166	TowgeN_I_27141	TC186950	Unknown Protein	Solyc12g005810	1	0.664746	0.665545	0.313376	0.343549	0.344802	0.177025	0.816959
167	TowgeN_I_16778	TC176587	GAME4	Solyc12g006460 (*21)	1	0.760254	0.353797	0.507858	0.36222	0.487326	0.365208	0.817387
168	TowgeN_I_35925	BI934641	3-beta-hydroxysteroid-Delta8 Delta7-isomerase	Solyc06g082980	1	0.833673	0.360284	0.470575	0.411772	0.55123	0.384672	0.823802
169	TowgeN_I_26269	TC186078	Genomic DNA chromosome 3 P1 clone MJL12	Solyc06g007790	1	1.46895	0.505773	0.301524	0.669338	0.611936	0.575258	0.824815
170	TowgeN_I_49642	AI771367	Cytochrome P450	Solyc12g042480	1	0.889398	0.402219	0.328534	0.581123	0.419037	0.309769	0.825493
171	TowgeN_I_24771	TC184580	Peptide transporter	Solyc05g005920	1	1.024803	0.368012	0.321886	0.621526	0.516429	0.371711	0.827999
172	TowgeN_I_30916	TC190725	Fructose-bisphosphate aldolase	Solyc01g110360	1	0.848071	0.649352	0.54922	0.381485	0.268832	0.272591	0.828334
173	TowgeN_I_46027	BE463031		no hit	1	0.763489	0.594545	0.758995	0.171572	0.170434	0.162146	0.828874
174	TowgeN_I_15931	TC175740	Mitochondrial transcription termination factor	Solyc03g124040	1	0.425792	0.317553	0.354169	0.267009	0.253302	0.240759	0.828931
175	TowgeN_I_18368	TC178177	Retinol dehydrogenase 12	Solyc03g025390 (*6)	1	0.791806	0.340494	0.440086	0.474342	0.562548	0.243989	0.831419
176	TowgeN_I_32146	CD003286	Glucose-6-phosphate 1-dehydrogenase	Solyc02g093830	1	1.020826	0.775358	0.545811	0.443769	0.300181	0.250082	0.833432
177	TowgeN_I_43624	BP901762	Squamosa promoter binding protein 15	Solyc10g078700	1	1.029226	0.608844	0.258024	0.51737	0.43947	0.581601	0.834261
178	TowgeN_I_22222	TC182031	Unknown Protein	Solyc01g065510	1	0.879906	0.628123	0.733959	0.347159	0.143931	0.20045	0.837045
179	TowgeN_I_46237	AW624314	LRR receptor-like serine/threonine-protein kinas	Solyc06g048950	1	1.137104	0.525702	0.239918	0.569744	0.636324	0.501225	0.837694
180	TowgeN_I_26694	TC186503	Aquaporin	Solyc03g120470	1	0.804852	0.353375	0.502521	0.560753	0.272101	0.226518	0.838857
181	TowgeN_I_25618	TC185427	Xyloglucan endotransglucosylase/hydrolase 12	Solyc09g008320	1	0.765652	0.537513	0.294728	0.567173	0.155394	0.216415	0.838951
182	TowgeN_I_16523	TC176332	Solute carrier family 15 member 2	Solyc05g005990	1	1.10598	0.360343	0.240659	0.710047	0.433105	0.421302	0.839226
183	TowgeN_I_22369	TC182178	Ripening regulated protein DDTFR10	Solyc07g016150	1	0.496902	0.305436	0.429296	0.265696	0.386178	0.261545	0.839229
184	TowgeN_I_28189	TC187998	Solute carrier family 15 member 4	Solyc05g005940	1	0.752094	0.3499	0.668373	0.398915	0.389153	0.246189	0.839365
185	TowgeN_I_21085	TC180894		no hit	1	0.424598	0.455853	0.329038	0.209501	0.237755	0.221337	0.83979
186	TowgeN_I_23666	TC183475	Octicosapeptide/Phox/Bem1p domain-containin	Solyc05g013530	1	0.91274	0.42002	0.450742	0.545777	0.394894	0.393556	0.8401
187	TowgeN_I_39889	BG735347	Nodulin-like protein	Solyc04g080940	1	0.809521	0.524397	0.837106	0.22829	0.24114	0.207177	0.840682
188	TowgeN_I_23062	TC182871	Heat shock protein 4	Solyc12g043110	1	0.763264	0.338322	0.267756	0.446443	0.565603	0.413625	0.841598
189	TowgeN_I_19645	TC177945	Receptor-like kinase	Solyc04g079710	1	1.009427	0.622035	0.492561	0.542211	0.353339	0.316015	0.842559
190	TowgeN_I_39008	AI779564		no hit	1	0.548189	0.21058	0.4349	0.468069	0.185247	0.188784	0.845165
191	TowgeN_I_29603	TC189412	Nitrate transporter	Solyc06g066620	1	1.200184	0.537103	0.517163	0.709376	0.272429	0.266031	0.84612
192	TowgeN_I_23960	TC183769	Isopentenyl-diphosphate delta isomerase (IDI)	Solyc05g055760	1	0.845317	0.372418	0.584029	0.546895	0.289853	0.255832	0.847041
193	TowgeN_I_24503	TC184312	Exocyst complex protein EXO70	Solyc11g073010	1	0.558423	0.06274	0.117388	0.575503	0.186597	0.157805	0.847591
194	TowgeN_I_15451	TC175260	Auxin responsive SAUR protein	Solyc08g079150	1	0.871585	0.119589	0.179328	0.76268	0.173568	0.107141	0.847937
195	TowgeN_I_36577	AW647926		no hit	1	0.906229	0.59212	0.924196	0.238223	0.13303	0.144452	0.848461
196	TowgeN_I_41156	BP895064	Cortical cell-delineating proteinprotein, helical	Solyc12g014630	1	0.579595	0.379775	0.395922	0.450615	0.214826	0.1558	0.848609
197	TowgeN_I_26399	TC186208	Unknown Protein	Solyc12g038560	1	0.896818	0.340016	0.217855	0.612031	0.41078	0.466774	0.849262

Table S5 *JRE*-regulated genes
Genes included in **Table S1** (red), **S2** (blue), or both (purple) are listed in order of Gene IDs. SGA biosynthesis genes are highlighted in yellow.

Description	Gene ID
Cytochrome P450	Solyc06g047300
Unknown protein	Solyc01g007760
Obtusifolial 14-alpha-demethylase	Solyc01g008110
Beta-1 3-glucanase	Solyc01g008620
Scarecrow transcription factor family protein	Solyc01g009110
Peptidyl-prolyl cis-trans isomerase	Solyc01g009990
Potassium/sodium hyperpolarization-activated cyclic nucleotide-gated channel 4	Solyc01g010080
Unknown Protein	Solyc01g065510
Receptor-like kinase	Solyc01g062510
Uncharacterized oxidoreductase	Solyc01g073640
Multidrug resistance protein ABC transporter family	Solyc01g080640
Glucose transporter 8	Solyc01g090680
JRE4	Solyc01g090760
Sterol 4-alpha-methyl-oxidase 2 (SMO2)	Solyc01g091520
Maleylacetoacetate isomerase/glutathione S-transferase	Solyc01g091330
Dihydroflavonol 4-reductase family	Solyc01g094070
Transporter major facilitator family	Solyc01g098740
Glucose transporter 8	Solyc01g098500
Calmodulin-binding protein	Solyc01g100240
bHLH transcription factor	Solyc01g102300
NAC domain protein	Solyc01g102740
Helix-loop-helix DNA-binding transcription factor	Solyc01g106460
Cytochrome P450	Solyc01g109150
Fructose-bisphosphate aldolase	Solyc01g110360
Unknown Protein	Solyc01g111180
Cinnamyl alcohol dehydrogenase-like protein	Solyc02g030480
2-oxoglutarate-dependent dioxygenase	Solyc02g062460
2-oxoglutarate-dependent dioxygenase	Solyc02g062500
Sterol C-5 desaturase (DWF7)	Solyc02g063260
Sterol side chain reductase (SSR2)	Solyc02g069490
Chlorophyll a/b binding protein	Solyc02g070940
Lipase-like	Solyc02g077000
LRR receptor-like serine/threonine-protein kinase FEI 1	Solyc02g078630
Sterol-4-alpha-carboxylate 3-dehydrogenase	Solyc02g081730
3-hydroxy-3-methylglutaryl CoA reductase (HMGR)	Solyc02g082260
Homeobox-leucine zipper-like protein	Solyc03g056630
Sterol C-5 desaturase (DWF7)	Solyc02g086180
Calmodulin-like protein	Solyc02g088090
Proline dehydrogenase	Solyc02g089620
Cytochrome P450	Solyc02g090340
Galactosyltransferase-like protein	Solyc02g092840
Glucose-6-phosphate 1-dehydrogenase	Solyc02g093830
Proteinase inhibitor II	Solyc03g020040
Retinol dehydrogenase 12	Solyc03g025390
Peptidoglycan-binding LysM domain-containing protein	Solyc03g026360
UDP-glucosyltransferase family 1 protein	Solyc03g058370
Aquaporin-like protein	Solyc03g096290
Unknown Protein	Solyc03g096410
MIN3-like protein	Solyc03g097870
Pectate lyase	Solyc03g111690
Peptide transporter	Solyc03g113430
Pol polyprotein	Solyc03g115130
Whitefly-induced gp91-phox	Solyc03g117980
Aquaporin	Solyc03g120470
Phospholipid diacylglycerol acyltransferase	Solyc03g121960
Hydrolase	Solyc03g123390
Mitochondrial transcription termination factor	Solyc03g124040
Peptide transporter	Solyc04g005070
Pyruvate kinase	Solyc04g008740
Carboxyl methyltransferase	Solyc04g055260
Isopentenyl-diphosphate delta-isomerase (IDI)	Solyc04g056390
Tubulin alpha-3 chain	Solyc04g077020
Erg28 like protein	Solyc04g077150
Serine/threonine kinase receptor	Solyc04g077270
Squalene monooxygenase	Solyc04g077440
Cytochrome P450	Solyc04g078340
Receptor-like kinase	Solyc04g079710
Mitogen-activated protein kinase 9	Solyc04g080730
Nodulin-like protein	Solyc04g080940
Peptide transporter	Solyc05g005920
Solute carrier family 15 member 4	Solyc05g005940
Solute carrier family 15 member 4	Solyc05g005950
Peptide transporter	Solyc05g005970
Solute carrier family 15 member 2	Solyc05g005990
Expansin12	Solyc05g007830
Mitogen-activated protein kinase 15	Solyc05g008020
Pyrimidine 5'-nucleotidase	Solyc05g011880
Primary amine oxidase	Solyc05g013430
Opticosapeptide/Phox/Bem1p domain-containing protein	Solyc05g013550
Unknown Protein	Solyc05g013780
Acetyl-CoA C-acetyltransferase (ACAA)	Solyc05g012760
Unknown Protein	Solyc05g024190
N-myc downstream regulated	Solyc05g026360
Calmodulin-binding heat-shock protein	Solyc05g034280
Chalcone synthase 2	Solyc05g053550
F-box protein PP2-B1	Solyc05g053620
Epoxide hydrolase	Solyc05g054320
Isopentenyl-diphosphate delta isomerase (IDI)	Solyc05g055760
Cytosolic ascorbate peroxidase 1	Solyc06g005160
Sterol 4-alpha-methyl-oxidase 2 (SMO2)	Solyc06g005750
Genomic DNA chromosome 3 P1 clone MJL12	Solyc06g007750
Auxin-regulated protein	Solyc06g030470
LRR receptor-like serine/threonine-protein kinase FEI 1	Solyc06g048950
UDP-sugar pyrophosphorylase	Solyc06g051080
Auxin-responsive family protein	Solyc06g053260
Non-specific lipid-transfer protein	Solyc06g054070
Nitrate transporter	Solyc06g060620
Acid phosphatase	Solyc06g062310
Acid phosphatase	Solyc06g062380
Ethylene responsive transcription factor 2a	Solyc06g063070
GDSL esterase/lipase 5	Solyc06g064970
Aquaporin	Solyc06g066560
Seed specific protein	Solyc06g072850
Sterol reductase (DWF5)	Solyc06g074090
Aquaporin	Solyc06g075650
3-beta-hydroxysteroid-Delta8 Delta7-isomerase	Solyc06g082980
Calmodulin-like protein	Solyc06g083000
Leucine-rich repeat receptor-like protein kinase PEPR2	Solyc06g084420
Senescence-associated protein	Solyc07g006280
S8-RNase	Solyc07g006570
CONSTANS-like protein	Solyc07g006630
Subtilisin-like serine protease	Solyc07g008900
Ripening regulated protein DDTFR10	Solyc07g016150
Cellulose synthase family protein	Solyc07g043390
Unknown Protein	Solyc07g043480
GAME11	Solyc07g043420
GAME6	Solyc07g043460
GAME17	Solyc07g043480
GAME1	Solyc07g043490
GAME18	Solyc07g043500
CONSTANS-like zinc finger protein	Solyc07g043510
Arabinogalactan-protein	Solyc07g053640
Expansin B1	Solyc07g054170
Xyloglucan endotransglucosylase/hydrolase 7	Solyc07g055990
Heme-binding protein 2	Solyc07g061800
Cytochrome P450	Solyc07g062510
Cytochrome P450	Solyc07g062520
Aquaporin	Solyc08g008050
Fatty acid oxidation complex subunit alpha	Solyc08g068390
Acyltransferase-like protein	Solyc08g075210
Unknown Protein	Solyc08g078060
Auxin responsive SAUR protein	Solyc08g079150
Hydroxymethylglutaryl-CoA synthase (HMGS)	Solyc08g080170
MYB transcription factor	Solyc08g082890
Glutathione S-transferase	Solyc09g007750
Xyloglucan endotransglucosylase/hydrolase 12	Solyc09g008120
Delta14-sterol reductase	Solyc09g009630
Alcohol dehydrogenase zinc-containing	Solyc09g059040
Acetyl-CoA C-acetyltransferase (ACAA)	Solyc09g061840
Sterol 3-beta-glucosyltransferase	Solyc09g061860
1-aminocyclopropane-1-carboxylate oxidase 2	Solyc09g066320
POT family domain containing protein	Solyc09g075230
POT family domain containing protein	Solyc09g075260
Inositol 1 4 5-trisphosphate 5-phosphatase	Solyc09g082370
Major allergen Mal d 1	Solyc09g090990
Light regulated protein-like protein	Solyc09g092210
Serine/threonine-protein kinase receptor	Solyc10g005630
RING finger protein 5	Solyc10g008410
Expressed protein	Solyc10g074540
Squamosa promoter binding protein 15	Solyc10g078700
Peroxidase	Solyc10g078890
F-box/LRR-repeat protein	Solyc10g080020
Ethylene-responsive methionine synthase	Solyc10g081510
Unknown Protein	Solyc11g008080
1-aminocyclopropane-1-carboxylate oxidase oxygenase	Solyc11g010410
Wax synthase isoform 3	Solyc11g012200
Blue copper protein	Solyc11g012310
Auxin response factor 17	Solyc11g013470
UDP-glucosyltransferase	Solyc11g066670
UDP-glucuronosyltransferase	Solyc11g066830
NBS-LRR	Solyc11g071830
Sentrin specific protease 1b	Solyc11g072220
Exocyst complex protein EXO70	Solyc11g073010
Unknown Protein	Solyc12g005810
GAME4	Solyc12g006460
GAME12	Solyc12g006470
Germacrene-D synthase	Solyc12g006570
Proline-rich protein	Solyc12g009650
Glucosyltransferase	Solyc12g009920
UDP-glucuronosyltransferase 1-6	Solyc12g009930
Transcription factor CYCLOIDEA	Solyc12g014140
Cortical cell-delineating proteinprotein, helical	Solyc12g014630
Unknown Protein	Solyc12g038560
Cytochrome P450	Solyc12g042480
Heat shock protein 4	Solyc12g043110
Exostosin-like	Solyc12g062940
Gibberellin-regulated protein 2	Solyc12g089300
UDP-D-glucuronic acid 4-epimerase	Solyc12g098480
Pistil extensin like protein	Solyc12g098780
Aldehyde dehydrogenase	Solyc12g099250

Table S6 Signal intensities of probes corresponding to *JRE*-regulated SGA biosynthesis genes.
Probes included in **Fig. 2** are listed. Signal intensities are shown relative to levels in wild-type control (WT1) or vector control line (VC1). Values in this tables were used to draw the heat maps in **Fig. 2**.

			Relative signal intensities (WT1=1)				Relative signal intensities (VC1=1)						
Gene Name	Gene ID	Accession	WT1	WT2	OX1	OX12	VC1	VC2	*JRE3-EAR* #1	*JRE3-EAR* #2	*JRE4-EAR* #1	*JRE5-EAR* #1	*JRE5-EAR* #2
ACAA	Solyc09g061840	AJ785227	1	0.961648	7.550433	8.483722	1	0.893444	0.413002	0.580993	0.21976	0.604076	0.404397
	Solyc05g017760	TC174045	1	1.104596	9.138964	7.339797	1	0.756805	0.398713	0.790009	0.666275	0.568014	0.40286
		BG133566	1	1.120552	9.130856	7.004796	1	0.785853	0.429466	0.83779	0.670355	0.590727	0.426306
HMGS	Solyc08g080170	TC181283	1	1.257646	11.70824	14.42098	1	0.946085	0.300229	0.329895	0.606184	0.44482	0.280459
		BI927518	1	1.15215	11.05402	13.94774	1	0.911264	0.307798	0.312061	0.739942	0.536676	0.318433
		TC170785	1	0.905634	9.976382	8.744177	1	0.834671	0.309451	0.48796	0.584477	0.49635	0.260957
		AW623849	1	1.065839	4.228345	5.149067	1	0.975909	0.314385	0.391644	0.602467	0.413759	0.236815
HMGR	Solyc02g082260	TC188523	1	0.686731	14.51534	10.96161	1	0.920892	0.428472	0.33892	0.992744	0.86245	0.738067
IDI	Solyc04g056390	TC183455	1	1.390309	17.961	21.13118	1	1.8915	1.239887	1.525859	0.479536	0.357135	0.263448
		AI490441	1	1.300929	7.192049	6.867939	1	0.958305	0.721383	0.727305	0.857842	1.161356	1.009374
		TC175619	1	0.803331	5.952957	4.840635	1	0.853952	0.79787	1.031414	0.149837	0.159689	0.107067
	Solyc05g055760	TC183769	1	0.719289	1.38069	0.883501	1	0.845317	0.372418	0.584029	0.546895	0.289853	0.255832
SQO	Solyc04g077440	TC177745	1	0.951095	21.17192	20.32349	1	0.75734	0.276342	0.375451	0.60095	0.490969	0.442029
		TC185030	1	0.93081	20.93639	19.88298	1	0.756938	0.280888	0.365963	0.606119	0.490286	0.457425
SSR2	Solyc02g069490	BG129290	1	0.817671	11.22924	10.93802	1	0.900372	0.686086	0.969607	1.221699	1.652738	0.964926
O14DM	Solyc01g008110	TC179459	1	1.032319	5.034661	5.56824	1	0.927137	0.404631	0.477067	0.658515	0.737435	0.480053
D14SR	Solyc09g009040	TC186795	1	0.849176	5.77837	5.032411	1	0.789349	0.650463	1.091788	0.551983	0.481941	0.313657
SCDH	Solyc02g081730	TC171310	1	0.895681	14.49682	16.75199	1	0.693252	0.351587	0.538969	0.531022	0.429762	0.283501
HYD1	Solyc06g082980	BI934641	1	0.917078	6.429609	6.799937	1	0.833673	0.360284	0.470575	0.411772	0.55123	0.384672
		TC170578	1	0.952229	6.360481	5.341404	1	0.825852	0.347642	0.591719	0.458181	0.588801	0.353596
SMO2	Solyc06g005750	TC186636	1	0.563219	48.24578	45.12938	1	0.833555	0.318685	0.430669	0.417558	0.370759	0.315918
	Solyc01g091320	TC173191	1	1.065271	90.66405	94.39727	1	0.916223	0.342875	0.646756	0.585214	0.648855	0.439169
DWF7	Solyc02g086180	TC180985	1	1.184102	110.5292	97.59696	1	0.818411	0.285162	0.362287	0.354693	0.442846	0.259922
	Solyc02g063240	TC171386	1	1.189806	16.94733	14.45596	1	0.825764	0.410796	0.489309	0.456078	0.559431	0.403913
DWF5	Solyc06g074090	BI423324	1	0.888223	16.06357	14.5303	1	0.995378	0.344677	0.400557	0.493111	0.416499	0.174973
		TC173365	1	0.986297	15.21924	15.18812	1	1.018198	0.353582	0.402966	0.526696	0.454028	0.188592
		BI210634	1	0.943085	14.71237	12.89597	1	0.866961	0.36492	0.582012	0.454865	0.412824	0.174957
GAME11	Solyc07g043420	TC172585	1	1.011034	110.1742	112.8818	1	0.852349	0.357757	0.324873	0.212764	0.267048	0.183102
		BI932634	1	0.955715	108.8269	98.0142	1	0.946928	0.316201	0.355442	0.289269	0.381599	0.213353
		BG135874	1	1.008802	93.73397	77.98379	1	1.045282	0.289951	0.279333	0.341455	0.674318	0.338237
		BI924489	1	0.791274	83.94899	69.74382	1	0.876317	0.341416	0.375024	0.378231	0.519336	0.323686
		BI927123	1	1.032108	67.46698	66.19639	1	0.924691	0.362548	0.381823	0.425863	0.593774	0.384314
		TC185907	1	0.52248	38.23898	30.52259	1	0.829837	0.639185	0.876107	0.291468	0.359069	0.218966
GAME6	Solyc07g043460	TC178028	1	0.923118	170.0818	178.4329	1	0.803286	0.19646	0.298423	0.372377	0.401699	0.199957
		BG129731	1	0.736299	77.12106	70.66887	1	0.9421	0.402957	0.28864	0.333418	0.532272	0.362124
		AI776710	1	0.852484	57.49373	55.93754	1	0.862819	0.420381	0.321604	0.325186	0.626143	0.424811
		TC170216	1	0.736903	35.61379	32.24015	1	0.864562	0.449834	0.419811	0.338007	0.581559	0.410132
		TC172348	1	1.632085	76.6278	46.81436	1	1.079942	0.410767	0.343589	0.257287	0.268776	0.12797
		AW929217	1	0.762952	9.338698	8.191618	1	0.447456	0.171542	0.330396	0.209258	0.264242	0.11471
		BI926887	1	0.563734	110.9421	156.4718	1	0.938304	0.285947	0.327803	0.444228	0.410215	0.244912
		TC174255	1	0.885596	102.7334	131.3099	1	0.810316	0.303888	0.30183	0.429597	0.323383	0.202977
GAME4	Solyc12g006460	TC186736	1	0.878452	49.28353	46.21897	1	0.813976	0.362929	0.414977	0.333048	0.460899	0.349059
		TC176587	1	0.822708	43.35172	38.7919	1	0.760254	0.353797	0.507858	0.36222	0.487326	0.365208
GAME12	Solyc12g006470	TC182755	1	0.931718	99.04693	106.2098	1	0.904166	0.231805	0.270111	0.167338	0.540936	0.32899
		AW928641	1	0.830709	89.24932	78.52043	1	1.034202	0.277494	0.289386	0.17769	0.570701	0.386981
		AW929410	1	0.764771	81.02268	74.86666	1	0.966394	0.235814	0.308445	0.224924	0.564927	0.374353
		AI482715	1	0.794899	52.24999	47.22228	1	0.900655	0.274536	0.333092	0.188508	0.695831	0.46265
		TC169925	1	0.858323	55.10971	53.90769	1	0.926267	0.290273	0.408015	0.263949	0.694388	0.455231
GAME1	Solyc07g043490	TC173982	1	1.002708	67.80652	74.71268	1	0.858718	0.242186	0.229215	0.376808	0.261688	0.134485
		TC178657	1	1.141792	57.31623	55.01481	1	0.895963	0.262972	0.385465	0.402354	0.2718	0.132259
GAME17	Solyc07g043480	TC183594	1	0.735856	161.7173	170.0751	1	0.828369	0.23519	0.457681	0.502314	0.322052	0.171699
		AW929708	1	1.123935	453.8576	574.5726	1	1.082934	0.239342	0.32511	0.488201	0.397026	0.190841
GAME18	Solyc07g043500	TC170299	1	1.066581	108.0615	112.6339	1	0.824651	0.280921	0.433828	0.393195	0.243955	0.175244

Table S7 SGA levels in transgenic tomato *JRE4-OX* plant and *JRE4-EAR* hairy root lines.
Metabolite levels were analyzed by LC-QTOF-MS. The levels were caluculated based on the assumption that all SGAs exhibit the same molar response as α-tomatine. Levels of α-tomatine (denoted with asterisk) are shown in **Fig. 4** as well. SGAs were extracted from leaves of *JRE4-OX* (line OX1) and wild-type plants exposed to MeJA vapor for 4 d and hairy roots of *JRE4-EAR* (line #1) and vector control line #1 treated with MeJA for 4 d. SGAs with bracketed numbers are schematically indicated in the metabolic pathway in **Supplementary Figure S5**.

SGA levels in leaves from plants exposed to MeJA vapors

				wild type		*JRE4-OX* line OX1	
Peak ID	retention time (min)	*m/z*	annotation	average (n=4)	SD	average (n=4)	SD
P_0132_1136	4.9369	1004.542	tomatidine dihexoside dipentoside isomer	0.21	0.08	0.59	0.11
P_0132_1154	4.3122	1034.552	α-tomatine isomer (31)	0.04	0.08	0.17	0.12
P_0132_1155	4.8078	1034.551	α-tomatine (31) *	20.46	4.71	43.47	8.42
P_0132_1163	4.2479	1032.53	dehydrotomatine isomer #1 (34)	0.07	0.08	0.11	0.15
P_0132_1160	4.7104	1032.536	dehydrotomatine isomer #2 (34)	2.80	0.61	4.15	0.38
P_0132_1173	4.7612	1064.561	tomatidine tetrahexoside	0.32	0.09	0.59	0.13
P_0132_1178	4.0942	1050.546	hydroxytomatine isomer #4 (32)	0.00	0.00	0.15	0.18

SGA levels in hairy roots treated with MeJA

				vector control line #1		*JRE4-EAR* line #1	
Peak ID	retention time (min)	*m/z*	annotation	average (n=5)	SD	average (n=5)	SD
P_0102_1782	4.9468	1004.537	tomatidine dihexoside dipentoside	0.12	0.01	0.00	0.00
P_0102_1807	4.1947	1030.522	didehydrotomatine isomer #1	0.76	0.19	0.00	0.00
P_0102_1777	4.3725	1030.519	didehydrotomatine isomer #2	0.09	0.05	0.00	0.00
P_0102_1801	4.2519	1032.535	dehydrotomatine isomer #1 (34)	1.82	0.26	0.09	0.13
P_0102_1802	4.7434	1032.535	dehydrotomatine isomer #2 (34)	2.90	0.17	1.31	0.19
P_0102_1793	4.3404	1034.552	α-tomatine isomer (31)	0.82	0.23	0.06	0.08
P_0102_1794	4.8356	1034.551	α-tomatine (31) *	19.32	1.14	9.10	1.04
P_0102_1815	3.8955	1050.546	hydroxytomatine isomer #1 (32)	0.12	0.11	0.22	0.02
P_0102_1818	3.9521	1050.545	hydroxytomatine isomer #2 (32)	1.27	0.08	0.60	0.06
P_0102_1813	4.027	1050.547	hydroxytomatine isomer #3 (32)	0.72	0.06	0.30	0.03
P_0102_1816	4.0961	1050.546	hydroxytomatine isomer #4 (32)	0.57	0.61	0.19	0.14
P_0102_1819	4.2015	1050.544	hydroxytomatine isomer #5 (32)	0.19	0.15	0.11	0.02
P_0102_1817	4.3192	1050.546	hydroxytomatine isomer #6 (32)	0.69	0.15	0.44	0.27
P_0102_1838	4.792	1064.562	tomatidine tetrahexoside	0.41	0.04	0.15	0.04
P_0102_1833	4.7294	1090.537	acetoxydehydrotomatine	0.11	0.01	0.00	0.00

Table S8 Top 10 sequences retrieved by MEME analysis.
The 5'-flanking regions (-1,500 to -1) of group R and SR genes were used as queries. Top 10 sequences retrieved are included. The match scores, which were calculated using position-specific probability matrices, represent similarlities of the sequences to each box. The scores range from 0 (no similarlity) to 1 (exactly same). The scores 0.5 or higher are highlighted in yellow. The orientations of the alighnments are denoted with the scores.

to

				match score					
rank	e-value	sequence logo	motif	P box		CS1 box		GCC box	
1	1.50E-52		[CT][CT][TC]C[TC]C[TC]C[TC]C	0.610	+	0.518	+	0.398	+
2	2.60E-19		[TC]TT[CT]TTCT[TC][CT]	0.376	+	0.403	-	0.311	+
3	3.00E-09		[GC]GG[CA][GA]G[GC][GA]G	0.580	-	0.507	-	0.573	-
4	3.50E-02		C[TC]C[GC]C[ACT]C[GAT][CA]C	0.615	+	0.578	+	0.444	+
5	9.60E-02		[CAT][AC]AC[AG]CAC[CA]C	0.623	+	0.644	+	0.370	+
6	3.30E+03		AAAAA[AG]AAAA	0.315	+	0.355	+	0.139	+
7	6.20E+05		GGACGG[TG]GGA	0.474	-	0.403	-	0.455	-
8	3.40E+04		C[CAT]C[CG]ACC[TA][ACT]C	0.458	+	0.457	+	0.459	+
9	7.50E+01		[TA]GG[AT]CCC[AC][CA]	0.466	+	0.537	+	0.436	+
10	1.00E+06		[AG]AGA[GA]AGAGA	0.471	-	0.391	+	0.328	-

group SR

				match score					
rank	e-value	sequence logo	motif	P box		CS1 box		GCC box	
1	1.40E-12		[AG][GC]G[GA][AT]G[GA]G[GA]G	0.553	-	0.452	-	0.427	-
2	2.60E-02		G[GA]GGGG[CG][GT]A	0.641	-	0.527	-	0.581	-
3	1.20E-01		C[TA]CT[CG]TC[CT][CA]	0.482	+	0.400	+	0.367	+
4	5.90E+02		C[TC]CC[AT][TC][TC]CCC	0.550	+	0.469	+	0.381	+
5	2.10E+04		TCCGG[CA]GGG[GA]	0.444	-	0.429	-	0.518	-
6	4.00E+04		[GT]GG[GA]GCT[GT][CG][GC]	0.484	-	0.530	-	0.497	-
7	4.90E+04		[CA][TC][GC]CC[CT]ACC	0.652	+	0.594	+	0.460	+
8	7.40E+04		AGGGGGG	0.464	-	0.439	-	0.502	-
9	1.30E+05		GAGCCGC	0.380	+	0.348	+	0.598	+
10	2.20E+05		GAA[AG]AGG[AG][GA]G	0.409	-	0.337	-	0.359	-

Table S9 Oligonucleotide primers used for qRT-PCR analysis.

Gene name	Gene ID or accession	forward or reverse (F or R)	sequences (5' to 3')
ACAA	Solyc09g061840	F	GGTGCTGGACTAGAGTTCATGACAG
		R	GGGCTTGTGCAAAAGCATC
HMGS	Solyc08g080170	F	CAATGTCGGATGCAGCCTAC
		R	GGATTCAAAGGGGGCCAGG
HMGR	Solyc02g082260	F	GAGCAGCTAATTATCGAGGAAG
		R	GGCAGGTTGCTGTGGAAC
IDI	Solyc04g056390	F	GTTGTGATAGCATCCTTCTGC
		R	CCGATTATACAGCACAACAGC
DWF7	Solyc02g086180	F	ATACCGTCGGAGATGGAGG
		R	GCCAATGTAGTTACGGAGCC
SMO2	Solyc06g005750	F	AGTGTCCAGTGTGCGTGTG
		R	GAACCAACTGAGACTCCGC
DWF5	Solyc06g074090	F	TCTGCTTGGGCGTTTCTTC
		R	CCAAACCACCCTGCCTTTTC
HYD1	Solyc06g0829080	F	TGGCATCTCATCCGTACTGG
		R	CCACCAGCACATGAGTACCC
GAME1	Solyc07g043490	F	TTGCCGGATGTTCCATGATCG
		R	CTAATGAAGAAACAGCGTCCTGG
GAME4	Solyc12g006460	F	ACCTGTTGCTCTTATGTCTGTC
		R	CCTCTTGTTCCTCTTTGGCTT
GAME6	Solyc07g043460	F	CTACTTTGTATGGTGGCGTCC
		R	GGTGCAATGGCATGGGTTTAG
GAME11	Solyc07g043420	F	TCCTTCCCTATAAATGGCCCTC
		R	GAGAGAAGATCCGCCATTGAC
GAME12	Solyc12g006470	F	GCGGAGGGTTCTTATGTCTATG
		R	GCTTCAATAAGACGAGGCTCAC
GAME17	Solyc07g043480	F	GCCATCTCCGACAACTTCTC
		R	GTTGCCTAGCTTCACGGTTAG
GAME18	Solyc07g043500	F	ATTTGTAACGCATTGTGGTTGG
		R	CTTGGGACCTCAACAGCTAC
JRE1	Solyc1g090300	F	CGATAGGAAAGGTGCTAGGC
		R	AGCCACGAATCTTATAAGCG
JRE2	Solyc1g090310	F	AGACAGTGGTGGCAAGTGTG
		R	CATTTTTCTTATCCGGATCC
JRE3	Solyc1g090320	F	CGCTACTACCATATTAGGTC
		R	GTGCTATCTCAAGTTTAGGTAGCTC
JRE4	Solyc1g090340	F	TGTTTCCTCCGGTGTTACGG
		R	CGATTTTTTCGAAACTCTTTCC
JRE5	Solyc1g090370	F	GATCATCAAAACGCGATCGC
		R	ATTTTTTCGGCCTATGCTC
JRE6	Solyc5g050790	F	ACGCGGCATTGGCTTATGATC
		R	TCAGCTCAGCAACATTCGTGTC
EF1α	Solyc05g005060	F	AAGCCTGGTATGGTTGTGAC
		R	CACCAGGGAGTGCCTCCTGG
GUS	AF485783	F	CTTTGATCGCGTCAGCGCCGTCG

	(for used template)	R	CGAAGTTCATGCCAGTCCAGCG
GFP	AB289767	F	CAAGATCCGCCACAACATCGAGG
	(for used template)	R	CTGGGTGCTCAGGTAGTGGTTGTC

Table S10 Sense and anti-sense oligonucleotides for probes used in EMSA. Sense oligonucleotide labelled with biotin at 5' end were commonly used to generate all the probes. Substituted nucleotides for mutant probes are underlined.

Probe name	sense or antisense (S or AS)	Sequence (5' to 3')
(for all)	S (labelled with biotin)	Biotin-ACACCGAGG
G1	AS	NNNNNNNNTAGCCCCCCANNNNCCTCGG
mG1	AS	NNNNNNNNTAAACAACCANNNNCCTCGG
G2	AS	NNNNNNNNCAACCCCGCANNNNCCTCGG
mG2	AS	NNNNNNNNCATTCTTGCANNNNCCTCGG
D1	AS	NNNNNNNNCAGCACGCCANNNNCCTCGG
mD1	AS	NNNNNNNNCATTACTTCANNNNCCTCGG
D2	AS	NNNNNNNNACGCACACTGNNNNCCTCGG
mD2	AS	NNNNNNNNACAAACAATGNNNNCCTCGG

Acknowledgements

I would like to express the deepest appreciation to Professor Takashi Hashimoto and Associate professor Tsubasa Shoji in the Laboratory of Plant cell function, Nara Institute of Science and technology for their continuous guidance, criticized ideas in research, encouragements and mentality supports. Both of them have been my personal investigator, supervisor, consultant and mentor throughout my study.

I would like to thanks, Dr. Shunsuke Imanishi, Institute of Vegetable and Tea Science, National Agriculture and Food Research Organization for his excellent help in Microarrays.

My appreciation is expressed to Dr. Toru Kudo, Department of Life Sciences, School of Agriculture, Meiji University for his help to accomplish the computational cis-element analysis.

I would like to give my gratitude to Dr. Ryo Nakabayashi and Prof. Kazuki Saito from RIKEN Center for Sustainable Resource Science, and Associate professor Kiyoshi Ohyama from Department of Chemistry and Materials Science, Tokyo Institute of Technology for their help on metabolite analysis and to polish our manuscript.

I would like to thanks, Dr. Koichi Kawamoto, Dr. Satoko Nonaka, Assistant professor Chiaki Matsukura and Prof. Hiroshi Ezura, Graduate School of life and Environmental Sciences, University of Tsukuba for their help in the generation of transgenic tomato used in this study and their comments throughout this research.

I deeply appreciate all kind helps, supports and friendships from all past and present members and staffs in the Laboratory of Plant cell function, Nara Institute of Science and Technology.

I would like to appreciate Ministry of Education, Culture and Science of Japan for the financial support and valuable education opportunity.

Last but not least, I would like to express the deepest gratitude to my mother, a lady from nowhere, for her support. Thanks to keeping telling me “It does not matter where you go, it matters how you are”.